Visualisation of Multi-dimensional Medical Images with Application to Brain Electrical Impedance Tomography

Yan Zhang

A thesis submitted to Middlesex University

in partial fulfilment of the requirements for the degree of

Doctor of Philosophy

Computing Science School

Middlesex University

June 2007

To my father …

Acknowledgements

I would like to express my sincere appreciation to my supervisors Dr. Peter J. Passmore and Professor Richard H. Bayford for their great support and inspiration. I am very much indebted to them for their professional guidance.

I would also like to thank researchers in the Electrical Impedance Tomography research group, University College of London, who provide their assistances in the study. Special thanks to Dr. Rebecca Yerworth for her help.

Thanks and acknowledgements go to administration staff at Middlesex University, especially, Professor Richard Comley, Professor Colin Tully, Dr. Claudia Kalay, Ms. Frida Attrams, Ms. Kerry Lane, and Ms. Emma Warren, for their support.

Many thanks to other research students, past and present, in the School of Computing Science, Middlesex University, for their friendship and support. Special thanks to Micheal Foster, Amala Rajan, Yoney Kirsal, Fatema Shaikh, Abhishek Agrawal, Jim Otieno, Mohammad Kamal, Saif Rehman, Nan Jiang, Yu Qian, Ming Nie, and Lin Wang.

Finally, I would like to thank my mum, my husband, my sisters, and all the family members, for their love.

Access Statement

I hereby declare that with effect from the date on which the thesis is deposited in the Library of Middlesex University, I permit the Librarian of the University to allow the thesis to be copied in whole or in part without reference to me on the understanding that such authority applies to the provision of single copies made for study purposes or for inclusion within the stock of another library. This restriction does not apply to the British Library Thesis Service (which is permitted to copy the thesis on demand for loan or sale under the terms of a separate agreement) nor to the copying or publications of the title and abstract of the thesis. IT IS A CONDITION OF USE OF THIS THESIS THAT ANYONE WHO CONSULTS IT MUST RECOGNIZE THAT THE COPYRIGHT RESTS WITH THE AUTHOR AND NO QUOTATION FROM THE THESIS AND NO INFORMATION DERIVED FROM IT MAY BE PUBLISHED UNLESS THE SOURCE IS PROPERLY ACKNOWLEDGED.

Signature: Date:

Contents

List of Figures

List of Tables

Abstract

Medical imaging plays an important role in modern medicine. With the increasing complexity and information presented by medical images, visualisation is vital for medical research and clinical applications to interpret the information presented in these images. The aim of this research is to investigate improvements to medical image visualisation, particularly for multi-dimensional medical image datasets. A recently developed medical imaging technique known as Electrical Impedance Tomography (EIT) is presented as a demonstration. To fulfil the aim, three main efforts are included in this work.

First, a novel scheme for the processing of brain EIT data with SPM (Statistical Parametric Mapping) to detect ROI (Regions of Interest) in the data is proposed based on a theoretical analysis. To evaluate the feasibility of this scheme, two types of experiments are carried out: one is implemented with simulated EIT data, and the other is performed with human brain EIT data under visual stimulation. The experimental results demonstrate that: SPM is able to localise the expected ROI in EIT data correctly; and it is reasonable to use the balloon hemodynamic change model to simulate the impedance change during brain function activity.

Secondly, to deal with the absence of human morphology information in EIT visualisation, an innovative landmark-based registration scheme is developed to register brain EIT image with a standard anatomical brain atlas.

Finally, a new task typology model is derived for task exploration in medical image visualisation, and a task-based system development methodology is proposed for the visualisation of multi-dimensional medical images. As a case study, a prototype

visualisation system, named EIT5DVis, has been developed, following this methodology, to visualise five-dimensional brain EIT data. The EIT5DVis system is able to accept visualisation tasks through a graphical user interface; apply appropriate methods to analyse tasks, which include the ROI detection approach and registration scheme mentioned in the preceding paragraphs; and produce various visualisations.

Chapter 1 Introduction

1.1 Background

Dr. Wilhelm Kornrad Roentgen discovered the X-ray in late 1895, and that led into a new era in the practice of medicine: it is now possible to look into the human body without having to open it (Morton and Hammer 1896). X-ray imaging is the oldest and perhaps the commonest medical imaging technique. Several other medical imaging approaches developed afterwards. Medical imaging plays an important role in modern medicine. With the increasing complexity and information presented by these images, visualisation is vital for medical research and clinical applications to interpret the information presented in these images. In this background section, an overview of medical imaging methods is presented first. Then a description of a particular medical imaging method, Electrical Impedance Tomography (EIT), which is used as a case study in this work, follows. Finally, an introduction on the visualisation of EIT images is given.

1.1.1 Overview of Medical Imaging Methods

Medical imaging methods can be divided into two global categories: *anatomical* and *functional* (Maintz and Viergever 1998). Anatomical medical imaging methods depict primarily morphology of subjects; functional medical imaging methods represent

information on the metabolism of the underlying anatomy. In the following, major medical imaging methods are introduced according to this classification.

1.1.1.1 Anatomical Medical Imaging Methods

Anatomical medical imaging methods generally include X-ray imaging, Computed Tomography (CT), Magnetic Resonance Imaging (MRI), Ultrasound imaging and Terahertz imaging. An introduction of these methods follows.

X-ray Imaging

X-ray image is formed by the interaction of X-ray photons with a photon detector. The photons emitted by an X-ray tube enter a patient, where they may be scattered, absorbed or transmitted without interaction. The photon detector records the transmitted photons and creates the image. X-ray imaging is very good at detecting problems in the bones, chest, and spine. It is difficult to distinguish soft tissue by X-ray imaging, and it is not possible to resolve spatial structures along the direction of X-ray propagation with this kind of image.

Computed Tomography

Computer Tomography (CT) was developed based on conventional X-ray imaging. Conventional X-ray images provide 2D projection of 3D objects, Computer Tomography has 3D resolution. With Computed Tomography, a planar slice of the body is defined and X-rays are passed through it only in directions that are contained within, and are parallel to the plane of slice. The resulting images show the human anatomy in section with a spatial resolution of about 1mm. Tissues, which could not be resolved on conventional transmission X-ray imaging, can be identified on CT reconstructions. CT scans are quick and accurate. It is commonly used on the head and abdomen scans. The

main drawback of CT scans is that it involves exposure to radiation in the form of X-rays.

Magnetic Resonance Imaging

Magnetic Resonance Imaging (MRI), which is based on the principles of Nuclear Magnetic Resonance (NMR), exploits the magnetic properties of hydrogen nuclei within the body (Mattson and Simon 1996). By detecting the signals of protons in hydrogen atoms and then locating their positions using a magnetic coil, MRI allows doctors to view images of organs and soft tissues within the body. The spatial resolution of MRI is a function of imaging time and signal-to-noise ratio. In clinical applications, the resolution is usually 1~3mm. MRI has been playing a vital role to study brain anatomy and their abnormalities. MRI can also be used to diagnosing problems of cardiovascular, spine, and joints. The advantage of MRI over other imaging modalities is obvious: MRI does not involve exposing the patient to ionising radiation; it is non-invasive and can create various contrasts to study different types of brain tissues. However, being placed in the MRI scanner can induce significant claustrophobia in some patients. Patients with certain kinds of medical devices – for example, pacemakers – cannot receive MRI. Besides these, MRI technology is extremely complex and expensive.

Ultrasound Imaging

Ultrasound imaging uses high-frequency (3~10 MHz) sound waves and their echoes. High-frequency sound pulses are transmitted into the body using a probe. The sound waves travel into the body and hit a boundary between tissues (e.g. between fluid and soft tissue, soft tissue and bone). The reflected waves are picked up by the probe and relayed to the machine, which displays the distances and intensities of the echoes on the screen, forming a two dimensional image. Ultrasound is a useful way of examining many of the body's internal organs. In particular, ultrasound has progressively become an indispensable obstetric tool and plays an important role in the care of pregnant

women. Ultrasound imaging uses no ionising radiation and provides real-time imaging. It is non-invasive, painless, cheap, widely available and easy to use. Nevertheless, ultrasound imaging still has some limitations: Ultrasound has difficulty in penetrating bone and therefore can only see the outer surface of bony structures and not what lies within. Ultrasound waves do not pass through air, therefore, in an evaluation of the stomach, small intestine and large intestine may be limited.

Terahertz Imaging

Terahertz imaging harnesses radiation called terahertz rays, which sit between microwaves and infrared in the electromagnetic spectrum, and typically include frequencies between 0.1 THz and 20 THz. Terahertz rays pass easily through most non-metals and can reveal both the structure and composition of the target. The dominant method of the terahertz imaging is TPI (Terahertz Pulsed Imaging) (Hu and Nuss 1995; Zhang 1997). The first medical applications of TPI is expected to be in dentistry (Ciesla, Arnone et al. 2000). Another important area where TPI may have benefits is in identifying surface cancers. One of the major advantageous of TPI relative to X-ray, MRI, and other conventional imaging technologies is that it provides terahertz spectral characteristics of the sample at each pixel in its image. TPI is non-ionising, has sub-millimetre lateral resolution and its frequencies scatter far less than infrared or optical frequencies. However the penetration depth of terahertz in biological tissue is limited to the order of millimetres. This will influence the focus of research into its medical applications.

1.1.1.2 Functional Medical Imaging Methods

Different from the structural information provided by CT, MRI or Ultrasound imaging, the information provided by functional medical imaging can reveal some physiological activity, which can provide a much earlier detection measure for certain forms of disease

than do anatomical changes over time. Functional medical imaging methods usually include Single Photon Emission Computed Tomography (SPECT), Positron Emission Tomography (PET), Functional Magnetic Resonance Imaging (fMRI), Electroencephalogram (EEG), Magnetoencephalography (MEG) and Electrical Impedance Tomography (EIT). An simple explanation of these methods follows.

Single Photon Emission Computed Tomography

Single Photon Emission Computed Tomography (SPECT), which is a nuclear medicine approach, involves the use of radioisotopes such as 99mTc to assess metabolic activity in various regions of the body (Frankle, Slifstein et al. 2005). The radioisotopes decay and emit a single gamma ray per nuclear disintegration from within the patient. A gamma camera collects these rays, which enable pictures to be reconstructed of where the gamma rays originated. From these pictures, the function of a particular organ or system can be determined. Typical applications of SPECT include the functional evaluation of the brain, heart, skeleton, liver, lung and kidneys.

Positron Emission Tomography

Positron Emission Tomography (PET) is another nuclear medical imaging technique, developed 10-20 years later than SPECT. In PET imaging, a radio pharmaceutical, such as fluorodeoxyglucose, which includes both glucose and a radioactive element, is injected into the body. The positron emitted from a radioactive element will travel less than one millimetre and then annihilates with an electron, producing a pair of photons in opposite directions. PET scanner detects this pair of gamma ray photons and reconstructs the signals into images.

Generally, PET is used to determine the presence and severity of cancers, neurological conditions, and cardiovascular disease. Compared with SPECT, PET has a higher spatial resolution (5×5×5 mm) and a similar temporal resolution (about 40 seconds). Compared

with X-ray or CT, the radioactivity in PET and SPECT is very short-lived, so the radiation exposure is extremely low. However, SPECT tracers are long lasting compared to PET. The PET process needs an on-site cyclotron to produce the short-lived radioisotopes for scanning. This facility is very expensive and few institutes can afford it.

Functional Magnetic Resonance Imaging

Functional Magnetic Resonance Imaging (fMRI), which was first demonstrated as an extension of anatomical MRI in 1991 (Belliveau, Kennedy et al. 1991), measures the quick, tiny metabolic changes that take place in the brain. The metabolism in an active part of the brain responsible for particular tasks will increase, which will require additional oxygen. Therefore, there will be an increase in oxygenated blood flow (oxyhemoglobin) to this local brain area. Oxyhemoglobin is diamagnetic like water and cellular tissue. Deoxyhemoglobin is more paramagnetic than tissue. MRI is able to detect a small difference between these two and provide a Blood-Oxygen Level Dependent (BOLD) signal.

In routine practice, fMRI is often used in planning brain surgery. FMRI can also enable the detection of strokes at a very early stage, help physicians monitor the growth and function of brain tumors and guide the planning of radiation therapy. FMRI images of brain and other head structures are clear and detailed because of its high spatial resolution (2.5mm) and temporal resolution (2~5 seconds). FMRI imaging involves less pain, does not involve radiation, or require injection or ingestion of any substance. Another advantage of fMRI is the natural correspondence to MRI structural images, which provides an anatomic basis to the functional localization. Although the occurrence of fMRI has challenged PET's supremacy in the field of functional imaging, it seems impossible for fMRI to take over PET. The main reason is that PET has a unique facility which is not possible with fMRI, it is that many kinds of different molecules can be radioactivity tagged, and then correspondingly detected using the PET

scanner. This enables the study of a variety of different metabolites, which extrapolates to different cognitive functions.

Electroencephalogram

Electroencephalography (EEG) is a technique that measures the brain function by analysing the scalp electrical activity. EEG recordings are obtained by placing electrodes on the scalp. Local current flows are produced when brain cells (neurons) are activated. The small electrical signals detected by the scalp electrodes are amplified thousands of times, then displayed on paper or stored in computer memory.

By identifying abnormal patterns such as spikes, sharp waves, EEG is often used to diagnose epilepsy, sleep disorders, stroke, tumours, head injuries and brain death. EEG is also widely used to study the brain organization of cognitive process such as perception, memory, attention, language, and emotion. EEG is non-invasive, no radiation, cheap and the equipment is portable. Unlike Techniques as SPECT, PET, and fMRI measuring neuronal activity in a relatively indirect manner, that is they detect changes in metabolism or blood flow that are coupled to neuronal activity, EEG records the electric fields that are directly generated by neuronal activity. In comparison to temporal resolutions of seconds to minutes for SPECT, PET and fMRI, EEG can track neuronal activity millisecond by millisecond. The major drawbacks of EEG are its poor spatial resolution (about a few centimetres), and that it can only measure activity on the cerebral cortex. The electrical activity inside the head is undetectable with EEG. In addition, from mathematical point of view, the reconstruction of EEG images is non-unique.

Magnetoencephalography

Magnetoencephalography (MEG) is based on the principle that all electric currents generate magnetic fields according to the right-hand rule. Accompanying the neuronal

activation, local current flows are produced in the brain. Some of these flows are longitudinal and form the main source of the extra cranial magnetic fields. These magnetic signals, which are extremely weak and vary from 1 fT to 100 pT, are detected.

Nowadays MEG is used in numerous hospital laboratories to investigate brain disease such as epilepsy, stroke, Parkinson's disease, Alzheimer's disease and, to perform pre-surgical mapping. Clinical applications of MEG are increasing, and quite a few centres have adopted MEG as a standard tool for pre-operation, non-invasive investigations (Gratta, Pizzella et al. 2001). Similar to EEG, MEG is non-invasive, does not involve radiation, and measures neuronal activity directly. MEG has a millisecond temporal resolution that is comparable to EEG. Theoretically, MEG has somewhat better spatial resolution than EEG because magnetic fields pass unaffected through the tissue of the head, but this benefit is partly cancelled by the greater distance imposed between MEG sensors and the brain. Source localization in MEG is still limited by the non-uniqueness of the inverse problem, which becomes increasingly troublesome as the number of signal generators increases. Some reports indicated that MEG could provide spatial discrimination of 2mm. Contrary to the cheapness and portability of EEG, MEG is costly and can only be carried out in a special magnetically shielded environment.

1.1.2 Electrical Impedance Tomography

Electrical Impedance Tomography (EIT) is a relatively new imaging technique with applications in medicine. EIT images the interior of human body based on electrical measurements made on the surface. The first impedance image was published by Henderson and Webster (Henderson and Webster 1978). They used a 2D matrix of 100 electrodes on the back of the thorax and a single large electrode on the front to produce a transmission image of the tissues. The first published tomography images were presented by Brown and his colleagues in 1983 (Barber and Brown 1984). They used a

ring with 16 electrodes, with current injection between adjacent electrodes, and reconstructed the images with a back-projection method.

EIT images will be used as a typical demonstration in this research, thus a relatively detailed introduction on EIT imaging is given in the following subsections, which include its physiological basis, imaging procedure, imaging instrumentation, and applications. The advantages and disadvantages of EIT imaging are also described by comparing with other major medical imaging methods.

1.1.2.1 Physiological Basis of EIT Imaging

Table 1.1: Resistivities of different tissues

[From: (Barber and Brown 1984)]

Tissue	Resistivity (Ωm)
CSF	0.65
Blood	1.5
Liver	3.5
Skeletal muscle (longitudinal)	1.25
Skeletal muscle (transverse)	18.00
Myocardium (longitudinal)	1.6
Myocardium (transverse)	4.24
Neural tissue	5.8
Gray matter	2.84
White matter	6.82
Lungs (out / in)	7.27 / 23.63
Fat	27.2
Bone	166

The physiological basis of EIT imaging is that different tissues have different impedances. The human body can be considered as a composite volume conductor comprising a number of spatially distributed tissues with differing electrical properties (Geddes and Baker 1967; Plonsey 1984). EIT is sensitive to changes in electrical conductivity and produces images of the distribution of impedance within the tissues. Unlike metallic conductors, electrical conduction within biological tissues is due to the

movement of ionic rather than electronic charge carriers (Plonsey 1969). Table 1.1 lists the values of impedances for different tissues. This shows that there is a large resistivity contrast between tissues in the body. For example, bone has a resistivity of 166 Ωm while blood is a much better conductor at only 1.5 Ωm.

1.1.2.2 EIT Imaging Procedure

During EIT Imaging, impedance signals are generated and collected using a set of electrodes placed on the imaged object or a part of the body. Electrodes usually form a ring in 2D imaging or are equally spaced around the imaging field in 3D measurement. A current source is applied between either an adjacent or opposite (across the object) pair of electrodes, and voltage signals are measured on all other electrode pairs in turn. Sequential pairs are then used for the current injection until all possible combinations have been used. Figure 1.1 illustrates signal generation and collection in an EIT imaging system.

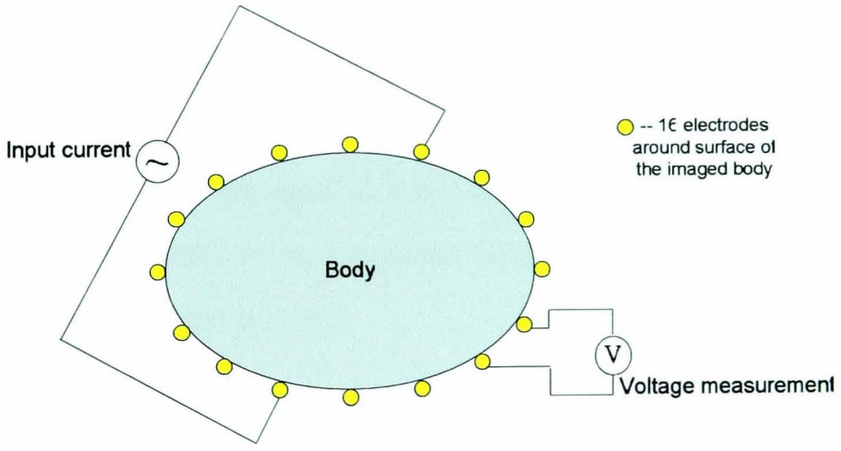

Figure 1.1 Signal generation and collection in an EIT imaging system

With the injected current and the measured voltages on the boundary, impedance or its reciprocal, conductivity, inside the object is estimated by reconstruction. An EIT reconstruction approach usually includes two parts: the solution of *forward problem* and the solution of *inverse problem*. The boundary voltages are linked to the object's

conductivity by known physical laws (Somersalo, Cheney et al. 1992). Such a relationship is called a forward operator. The inverse operator, which given the voltages would return the conductivity, is not known in the general case. For an accurate EIT reconstruction it is a prerequisite to have a model capable of predicting the voltages on electrodes for a given conductivity distribution (Lionheart 2004).

1.1.2.3 EIT Imaging Instrumentation

EIT imaging systems are generally about the size of a video recorder, but some may be larger. They usually comprise a box of electronics and a PC. Connection to the subject is usually made by coaxial cables a meter or two long, and ECG (electrocardiogram) type electrodes are placed in a ring or rings on the body part of interest.(Holder 2005) Up to now, only one commercial medical EIT system (Maltron International Ltd) is available although some research systems have been duplicated many times (Brown 2003). EIT systems used in medical research can be classified into three types: *absolute*, *dynamic* and *spectroscopic* (Boone, Lewis et al. 1994).

Absolute EIT imaging, sometimes referred to as static imaging, is an attempt to quantify the conductivity of an object in an absolute way. Usually, a current is applied though many electrodes in a pattern designed to maximise sensitivity. Examples of this kind of EIT system include the ACT or ACT3 systems from the Renssalaer Technical Institute in the USA (Saulnier, Blue et al. 2001).

A dynamic EIT system collects data over time to observe relative changes in impedance-time difference imaging. The Sheffield Mark 1 system is an example of a dynamic EIT system. This is a 2D system, using 16 electrodes with the applied current of 5mA at 51 kHz (Barber and Seagar 1987). The UCLH Mark 1b system is another time difference EIT imaging system that can use up to 64 independent electrodes. This system, which was designed specially for brain EIT imaging, employs a single impedance-measuring

circuit and multiplexer so that electrode combinations may be addressed flexibly using software installed on a laptop (see Figure 1.2). The system is a single frequency one, and can be set up to supply 18 different frequencies between 77 Hz and 225 kHz. The current recording protocol requires 258 measurements to be made for the acquisition of one image, which takes just about one third of a second (Yerworth, Bayford et al. 2002).

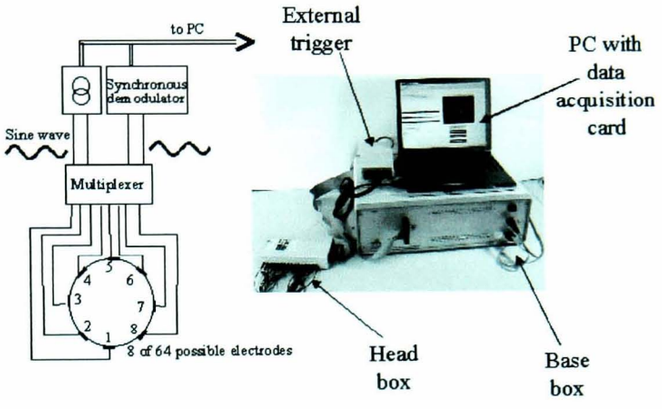

Figure 1.2 Schematic diagram and a photo of UCLH Mk1b EIT system

[From: (Yerworth, Bayford et al. 2002)]

Figure 1.3 UCLH Mk2 EITS system and the author as a subject

Spectroscopic or multiple frequency EIT imaging systems allow images of frequency-dependent impedance changes to be obtained. This can take the form of imaging the difference between two frequencies or injecting current at many frequencies and deriving parameters which can summarise the frequency dependent Cole Parameters. The Sheffield Mk3.5 system is an example of an EITS (Electrical Impedance Tomography Spectroscopy) System, where eight electrodes are used in an adjacent drive/receive protocol to deliver sine waves at frequencies between 2 kHz and 1.6 MHz

(Wilson, Milnes et al. 2001). A new multi-frequency EIT design has been developed at UCL, which adapts the Sheffield Mark 3.5 system for use with up to 64 electrodes (Yerworth, Bayford et al. 2003). The UCLH Mk2 EITS system, which injects currents from 2 kHz to 1.6 MHz, composes of a power supply, a base box and a headnet. Figure 1.3 shows a photo of the author of this thesis in an experiment using the UCLH Mk2 EITS system.

1.1.2.4 Potential Clinical Applications of EIT

Currently, EIT is not in routine biomedical use. Research results imply many possible applications, which include gastrointestinal function, pulmonary measurement, breast tumours, and brain function.

Gastrointestinal function

The most promising clinical use of EIT is in the measurement of gastric emptying, which is an important test in the management of some gastric disorders. A meal can be used as a label and then EIT is used to measure the rate of gastric emptying (Avill, Mangnall et al. 1987; Mangnall, Barnish et al. 1988). The utility of EIT imaging in pyloric stenosis (Nour, Mangnall et al. 1993) and gastroesophageal reflux (Ravelli and Milla 1994) has also been demonstrated.

Pulmonary measurement

Lung tissue has a resistivity which is about five times greater than most other soft tissues in the thorax. This resistivity increases considerably with inspiration as the alveoli swell and electrical currents have to flow around them. By imaging this change in resistivity, the distribution of ventilation can be seen. A review of the experimental and clinical application of EIT imaging for lung was published by Frerichs (Frerichs 2000). The

research in Sheffield shows that EIT pulmonary measurement can be applied to both adults and neonates (Eyuboglu, Brown et al. 1989; Brown, Barber et al. 1994; Brown, Primhak et al. 2002a; Brown, Primhak et al. 2002b).

Breast tumours

Early detection and treatment of breast tumours increases the survival rate amongst women who develop breast cancers. Because the electrical properties of tumour cells, particularly malignant ones, are very different to the surrounding normal tissue (Joines, Zhang et al. 1994), several EIT groups have been developing EIT systems that could be used to image breast tumours and cysts. A EIT research group in Moscow has produced 3D tomographic images of *in vivo* breast tissue amongst women with different hormonal status using a circular grid of 256 electrodes (Cherepenin, Karpov et al. 2002; Kerner, Paulsen et al. 2002). The EIT group at Dartmouth College has developed a multi-frequency EIT system for breast imaging (Soni, Hartov et al. 2004).

Brain function

In brain EIT imaging, functional impedance changes with time may occur through three main mechanisms: a) cells outrun their energy supply and swell, which cause tissue impedance rises by tens of percent over minutes (Holder 1992a; Holder 1992b); b) blood volume and flow increase during normal functional activity, which decrease the local brain impedance by a few percent over minutes (Adey, Kado et al. 1962; Tidswell, Gibson et al. 2001a; Tidswell, Gibson et al. 2001b); c) during neuronal depolarisation, ion channels open in the dendritic membrane causing its resistance to decrease a few percent over tens of milliseconds (Liston 2004).

Unfortunately, EIT imaging of brain function is obviously challenged by the low conductivity of the skull, since much of the current is shunted through the scalp and does not enter the brain compartment (Rush and Driscoll 1969; Malmivuo and Plonsey 1995).

The EIT research group in UCL (University College of London) has been addressing this problem over the past decade: one of the significant progresses having been made is using diametric excitation, which means the current injecting electrodes need to be diametrically opposed to each other across the head, instead of adjacent excitation, where the current is injected through two adjacent electrodes. The sensitivity of the diametric excitation is approximately 100 times more than that of the adjacent excitation (Bayford, Boone et al. 1996). To date, studies have applied EIT to measure functional brain activity during strokes (Holder 1992a; Clay and Ferree 2002), cortical spreading depression (Holder 1992b; Boone, Lewis et al. 1994), visual evoked responses (Holder, Rao et al. 1996; Tidswell, Gibson et al. 2001b; Ahadzi, Gilad et al. 2004) and epilepsy (Rao, Gibson et al. 1997; Fabrizi, Sparkes et al. 2004).

1.1.2.5 Advantages and Disadvantages of EIT Imaging

EIT imaging has several advantages over other current medical imaging methods:

- It is relatively cheap. The Sheffield Mk 3.5 system costs around £15,000.
- It is safe. EIT provides a non-invasive method to probe the body using non-ionising radiation. There are no known hazards attached to its use. Therefore, it is possible for long-term monitoring of physiological function with EIT.
- It is relatively portable and allows use at the bedside.
- It has good temporal resolution. For instance, the UCLH Mk1b EIT system can take more than 600 measurements per second, which corresponds to about 3 images a second using 31 electrodes and 258 electrode combinations (Yerworth, Bayford et al. 2002). Furthermore, EIT can, in principle, record thousands of images per second. Because neuronal depolarisations, which underlie all mental processes, last only a few milliseconds, EIT is probably the only existing imaging technique with the potential to image these events directly.
- It images the electrical properties of tissue that are not provided by other medical imaging techniques.

The main disadvantage of EIT is its poor spatial resolution. This problem is related to the number of electrodes used (Seagar, Barber et al. 1987). However, it is not a case of simply increasing the number of electrodes to overcome this problem. This is due to the practical difficulties of applying large numbers of electrodes to the body, the associated complexity of the electronics which can accurately measure signals with large dynamic range, and the computational difficulties of processing vast quantities of data.

The description in section 1.1.1 and 1.1.2 reveals that different medical imaging methods are based on separate physical interactions of energy with biological tissues and thus provide measurements of different physical properties of biological structures or functions. Different imaging approaches have different advantages and disadvantages, and so have particular application areas in medicine. It is possible that two (or more) tissues similar in one physical property may well differ widely in another. So almost without exception, new imaging techniques always come to be regarded as complementary rather than replacing existing ones. It is quite reasonable that all these imaging modalities exist together in one health centre. As a conclusion, table 1.2 outlines some of the main characteristics of the imaging approaches.

Table 1.2: Summary of medical imaging methods

Method	Anatomical/ Functional	Spatial Resolution	Temporal Resolution	Ionising Radiation	Portable	Cost*
X-ray	anatomical	few cm	-	yes	no	1
CT	anatomical	1 mm	-	yes	no	2
MRI	anatomical	1~3 mm	-	no	no	3
Ultrasound	anatomical	0.6 mm	-	no	yes	1
Terahertz	anatomical	200 μm	-	no	no	2
SPECT	functional	9 mm	40 secs	yes	no	2
PET	functional	5 mm	40 secs	yes	no	4
fMRI	functional	2.5 mm	2~5 secs	no	no	3
EEG	functional	few cm	few msecs	no	yes	1
MEG	functional	few cm	few msecs	no	no	3
EIT	functional	few cm	few msecs	no	yes	1

* Because the costs of instrumentation for different imaging methods change according to their type and application, they are rated on a 4-point price scale, where '1' represents the cheapest case and '4' is the most expensive one.

1.1.3 Visualisation of EIT Images

When a current is flowing between two electrodes applied to a body, clearly the flow of that current is three-dimensional. So if a two-dimensional ring of electrodes is applied to an object, the measurements are sensitive to off-plane conductivity variations. Therefore EIT is inherently three-dimensional. In spite of these considerations, for some other reasons, 2D imaging is very common in EIT, particularly in the early stage of EIT research. For 2D EIT imaging, reconstructed results can be displayed as 2D images directly. Presentation of these images is relatively straightforward, and will not be discussed here.

With the development of EIT imaging, especially the progress of reconstruction algorithms, the EIT imaging trend has moved towards 3D in recent years (Goble, Cheney et al. 1992; Metherall, Barber et al. 1996; Vauhkonen, Vauhkonen et al. 1999; Polydorides and Lionheart 2002). Dynamic EIT imaging systems conduct measurements during a time interval, therefore a temporal-spatial EIT dataset, which is 4D, can be reconstructed by using a 3D reconstruction algorithm at each sample time point. Similarly, spectroscopic EIT imaging systems are able to produce 4D image datasets as well. Furthermore, if a spectroscopic EIT imaging system is adopted to examine impedance variation during a time interval, a spectral-temporal-spatial EIT dataset, which is 5D, will be obtained after reconstruction. Visualisation of EIT image datasets with three or more dimensions is more challenging than the two dimensional case. In the following, commonly used visualisation methods for EIT images are mentioned first, then researches on EIT visualisation are reviewed, finally, the challenges of EIT visualisation are summarized.

1.1.3.1 Commonly Used Visualisation Methods for EIT Images

To understand the normally used visualisation methods for EIT images, some typical cases from the EIT literatures are described first.

Case 1: Visualisation of multi-frequency EIT images of breast [From: (Soni, Hartov et al. 2004)]

In this case, the multi-frequency breast EIT images were collected with a single array of 16 electrodes at ten discrete frequencies in the range 10kHz – 1MHz. The electrode array was placed at various planes on the breast during the measurement. The reconstruction results are four-dimensional with three dimensions for space and one dimension for frequency. Some figures are presented in the paper to visualise the results. In the top schematic of those figures, the location and positions of an irregular mass and various planes of data acquisition are illustrated. Below, conductivity and permittivity images corresponding to each imaging plane at the excitation frequency are presented.

Case 2: Visualisation of functional EIT (f-EIT) and absolute EIT (a-EIT) images of lung diseases [From: (Hahn, Just et al. 2006)]

The dataset involved in this case was acquired by applying EIT imaging on four patients with different lung diseases. The measurements were conducted at a rate of 13 frames per second for a period of 60 seconds. Using different reconstructed techniques, a series of f-EIT images and a-EIT images were obtained. The reconstructed f-EIT and a-EIT images are four-dimensional, with three dimensions for space and one dimension for time. To visualise the lung EIT images, the authors presented CT scans of those patients in the left column images in the figure, where areas marked by green dashed lines are expected to be ventilated; areas marked by red dashed lines indicate high air content; areas marked by blue dashed lines correspond to a higher absorption of x-rays due to infiltration. The middle column displays mean f-EIT images, and the right column shows mean a-EIT images with white dashed lines marking the lung areas.

Case 3: Visualisation of EIT images of cardiac activities [From: (Isaacson, Mueller et al. 2006)]

In this case, data corresponding to cardiac activities were collected by placing electrodes of the EIT imaging instrument around the circumference of a human chest, and then reconstructed into a series of 2D cross-section EIT images of the torso. Therefore, the reconstructed dataset is three-dimensional, where one dimension is time and the other two are used to describe a location in the measured plane. Isaacson et al. adopted a sequence of 24 consecutive images to visualise the impedance change during one cardiac cycle. At the same time, a movie view of the sequence images is provided online as another visualisation approach for the dataset.

The above examples reveal that, although EIT datasets may have different dimensions (e.g. in above cases, the EIT datasets are 4D or 3D), they are generally displayed as a series of 2D slices, which is a traditional visualisation method for medical tomography images. The 2D slice display approach is able to illustrate some important information in EIT datasets, while it also has some natural shortcomings, especially when it is adopted to visualise datasets with more than three dimensions. Taking the preceding cases as examples again, in case 1, the displayed figures presented images corresponding to the excitation frequency. If images at ten frequencies are visualised simultaneously, there would be too many small images to be understood properly by the observer. Similarly, in case 2, for each subject, the figure provided only displays the mean f-EIT and a-EIT images at one single cross section instead of the whole series of images at different sections.

Except for the 2D slice display method, some other approaches are also used to enhance the visualisation: In case 1, the ROI (Region of Interest), the location for an irregular mass, is highlighted with black slashes or discrete dots. In case 2, the ROIs are marked out with dashed lines in different colours and anatomical information corresponding to

the EIT imaging area is presented as reference. In case 3, animation is used to reveal impedance change along a time interval.

1.1.3.2 Researches on EIT Visualisation

Visualising multi-dimensional EIT datasets by a series of 2D slices is a relatively simple method. Radiologists usually have some experience of understanding this form of presentation and are able to mentally construct the corresponding 3D situation in the patient's body. This construction largely depends on personal experience, it would be helpful to use some advanced visualisation approach to perform this kind of task automatically. Furthermore, before EIT can be used as a routine tool with patients, it is necessary to develop a convenient visualisation interface for clinical decision making. Nowadays, most researches in EIT field aim to improve EIT reconstruction algorithms and imaging instruments, while some efforts have been given to improve the visualisation of EIT images. In the following, some researches made in the EIT visualisation area are introduced.

EIT volume visualisation in the University of Salford

According to the literature search, Briggs and colleagues from the University of Salford in UK published the first paper specific to EIT visualisation (Briggs, Avis et al. 2000). In the paper, Briggs et al. presented a volumetric visualisation result for a sub-dataset corresponding to one sample time point in a temporal-spatial (4D) EIT dataset. The temporal-spatial dataset represents impedance changes in the brain during visual evoked responses.

Briggs et al. were pioneers for EIT visualisation. However, the visualisation result presented in their paper looks relatively rough. First, the outline of the volumetric

visualisation, which should be head-shaped ideally, looks more like a cylinder. Secondly, it is not easy to identify regions of interest in this view. Finally, Briggs et al. aimed to present a system to visualise EIT dataset volumetrically in real-time, and described that the rendering rates of the system were 1.16 ~ 4.55Hz for every frame and changed according to the rendering methods adopted. Unfortunately, these rates did not include the time needed to reconstruct EIT image data from the measured boundary data, which is a serious bottleneck for real-time EIT imaging systems.

Visualisation features in EIDORS

EIDORS (Electrical Impedance Tomography and Diffuse Optical Tomography Reconstruction Software) is a software suite for image reconstruction in EIT and DOT (Diffuse Optical Tomography). It aims to provide a freely distributable and modifiable software for image reconstruction of electrical or diffuse optical data (Adler and Lionheart 2006). After publications of the first and second version in 2000 and 2002, EIDORS (version 3) moves its attention away from basic reconstruction algorithms, and focuses on issues such as mesh generation, electrode modelling, electrode error detection and visualisation.

Although EIDORS was not developed for EIT visualisation particularly, it still presented some exciting features in visualisation. First, volumetric visualisation is realized based on Matlab to view the FEM (Finite Element Mesh) model and conductivity changes. Secondly, arbitrary two-dimensional slices through a volume can be generated. Finally, EIDORS includes a function to write data into the VTK (Visualisation Toolkit) format, which allows further visualisation using Mayavi (Ramachandran 2003). Mayavi is a general visualisation software developed in Python with using VTK for visualisation support. Mayavi provides various methods, such as, 2D slice, 3D volume rendering, 3D surface rendering, isosurface detection, and animation, to visualise 3D or 4D image datasets.

EITviewer

EITviewer was first mentioned in a short abstract (van Genderingen and Verbunt 2005) in the proceeding of the 6th EIT conference held in London, 2005. EITviewer was developed to be a clinical visualisation tool for thoracic EIT. It includes a region-of-interest analysis function. The authors of EITviewer claimed that "*data can be visualised and adapted easily with a user-friendly interface (in EITviewer)*". Unfortunately, there are no further details about its visualisation approaches or visualisation result demonstrations that have been published in any paper or are available online until the thesis is written.

NIM image display software

NIM image display software was developed by the UCL EIT research group for the visualisation of 4D temporal-spatial EIT dataset. Two main views provided by NIM are *Orthogonal display* and *Time series display*.

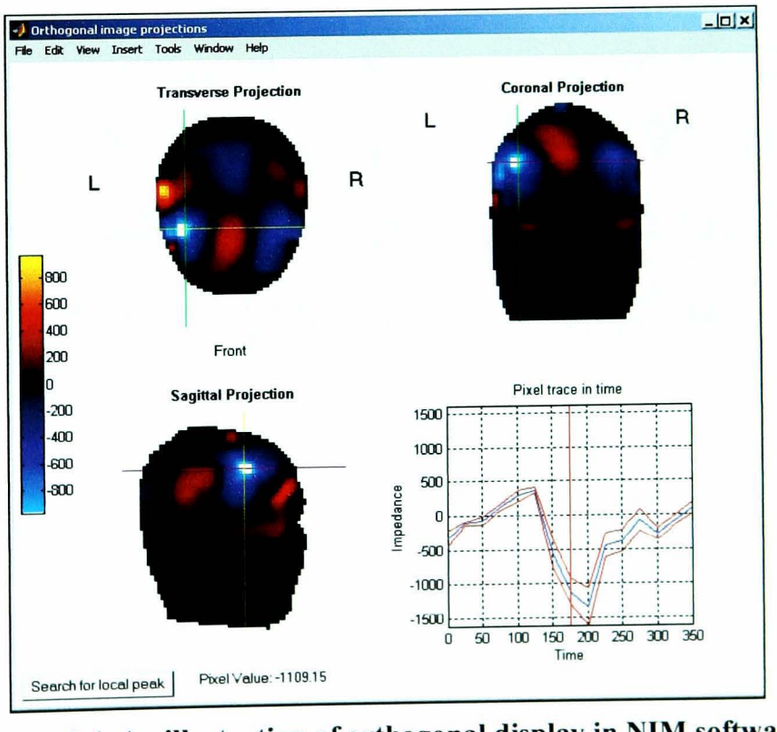

Figure 1.4 An illustration of orthogonal display in NIM software

The orthogonal image viewer displays three orthogonal slices of a temporal-spatial EIT dataset at one sample time point, centred at the point indicated by the cross hairs. The time series of the pixel value at that cross hair is indicated in the pixel profile graph on the lower right of the view. The time point of the image displayed is indicated by a red line on the pixel profile graph. Figure 1.4 is an illustration of the orthogonal display in NIM.

The time series display presents a temporal-spatial dataset as a 2D image matrix. Each column of the matrix, which can be composed of a stack of transverse, coronal, or sagittal image planes, corresponds to a sample time point. Each row of the matrix describes a series of 2D images on a particular plane along the whole sample time period. Figure 1.5 demonstrates a time series display composed of transverse image planes.

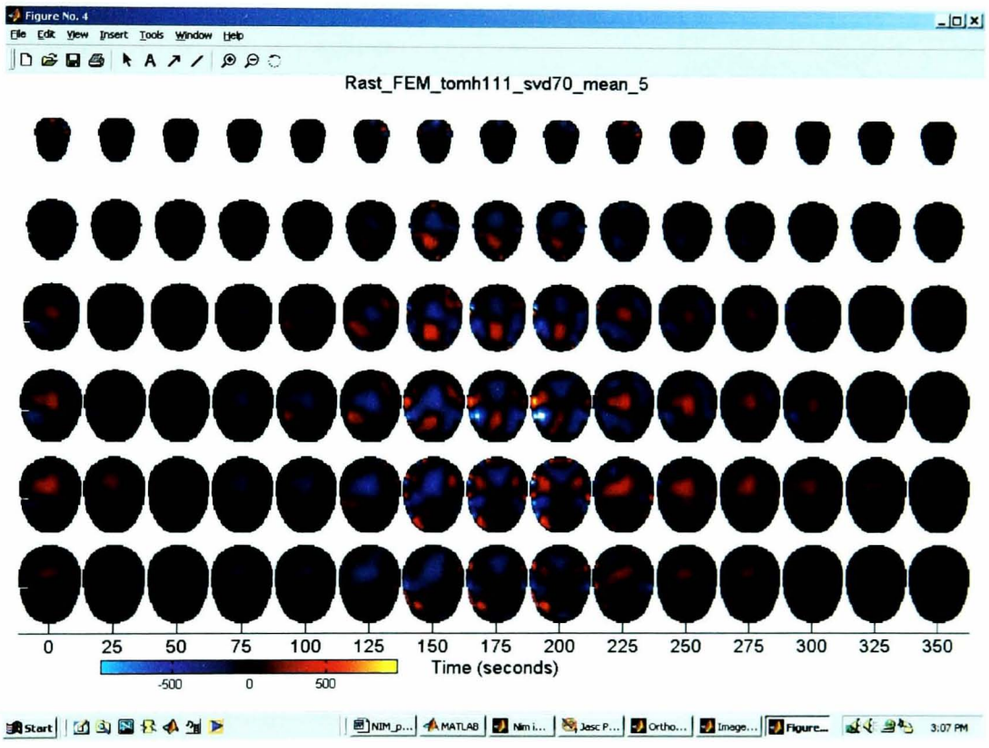

Figure 1.5 A time series display composed of transverse image planes in NIM software

With NIM software, a 4D EIT dataset can be visualised in various ways interactively. It is possible to display the three most significant planes in one view. But the visualisation

approaches provided by NIM are 2D based. Mental effort is necessary to understand the spatial situation included in the dataset.

As a summary, table 1.3 lists the advantages and shortcomings of the research work mentioned above. Each work achieved some progresses and inevitably has some limits. More work needs to be done to improve the visualisation of EIT image datasets. Furthermore, with the development of EIT imaging technology, new challenges are presented for EIT visualisation, as discussed in the next section.

Table 1.3: Summary of previous research work in EIT visualisation

	Dimensions of input dataset	**Progresses**	**Shortcomings**
EIT visualisation in Salford Uni.	4D	First applying volumetric visualisation to EIT images; Real-time visualisation system.	Visualisation results are relatively rough; Excluding image; reconstruction time from the real-time system.
EIDORS	3D	Volumetric visualisation by surface rendering; Arbitrary 2D slicing; Interact with a general visualisation software – Mayavi.	No volume rendering; Specific function is needed for the interaction with Mayavi.
EITviewer	N/A	Region-of-interest analysis; User-friendly interface.	N/A
NIM	4D	Displaying three orthogonal planes in one view; Presenting 4D dataset as a 2D image matrix.	Visualisation methods are 2D based; No volumetric visualisation.

1.1.3.3 Challenges on EIT Visualisation

Visualisation is a tool to prompt EIT research and is necessary for EIT clinical applications. To develop a successful EIT visualisation system, advanced visualisation approaches in computer science must be adopted; currently available visualisation

systems for other medical images should be referred. The most important, special challenges brought up by EIT images must be faced. Three main challenges included in EIT visualisation are described below.

Identification of Regions of Interest (ROI)

Pulletz et al. (Pulletz, Genderingen et al. 2006) pointed out that one of the essential issues in the process of regional lung function evaluation by EIT is to define appropriate Regions of Interest (ROI) within the EIT scan. In fact, as the usability of EIT imaging to other parts of human body has developed, the identification of ROI is essential for all them, not just for lung functional EIT images.

To date, there is only limited data available on the approaches to ROI definition in EIT images, which can be classified into two main types. The first type is based on the calculation of the pixel values (Smallwood, Hampshire et al. 1999; Frerichs, Dudykevych et al. 2001; Frerichs, Bodenstein et al. 2005). The selection of a proper edge criteria value is the key issue for this kind of method: too low values of the edge criterion would make the selected ROIs too large and vice versa. The second kind of method defines ROI as a simple geometrical object (Victorino, Borges et al. 2004; Odenstedt, Lindgren et al. 2005). Pulletz et al. demonstrated that, for ROI definition in lung functional EIT images, the first kind of approach is more convenient than the later one (Pulletz, Genderingen et al. 2006). Nevertheless, defining the ROI suitably is still a challenge for EIT researchers.

Combination of anatomical information with EIT images

Faes et al pointed out that, "*clearly it is not anatomical information that will sell EIT, and therefore we have to sell EIT as the imaging modality of physiological function*" (Faes, Genderingen et al. 2006). However, even EIT aims to be used as a functional

imaging method, and supposing that ROI in EIT images can be identified properly, it would be unacceptable if the anatomical information corresponding to the functional information cannot be seen by the clinicians.

To deal with the absence of anatomical information in EIT images, researchers tried to display a simple structure schematic (as used in case 1 in section 1.1.3.1) or anatomical information obtained by other imaging methods (as adopted in case 2 in section 1.1.3.1) simultaneously with EIT images. Besides these two relatively intuitive methods, more sophisticated approaches are still under development. However, to link anatomical information with functional information included in EIT dataset is another challenge for EIT visualisation.

Visualisation of 5D EIT data

As mentioned at the beginning of section 1.1.3, EIT imaging is able to collect spectral-temporal-spatial data, which is five-dimensional. In the medical image visualisation area, researchers usually process three-dimensional spatial datasets or four-dimensional temporal-spatial datasets. To date, no publication on the visualisation of five-dimensional spectral-temporal-spatial datasets has been found in the literature review. Therefore, handling 5D EIT datasets in a visualisation system is another challenge to be solved.

1.2 Aim and Objectives

The background introduction described above shows that medical imaging technology is progressing continuously: new imaging methods are coming up; traditional imaging modalities are providing more accurate and complex information. As a vital tool for medical research and clinical application, medical image visualisation needs to be

improved simultaneously to keep pace with the development of medical imaging technology. One particular phenomena appearing in medical imaging is that the dimension of the result dataset is increasing. In other words, former medical imaging may produce 2D, or 1D datasets, while information collected by modern medical image approaches generally need 3D, 4D, or even 5D datasets to be processed. How to visualise those multi-dimensional medical image datasets is the research topic of this thesis. It is worth noting that medical images obtained through different imaging modalities, or even collected by the same imaging method but corresponding to different parts of human body, have different features, and different challenges may be presented in the visualisation of different kinds of medical images. Such differences will affect the selection of particular visualisation methods to some extent. The research work mentioned in this thesis is mainly focussed on EIT images of the brain. The aim of this research is to investigate improvements to medical image visualisation, particularly for multi-dimensional medical image datasets. And EIT images of the brain are presented as a demonstration.

In order to fulfil this aim, the following objectives were to be achieved:

- To propose a method to define ROI in functional brain EIT images

- To develop a registration scheme to combine human morphology information obtained by other imaging modality with brain EIT images

- To derive a system development methodology for the visualisation of multi-dimensional medical images, and construct a prototype visualisation system for five-dimensional brain EIT datasets

1.3 Outline of the Thesis

This thesis is composed of six main chapters. The first chapter provides a background introduction and motivation for this research project.

In the second chapter, published literature on visualisation is reviewed from three aspects: first, an overview of visualisation in different applications is presented; then, approaches for medical image visualisation are surveyed; finally, the state of art for exploratory visualisation is mentioned.

The third chapter concentrates on the first objective of this research. That is, by evaluating the feasibility of processing brain EIT data with an existing statistical analysis method, a ROI definition approach is proposed for 4D spatial-temporal brain EIT images. Furthermore, experiments based on simulated and clinical EIT data are described and the experimental results are analysed.

Chapter four details an innovative landmark-based registration scheme to register brain EIT dataset with a standard anatomical brain dataset.

The last objective of this research is fulfilled in chapter five. In detail, a novel task typology model is derived for task exploration, a task-based system development methodology is proposed for the visualisation of multi-dimensional medical image data, and a prototype visualisation system, named EIT5DVis, is developed according to this methodology for the visualisation of 5D brain EIT datasets.

The thesis concludes with chapter six in which this work is assessed, and the final conclusions and suggestions for further research are discussed.

Chapter 2 Literature Review of Visualisation

2.1 Overview of Visualisation

> **Visualise** -- "To form a mental vision, image, or picture of (something not visible or present to the sight, or of an abstraction); to make visible to the mind or imagination." [The Oxford English Dictionary, 1989]

Visualisation has been an efficient way to communicate both abstract and concrete ideas since the dawn of humanity. The first application of visualisation can be traced back to cave painting in prehistoric times. Today, we see an increasing and diverse application of visualisation ranging from more traditional areas such as geography, medicine and weather to more recent and exotic areas such as bioinformatics and Web visualisation. In this thesis, visualisation just refers to *computer visualisation*, which may be the most important development for the visualisation field ever, if no other explanation is given.

According to the importance of displaying a physical "thing", visualisation can be divided into two classes: *information visualisation* and *scientific visualisation*. Information visualisation tends to deal with abstract quantities such as football scores, electrical voltages, fluctuating exchange rates. These quantities relate to real things, but there is little to be gained, for example, by displaying pictures of pound notes when trying to communicate fast changing exchange rates to a currency dealer. In scientific

visualisation what is seen primarily relates to, and represents visually, something "physical". Thus, the flow of water in a pipe, the nature of the weather in a mountain area, and the physiological change in a body are usually – and usefully – displayed directly superimposed on, or at least close to, a realistic representation of the physical thing (Spence 2001). At the same time, there is currently no clear consensus on the boundaries between these two terms of visualisation. Inevitably some overlaps exist between these two. Many visualisation techniques can be applied in both situations. This section will review applications of visualisation in different areas by sorting them into information visualisation and scientific visualisation.

2.1.1 Information Visualisation

Information visualisation can be defined as: "*the use of computer-supported, interactive, visual representations of abstract data to amplify cognition*" (Card, Mackinlay et al. 1999). The main design challenge in information visualisation is the mapping of complex, non-spatial, abstract data onto cognitively useful forms. Software visualisation, network visualisation, and bioinformatics visualisation, are three typical information visualisations.

2.1.1.1 Software Visualisation

Software visualisation is defined as the use of the crafts of typography, graphic design, animation, and cinematography with modern human-computer interaction technology to facilitate both the human understanding and effective use of computer software (Price, Baecker et al. 1993). Software visualisation techniques are widely used in the areas of software maintenance, reverse engineering, and re-engineering, where typically large amounts of complex data need to be understood and a high degree of interaction between software engineers and automatic analyses is required.

In creating a software visualisation tool, several inherent tasks are present, which mainly include: data collection, data analysis, storage of both raw and processed data, and data display (Kraemer and Stasko 1993). A number of display facilities have been associated with debugging tools, performance evolution tools, and program visualisation systems. These include: program graphs, communication graphs, statistical displays, memory access displays, bar-scope views, XY plots, application-specific and abstract displays.

2.1.1.2 Network Visualisation

Network information visualisation involves gaining insight into the network structure and understanding the users' behaviour patterns. With the explosive growth of the Internet, network structure visualisation efforts focus on visualising the global network topology of the entire Web. With the goal of "understanding the organization," these efforts visualise the connectivity of major traffic servers around the world. In the past decade, some researchers have explored visualisation methods to help understand usage data and identify major traffic patterns. To some extend, understanding the users' behaviour patterns is more important than understanding the Web's structure (Chi 2002).

A network consists of hierarchical nodes and links, where a node represents a data point, and a link represents a relationship between two nodes. Much of the work done in network visualisation came about from graph drawing. Most interface representations include two-dimensional or three-dimensional node-and-link diagrams:. Some visualisation techniques add animation, distortion, and a tightly-coupled overview window to reveal even more information about a network.

2.1.1.3 Bioinformatics Visualisation

Bioinformatics is a newly emerging interdisciplinary research area which aims to exploit information technology in biological data analysis. With the data explosion in biology, especially as the genome sequencing projects proceed, scientists have gained access to tremendous amounts of biological information. Due to the difficulties inherent in understanding large quantities of data, information visualisation techniques have become an attractive option for the field of bioinformatics. Using information visualisation, researchers can see experimental results more clearly than by simply viewing raw numbers.

Bioinformatics visualisations generally should provide biologists with data overviews, followed by the ability to study Regions of Interest (ROI) in detail, within the context of the overall data set and to highlight patterns within the data (Dadzie and Burger 2005). A number of visualisation methods and techniques already exist for complex data analysis, both within and outside of the field of bioinformatics, including 2D and 3D scatter plots, parallel coordinates, 2D and 3D hierarchical graphs, information maps, and physical space metaphors such as rooms, windows and desktops. Hyperbolic or fish-eye views aid detailed study of ROI especially in large data sets.

2.1.2 Scientific Visualisation

Scientific visualisation is typically constructed from measured or simulated data representing objects or concepts associated with phenomena from the physical world. As such, the data and, hence, its derived visual representations represent objects that exist in a 1D (one-dimensional), 2D, or 3D object space. Scientific visualisation strives to display measurements of physical quantities so the underlying physical phenomena can be interpreted accurately, quickly, and without bias. In the following sections, geographic visualisation and flow visualisation are mentioned as two examples of

scientific visualisation. In a later section, medical visualisation, which is the core of this thesis and one of the most important domains for scientific visualisation, is detailed.

2.1.2.1 Geographic Visualisation

Geographic Visualisation (GVis), sometimes called cartographic visualisation, integrates principles from cartography, geographic information systems (GIS), and Exploratory Data Analysis (EDA) in the development and assessment of visual methods that facilitate the exploration, analysis, synthesis, and presentation of geo-referenced information.

The goal of cartographic visualisation is the understanding of spatial information and knowledge through interactive visual display. Researchers have developed numerous recommendations and software tools to enhance geographic visualisation, which can be categorized as query, re-expression, multiple views, linked views, animation, and dimensionality (Kraak 1999).

2.1.2.2 Flow Visualisation

In fluid dynamics, it is critically important to see the patterns produced by flowing fluids. While most fluids (air, water, etc.) are transparent, their flow patterns are invisible without using some special methods. Flow visualisation is the art of making these patterns visible. Flow visualisation has always been a significant area of scientific data visualisation; it has also been one of the most challenging areas, especially when looking at volumetric data.

Three different approaches are widely used in flow visualisation (Laramee, Weiskopf et al. 2004): *Direct flow visualisation*: This category of techniques uses a translation that is

as direct as possible for representing flow data in the resulting visualisation. The result is an overall picture of the flow. Common approaches are drawing arrows or colour coding for velocity. *Geometric flow visualisation*: These approaches often first integrate the flow data and use geometric objects in the resulting visualisation. The objects have a geometry that reflects the properties of the flow. Examples include streamlines, streaklines, and timelines. Not all geometric objects are based on integration. Another useful geometric approach is generating isosurfaces, e.g., with respect to an isovalue of pressure or magnitude of velocity. *Dense, texture-based flow visualisation*: A texture is computed that is used to generate a dense representation of the flow. A notion of where the flow moves is incorporated through co-related texture values along the vector field. In most cases this effect is achieved through filtering of texels according to the local flow vector. Texture-based methods offer a dense representation of the flow with complete coverage of the vector field.

In conclusion, this section reviewed visualisation applications in some typical areas by classifying them into two types. Visualisation researchers meet different challenges related to the natural features of different application fields. Each field has its own suitable visualisation approach. At the same time, many visualisation methods can be adopted in more than one field. Medical visualisation is a very important domain in scientific visualisation. The research presented in this thesis is a specific project in this domain. Therefore, a more detailed literature review on medical image visualisation follows in the next section.

2.2 Approaches for Medical Image Visualisation

The practice of medicine has always relied upon visualisations to study the relationship of anatomic structure to biologic function and to detect and treat disease and trauma that disturb or threaten normal life processes (Robb 2000). Traditionally, these visualisations

have either been direct, via surgery or biopsy, or indirect, requiring extensive mental reconstruction. With the development of medical imaging methods, imaging has become an essential component in medical research and clinical practice. For example, virologists generate 3D reconstructions of viruses from micrographs, radiologists identify and quantify tumours from MRI and CT scans, and neuroscientists can detect regional metabolic brain activity from PET and fMRI scans. Analysis of these diverse image types requires advanced visualisation tools.

A variety of methods have been developed for image visualisation. Most of them are transferable between different application areas, and may also be applied to the special case of medical images. From different perspectives, visualisation in medicine can be divided into different catalogues. For example, Solaiyappan grouped them into three classes: illustrative visualisation, investigative visualisation, and imitative visualisation (Solaiyappan 2000). This section reviews approaches for medical image visualisation based on dimensions of datasets involved in the process.

2.2.1 Terminology

As Wong and Bergeron mentioned in their survey of Multi-Dimensional Multi-variate Visualisation (MDMV), the MDMV literature suffers from ill-defined and inconsistent terminology, the term *dimensionality* is especially overloaded (Wong and Bergeron 1997). A similar situation exists in medical image visualisation, therefore a clarification of the terminologies used in this thesis is presented.

Dimension and Variate

To define the dimension and variate of a medical image dataset, a functional view of the data structure is adopted. A function is a relation between two or more variables such that the values of some variables, which are dependant variables, are dependent on,

determined by, or correspond to values of the other variables, which are independent variables. An image dataset can be divided into two conceptually different parts: one part defines the context in which the data is obtained, while the other part represents results of measurements, observations, calculations, etc. obtained in that context. From the functional view, the image dataset structure can be presented as:

$$(s_1, s_2, \cdots, s_m) = f(x_1, x_2, \cdots, x_n) \tag{2.1}$$

Where $x_1, x_2, \cdots, x_n$ are independent variables, which define the measurement context in the dataset; n is the number of independent variables.

$s_1, s_2, \cdots, s_m$ are dependent variables, which present measurement results in the dataset; m is the number of dependent variables.

f is a data function, which describes the correspondence between measurement context and results.

In this thesis, the *dimension* of an image dataset is defined as the number of independent variables in the dataset, and dependant variables included in the dataset are termed as *variates*.

Multi-dimensional & Multi-variate

The prefix, 'multi', is frequently interchanged with another prefix, 'hyper'. In statistics literatures, the prefix multi means two or more, indicating a natural breakpoint between one and two dimensions in probabilistic methods. For the breakpoint between three and four (or beyond), sometimes the prefix hyper is used, and sometimes the prefix multi is adopted. In this thesis, the expression multi-dimensional is chosen to refer to dimensionality of four or more. Datasets with four or more dimensions are multi-dimensional datasets correspondingly. While, the term multi-variate is defined as more than one variate, the dataset having two or more variates is a multi-variate dataset.

After the terminology definition, the following sections will review approaches for medical image visualisation by classifying them into four categories according to the number of dimensions and variates of the processed dataset. These are one-, two-, or three-dimensional, and multi-dimensional and multi-variate.

2.2.2 One-dimensional Visualisation

An one-dimensional (1D) medical image dataset can be described as:

$$s = f(x) \tag{2.2}$$

where s represents imaging results, x stands for the only independent variable to define the measurement context, which is usually time.

The commonest visualisation form for a one-dimensional image dataset is to present it as a waveform, which can be seen on such devices as ECG (Electrocardiogram) monitors and EEG (Electroencephalography) equipments. This form of visualisation is quite elementary, while it is a convenient and powerful tool for conveying the physiological property of the subject. By observing these waveforms, clinicians can rapidly understand the present state of the subject and possibly deduce the trend condition during a clinical intervention. These early developments obviously indicated the potential benefits of visualisation in medicine.

2.2.3 Two-dimensional Visualisation

A two-dimensional (2D) image dataset can be presented as:

$$s = f(x, y) \tag{2.3}$$

where s stands for the imaging results, x, y are two independent variables to define measurement context, which are commonly two orthogonal coordinates in Cartesian space and used as pixel positions in visualisation.

Although modern X-ray imaging is able to provide images in three-dimensions, the emergence of X-ray imaging once announced the arrival of two-dimensional medical image datasets. It is easy to display two dimensional medical datasets on a piece of paper or a monitor screen. Approaches have been developed to enhance image features that otherwise may have been ignored. In the following, three typical examples of those approaches, which are interpolation, 2D contours detection, and 2D texture mapping, are reviewed.

In medical images, the number of pixels might vary according to imaging modality, and it is usually in the range of 128×128 to 512×512. The resolution of computer displays is usually high, above 72 pixels/inch. If viewing the measurement results directly on the screen, the displayed images will be relatively small. To enlarge these images to a proper display size, different interpolation techniques are developed. Interpolation is able to create a continuous presentation of discrete image data. Commonly used interpolation approaches include nearest-neighbour interpolation, linear interpolation, B-splines interpolation, and sinc interpolation.

Manipulation of an entire 2D image appears to be a cumbersome approach when the feature of interest could be delineated through contour lines. Both manual and automatic techniques were developed to define contours. Contour detection algorithms work either in the spatial or frequency domain of an image. Examples of spatial filters for contour detection include the Roberts' Cross (Roberts 1965), Sobel filter (Sobel 1970), Prewitt filter (Prewitt 1970), and Canny filter (Canny 1983; Canny 1986). Frequency domain filters include the ideal high pass filter and the high pass Butterworth filter (Fisher, Perkins et al. 1996).

Texture mapping is a concept introduced in computer graphics for providing high visual realism in a scene (Haeberli and Segal 1993). An image (the texture) is added (mapped)

to a shape in the scene, like a decal pasted to a flat surface. This reduces the amount of computing needed to create the realistic effects when each time the elements appear in the scene. The way the resulting pixels on the screen are calculated from the texels (texture pixels) is governed by texture filtering. In medical image visualisation field, texture mapping contributes to realism and speed.

2.2.4 Three-dimensional Visualisation

A three-dimensional (3D), or volumetric, image dataset can be described as:

$$s = f(x, y, z) \tag{2.4}$$

where s represents imaging results; x, y, z are three independent variables to define measurement context, which are usually three orthogonal coordinates in Cartesian space and are able to be used as voxel positions in visualisation.

Modern anatomical medical imaging methods generally produce three-dimensional datasets. With the constant improvement to imaging instrumentations, medical imaging resolution can be quite high, which consequently makes the size of volumetric dataset very large. Another important factor in the development of three-dimensional visualisation is that the data has one dimension more than the computer display. Visualising three-dimensional medical datasets efficiently has been an active research area for many years. Different techniques have been developed, which can be classified into two main categories: 2D display and 3D rendering.

3D rendering of volumetric medical datasets can be further divided into different types from different perspectives. It can be classified as *indirect* and *direct* methods (Csebfalvi 2001): for indirect volume rendering, there is a preprocessing step to convert the dataset to an intermediate representation, such as a surface model or a presentation in another domain; direct volume rendering methods process the dataset without generating any intermediate representation and assigning optical properties directly to the voxels in

spatial domain. 3D rendering approaches can also be grouped into another two types: *surface rendering* and *volume rendering* (Kaufman 2000; Tian, Bao et al. 2003): surface rendering techniques construct surfaces in the dataset first and then render these surfaces into displayable images; volume rendering techniques display the volumetric data sets in their entirety. In this review, the later classification is adopted.

In the following, 2D display for 3D datasets is mentioned first. Then surface rendering techniques are introduced. Next, volume rendering methods are described. Finally, a comparison between surface rendering and volume rendering for volumetric visualisation is conducted.

2.2.4.1 2D Image Generation and Display

A three-dimensional medical image dataset can be obtained by either imaging a series of cross sections or a 3D reconstruction from measurements. Traditionally, radiologists check 2D tomography images on a light box. It is natural to adopt this light box viewing method to 3D dataset before volume visualisation is available. Even in an innovative visualisation system, 2D slice presentation is still a necessary feature, because there are many situations in which identification, generation, and display of the optimal image plane are critical.

2D image generation and display techniques aim to avoid the structure positioning and scanner orientation restrictions of most imaging systems and present important features in a clear, unrestricted view. Descriptions of three types of 2D image generation approaches, orthogonal sectioning, oblique sectioning and curved sectioning follows.

Orthogonal sectioning

The 3D nature of volumetric dataset, when isotropic, allows for simple and efficient computation of images that lie along the non-acquired orthogonal orientation of the volume (Glenn, Johnston et al. 1975). For example, in CT imaging, transverse images are reconstructed directly after measurement, coronal or sagittal images can be displayed by orthogonal sectioning after some processing, such as deconvolution, to the dataset.

Oblique sectioning

A desired 2D image may not be parallel to an orthogonal orientation in which the 3D volume image was acquired, but is more likely to lie along an arbitrarily orientated plane at some oblique angle to the orthogonal axes of the volume image (Robb 1999). Although geometric principles describing planes oblique to an orthogonal image data set are well understood, the specification of the orientation and efficient generation of the oblique image in volumetric image dataset require additional visualisation and computation techniques (Rhodes, Glenn et al. 1980; Bates, Hanson et al. 1998).

Curved sectioning

It is quite often in medical image dataset that objects of interest may have curvilinear morphology and not located entirely within a single plane, and orthogonal or oblique sectioning cannot capture them in a single 2D image. This restriction can be overcome using curved sectioning techniques (Robb 1999; Kanitsar, Fleischmann et al. 2002). With this technique, a trace along an arbitrary path defines a set of pixels that have a corresponding row of voxels through the volume image. Each row of voxels for each pixel on the trace can be displayed as a line of a new image, which corresponds to the curved planar structure lying along the trace. The curved plane can be viewed through projection, stretching and straightening (Kanitsar, Fleischmann et al. 2002).

2.2.4.2 Surface Rendering

In the 1980s, no rendering techniques were available for the visualisation of volumetric data directly. The existing computer graphics methods, like ray tracing or z-buffering, had been developed for geometrical models rather than for volume data sets. Therefore, there was a need to convert the volume defined in a discrete space into a geometrical representation and rendering it with methods developed in computer graphics domain. This approach is called surface rendering.

The key step in surface rendering is to construct surfaces in a volume. Early surface reconstruction methods were based on the traditional image-processing techniques, such as edge detection and contour connection (Artzy, Frieder et al. 1980; Udupa 1982). The most important milestone in this research direction was the marching cubes algorithm (Lorensen and Cline 1987). In the following, the main algorithms for surface reconstruction in volume data are introduced.

Contour connection

Before the introduction of isosurface techniques, contour connection approaches were widely used in visualisation of volumetric dataset. In a semiautomatic or manual method the contours of structures of interest were identified on single slices first. Geometrical algorithms were then used to connect the contours of adjacent slices in order to form a closed surface (Meyers, Skinner et al. 1992; Arvo and Novins 1994; Meyers 1994). Enhancements to this technique include the generation of meshes with more or less uniformly shaped triangles, which could be reduced in size (and detail) by standard mesh reduction algorithms (Fuchs, Kedem et al. 1977). The major problem of this kind of surfacing technique was the handling of branches in the objects' structures (Shantz 1981).

Marching cubes

The *Marching Cubes* technique (Lorensen and Cline 1987) is the best established isosurface extraction approach. It is called "marching cubes" because it marches through all the cubic cells and generates a local triangular mesh inside those cells which are intersected by an isosurface. This algorithm does not rely on image processing performed on the slices and requires only one parameter, a density threshold, to define the isosurface.

The marching cubes algorithm provides a fast and easy way to get a high-resolution 3D surface from serial sections up to a complete 3D object. However, it is computationally expensive. This time consuming process motivated researchers to come up with acceleration strategies (Wilhelms and Gelder 1992; Itoh and Koyamada 1994; Montani, Scateni et al. 1994a; Livnat, Shen et al. 1996; Li and Agathoklis 1998; Delibasis, Matsopoulos et al. 1999). Furthermore the number of triangles produced by the method in a typical set of volume image data is very high, the decimation of triangle number was another problem (Shekhar, Fayyad et al. 1996). The original marching cubes technique suffered from the problem of ambiguities in the surface construction scheme, which would result in holes in the extracted surfaces. Further research work has been done to correct this problem (Nielson and Hamann 1991; Matveyev 1994; Montani, Scateni et al. 1994b).

Dividing cubes

Dividing cubes algorithm, which is also developed by Cline and Lorensen (Cline, Lorensen et al. 1986), is a variation of marching cubes algorithm. As the resolution of the 3D medical data increases, the number of triangles generated with the marching cubes algorithm approaches the number of pixels in the displayed image. The dividing cubes algorithm eliminates the scan conversion step and approximates the polygons with points.

Surface producing for noisy data

Isosurface extraction works very successfully for volume image data with high signal-to-noise ratio, which allows effective classification of constituent structures. However when the data are noisy or when the structure cannot be segmented well, results of isosurface extraction (e.g. marching cubes) could become unpredictable. Elastic surface approaches were proposed to solve the problems. These surfaces are sometimes called balloons, for their expanding properties, or shrink-wrapping surfaces with elastic properties, or, in general, deformable surface. These techniques usually tend to be computationally intensive because of their iterative steps. "Statistical" surface is another approach that attempt to produce efficient results for noisy data. It employs space partitioning techniques based on local statistical measurements to produce a mean estimated surface within a given error deviation. This technique may not preserve the topology connectivity that deformable techniques could provide.

2.2.4.3 Volume Rendering

Volume rendering methods provide direct visualisation of volume images without the need for prior surface construction or object segmentation, and preserving the values and context of the original image data. The optical attributes like color, opacity, or emission are assigned directly to the voxels. The pixel colours in the displayed image depend on the optical properties of the voxels intersected by corresponding viewing rays.

Volume rendering can be achieved using an *image-order*, an *object-order*, or a *domain-based* technique. The image-order methods produce the image pixel-by-pixel by casting a ray though each pixel and re-sampling the volume along the viewing rays. The object-order methods process the volume voxel-by-voxel by projecting them onto the image plane. The domain-based methods transform spatial volume into an alternative domain first, and a projection is then generated directly from that domain. In the following, typical algorithms included in the three kinds of methods are presented.

2.2.4.3.1 Image-order methods

Image-order volume rendering algorithms, which represent a *backward mapping* scheme. cast rays from each pixel in the image plane through the volume data to determine the final pixel value. They are also called *volume ray casting* techniques and are similar to the common computer graphics polygon- or surface-rendering procedure of *recursive ray tracing*, with the difference that secondary reflection and refraction rays are not spawned. During the process to accumulate all data points along a ray with appropriate weights and to produce an aggregate value that is projected on the viewing plane, different techniques can be adopted. Some of those techniques are mentioned below.

Binary ray casting

The first generation of image-order volume rendering methods were developed for binary volumetric data. One of these techniques, *binary ray casting*, (Tuy and Tuy 1984), detects the first intersection of the ray with data volume, and so can show the outer surface of the data without the need to explicitly perform boundary detection and hidden-surface removal.

Discrete ray casting

Instead of traversing a continuous ray and determining the closest data sample for each step with a zero-order interpolation function, as in the previously mentioned binary ray casting algorithm, a discrete representation of the ray could be traversed, which is referred to as *discrete ray casting* (Yagel, Cohen et al. 1992). In this method, a ray is discretixed into a 6-, 18-, or 26-connected path, which is based upon the three adjacent relationships between consecutive voxels along the path.

Density integral

The purpose of a volume ray casting model is to define the geometry of the rays cast through the volumetric data. To generate the displayed image, the pixel values are assigned appropriate intensities "sampled" by the rays passing everywhere through the scene (volume of data). Different ray functions are used to determine the contribution of a voxel to the final image. One possibility is to calculate each pixel value as the *density integral* of the voxels along the corresponding viewing ray.

Maximum intensity projection

Maximum Intensity Projection (MIP) (Sakas, Grimm et al. 1995) is another method to calculate the pixel intensity. As the name suggests, the maximum intensity value encountered along each ray is projected on the viewing plane. This projection is capable of revealing some internal parts of the data, specifically those with high density, such as blood vessels in MRI data.

Local maximum intensity projection

The main limitation of MIP is that it cannot adequately depict the spatial relationships of overlapping objects. In order to avoid this problem, Sato (Sato, Shiraga et al. 1998) proposed a technique called Local Maximum Intensity Projection (LMIP). Different from MIP, LMIP assigns the first local maximum, which is above a predefined threshold, along the corresponding viewing ray to each pixel.

Acceleration techniques for volume ray casting

Volume ray casting is able to generate images of high quality, while sampling data volume along the viewing rays at equidistant locations is computationally expensive. Several acceleration techniques have been proposed in order to speed up the process. Some approaches are exploiting the fact, that there are regions in the volume data set

that do not contribute to the final image (Yagel and Shi 1993; Sramek and Kaufman 2000). Other approaches try to optimize the method viewing rays are sampled, either by taking the final image into account, or by using adaptive sampling strategies (Kreeger, Bitter et al. 1998; Ogata, Ohkami et al. 1998; Wan, Kaufman et al. 1999). Also the way, viewing rays are traversed through data volume are subject to acceleration approaches (Yagel and Kaufman 1992; Law and Yagel 1996). Although these acceleration techniques yield a significant reduction in rendering times, volume ray casting (without a tradeoff in image quality) is far from being an interactive technique.

2.2.4.3.2 *Object-order methods*

Different from image-order algorithms, object-order volume rendering methods represent a *forward mapping* scheme. Here each voxel in the volume is processed to determine its contribution to the final image. In its simplest form, an object-order algorithm loops through the volume data, projecting each voxel onto the image plane. There are two orders in which the volume is traversed: *back-to-front* or *front-to-back.* According to back-to-front projection, if two voxels project to the same pixel on the image plane, the first processed voxel must be farther away from the image plane than the second one. In front-to-back methods, voxels are traversed in the order of increasing distance from the image plane. The first object-order methods, similarly to the early image-order methods, aimed to render binary volumes. More sophisticated object-order methods are not restricted to the rendering of binary volumes. In the following, two typical object-order volume rendering approaches: splatting algorithm and sheer warp factorization methods, are described.

Splatting algorithm

The splatting algorithm (Westover 1990) computes the contribution of a voxel, in volume data, to a displayed image by a process called *splatting*. The splatting process

convolves a voxel with a filter that distributes the voxel's value to a neighbourhood of pixels (Westover 1989). The final displayed images are composed by accumulating "splatted" footprints of voxels on the image plane.

The splatting approach supports incremental rendering in back-to-front or front-to-back order. In principle, the splatting algorithm can achieve the same image quality as a ray caster provides. The advantages of splatting over ray casting are twofold: first, ray casting requires access to volume voxels along the viewing ray, while splatting algorithm traverses voxels sequentially in the same order as they are stored in memory, so the cache coherency is exploited; secondly, with splatting, smooth surfaces can be rendered without staircase artefacts, unlike the case of ray casting. The main drawback of splatting comparing with ray casting is that, images generated by splatting are blurred, while sharp object boundaries can be reserved with ray casting.

It has been showed that the splatting algorithm can be optimized by using strategies such as sparse data sets, (Laur and Hanrahan 1991; Mueller and Yagel 1996; Huang, Mueller et al. 2000; Orchard and Möller 2001). Further researches on splatting techniques are focused on the reduction of aliasing artefacts, (Swan, Mueller et al. 1997; Mueller, Moller et al. 1998) and the improvement of the visual quality of images (Mueller, Moller et al. 1999).

Shear warp factorization method

The shear warp factorization method was introduced by Philippe Lacroute and Marc Levoy (Lacroute and Levoy 1994). This object-order volume rendering approach aimed to avoid the expensive computation of ray-casting algorithms and achieve some advantages involved in image-order methods. In this technique, the voxels are rearranged such that the nearest face of the volume becomes axis aligned with an off-screen image buffer with a fixed scale of voxels to pixels (shearing of the volume data set). The volume is then rendered into this buffer using the far more favorable memory

alignment, fixed scaling and blending factors. Once all slices of the volume have been rendered, the buffer is then warped into the desired orientation and scale in the displayed image (warping the image).

Shear warp rendering is capable of generating images of reasonably sized data volumes at interactive frame rates, but at the cost of less accurate sampling and potentially worse image quality compared to ray casting. To further speed up the rendering, several acceleration techniques have been developed, such as, parallel rendering approaches (Lacroute 1996; Jiang and Singh 1997; Schulze and Lang 2002), and optimized sparse data representations (Csébfalvi 1999).

2.2.4.3.3 Domain-order methods

Traditionally, displayed images for volume datasets are rendered in the spatial domain. Volumetric datasets can also be transformed into an alternative domain and rendered from that domain. This kind of approach belongs to domain-order volume rendering, which generally includes frequency domain, compression domain, and wavelet domain volume rendering.

Frequency domain volume rendering

Frequency domain Volume Rendering (FVR) was first proposed by Levoy and Malzbender (Levoy 1992; Malzbender 1993). The motivation for FVR is that the Fourier Projection-Slice Theorem allows 2D projections of 3D data sets to be generated using only a 2D slice of the data in the frequency domain Although the calculation of the 3D Fourier transform is very time-demanding, it has to be performed only once in a preprocessing step. Afterwards, an arbitrary projection of the volume can be generated by a relatively cheap 2D inverse Fourier transformation of a single slice. This inverse transformation can be rapidly executed even on low-end hardware. In the final image,

each pixel contains the density integral along the corresponding viewing ray, thus FVR can be considered as an X-ray simulation.

FVR reduces the rendering complexity from $O(N^3)$, which ordinary volume rendering methods usually have, to $O(N^2 \log N)$ for a volume of size N^3. The main drawback of this approach is the lack of depth information, since for the calculation of density integrals, a distance-dependent weighting function or an opacity manipulation cannot be used. An algorithm had been presented to replace much of the missing depth and shape indications by performing shading calculations in the frequency domain during slice extraction (Totsuka and Levoy 1993), but the images generated by FVR are still not comparable with those generated by spatial domain based methods.

Compression domain volume rendering

Considering the large amount of volume data, compression methods are usually applied to improve the efficiency. There are four possible approaches to integrate visualisation and compression: decompression before rendering, on-the-fly rendering during decompression, on-the-fly decompression during rendering, and rendering in the compression domain (Yang 2000). Compression domain rendering approaches perform volume rendering from compressed data without decompressing the entire data set, and therefore reduces the storage, computation, and transmission overhead of otherwise large volume data.

One of the first compression domain volume rendering was presented by Ning and Hesselink (Ning and Hesselink 1992; Ning and Hesselink 1993). Later progress in this field include dividing volume data into subcubes and replacing discrete cosine transform used in the JPEG still image compression algorithm with discrete Fourier transform (Avila, He et al. 1994; Chiueh, Yang et al. 1997). The subcube-based scheme not only achieves higher compression efficiency by exploiting local coherency, but also improves

the quality of resultant rendered images because it approximates the occlusion effect on a subcube by subcube basis.

Wavelet domain volume rendering

A wavelet is a fast-decaying function with zero averaging. The attractive features of wavelets are that they have local property in both spatial and frequency domains, and can be used to fully represent volumes with a small number of wavelet coefficients.

The first application of wavelet to volume rendering was presented by Muraki (Muraki 1993). In Muraki's algorithm, the volume dataset is transformed into a wavelet expression by using a decreasing 3D orthogonal wavelet. The main shortcoming of this approach is that the rendering speed of the wavelet expression data is slow. Westermann (Westermann 1994) introduced a method for the approximation of volume rendering integrals by taking advantage of the sparse representation of a signal projected into a wavelet basis, and suggested that the choice of "right" basis function would give the best trade-off between rendering time and compression rate. Gross and Lippert (Gross, Lippert et al. 1995; Gross, Lippert et al. 1997) described approximate solutions of the low–albedo volume rendering equation in wavelet spaces and introduced two methods for wavelet domain rendering of volume data sets. Horbelt (Horbelt, Unser et al. 1999) further extended Gross's volume wavelet rendering methods by computing splats via an orthogonal projection operator. Yu and Chang (Yu, Chang et al. 2004; Yu, Chang et al. 2005) presented a fast rendering algorithm for foveated volumes by processing it directly in the wavelet domain.

As a summary, the hierarchy of approaches mentioned in this section is presented in figure 2.1. In the next section, a comparison between the two 3D rendering methods: surface rendering and volume rendering, is conducted.

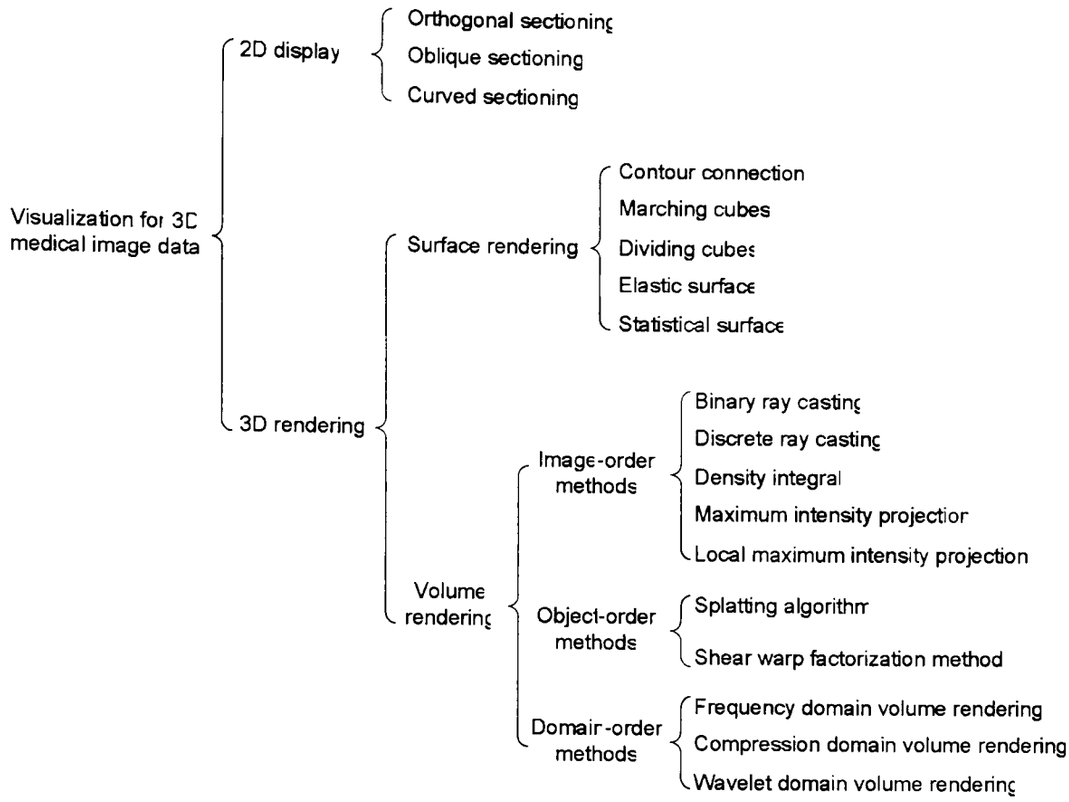

Figure 2.1 Hierarchy scheme of visualisation methods for 3D medical image data

2.2.4.4 Comparison of Surface Rendering and Volume Rendering

In the early stages, surface rendering was commonly used for three-dimensional medical dataset visualisation, but recent advances in hardware and software technology have made it possible to use volume rendering. Both surface rendering and volume rendering have some advantages and disadvantages.

The advantage of surface rendering lies in the relatively small amount of surface data. After the determination of the surface representation, a fast rendering speed and interactive manipulation is available with surface rendering. Standard computer graphics techniques can be applied, including shading models. In addition to the advantages, the following disadvantages are inherent to the surface rendering algorithm. First, the determination of the surface representation is time-consuming and has to be performed each time a threshold is changed. Second, since only a surface representation is used,

much of the information contained within the data is lost during the rendering process. Third, in the case where the anatomical structures of interest cannot be extracted with a unique threshold, surface rendering may be difficult to use.

Volume Rendering retains all of the volume data during rendering, and all acquired voxels may contribute to each rendered image. This provides the capability to section the rendered image and visualise the actual image data in the volume image, and to make voxel value-based measurements for the rendered image. Also, transparency can be assigned to view internal structures or structures in the background, and three-dimensional unambiguous images are obtained with good depth indications. Some disadvantages of volume rendering are; First, volume rendering is computationally expensive, which could result in less interactive rendering. Even on high-end workstations volume rendering is still relatively slow. Second, volume rendering blends the data over a range suitably weighted by a transfer function. However, in its original form, it does not take into account the spatial connectivity between various structures in the data, thus making it sometimes difficult to select a particular structure of interest. Third, determination of the optimal settings is difficult because of the large number of parameters that can be set, possibly leading to over visualisation.

A comparison between the main features of surface rendering and volume rendering is given in table 2.1. In clinical practice, it is the application that determines which rendering method should be applied. For example, Soyer and Heath (Soyer, Heath et al. 1996) indicated that maximum intensity projection appeared to be an satisfactory technique to perform 3D imaging of intrahepatic venous structures with helical CT data when slices 8 mm thick overlapping every 4 mm are used. Hong and Freeny (Hong and Freeny 1999) proposed that 3D volume rendering is superior to MIP and shaded-surface displays in the depiction of pancreaticoduodenal arcades and dorsal pancreatic arteries. Van Ooijen and van Geuns (van Ooijen, van Geuns et al. 2003) demonstrated that volume rendering produces images of higher quality than those produced with surface

rendering for the visualisation of the coronary artery tree. At the same time, Kuszyk and Heath (Kuszyk, Heath et al. 1996) illustrated both volume rendering and surface rendering had some limitations for 3D visualisation of skeletal pathology. Fishman and Ney (Fishman, Ney et al. 2006) emphasized that it is important that radiologists understand when and how each technique should be used.

Table 2.1: Comparison between surface rendering and volume rendering

Features	Surface rendering	Volume rendering
Using surface to present volume data	Yes	No
Retaining the whole volume data during rendering	No	Yes
Rendering speed	Fast	Slow
Supporting standard computer graphics techniques	Yes	No
Transparency can be assigned to view internal structure	No	Yes
Rendered images can be sectioned to present the actual volume data inside	No	Yes
Parameters need to be settled during rendering	Simple	Complex

Rendering methods are continuously progressing. One opinion is that, as the speed and cost of image-processing hardware improve, the relatively rapid processing of surface rendering will become less of an advantage. Hardware-assisted real-time volume rendering and improved segmentation techniques promise to make volume rendering a more practical and widely used tool (Shahidi, Lorensen et al. 1996). Meanwhile, many techniques have been investigated to combine the strengths of surface rendering and volume rendering and reduce their weaknesses. Shell rendering technique is a notable one among them (Udupa and Odhner 1993). Nevertheless, it seems that one particular rendering approach will not replace all others. The future will more likely see an integration of many approaches into one manageable toolbox (Tietjen, Isenberg et al. 2005). Volume rendering will be an important component in the toolbox, but not the only one.

2.2.5 Multi-dimensional and Multi-variate Visualisation

A multi-dimensional and multi-variate (MDMV) image dataset can be presented as:

$$(s_1, s_2, \cdots, s_m) = f(x_1, x_2, \cdots, x_n) \tag{2.5}$$

where $s_1, s_2, \cdots, s_m$ are variates in the dataset, and $m \geq 2$. In the medical imaging domain, the method usually collects one type of physical property associated with biological structures or functions. Consequently, only one variate included in an imaging dataset. Because different imaging approaches provide complementary information, it is common to fuse features from different imaging modalities. Such fused data include more than one variate.

$x_1, x_2, \cdots, x_n$ are independent variables, which compose the dimensions of the dataset, and $n \geq 4$. The four commonest dimensions in a medical dataset are three orthogonal coordinates in Cartesian space and time. Frequency is the other constantly used dimension.

MDMV visualisation techniques can be categorized in different ways. Possible criteria for such a categorization include the type and/or dimensionality of the data, the dimensionality of the visualisation technique, and the goal of the visualisation. In this section, general approaches for MDMV visualisation are introduced, and then visualisation methods for two typical MDMV datasets in medical image field, spatial-temporal datasets and multi-variate datasets, are described.

2.2.5.1 General Approaches for MDMV Visualisation

Various approaches have been developed to visualise MDMV datasets. Some of these techniques attempt to show all dimensions and all variates visually as one display, some try to reduce the dimensionality of the dataset before visualisation, whereas others allow the user to select subsets for display.

2.2.5.1.1 *Approaches show all dimensions and all variates as one display*

This section highlights approaches showing all dimensions and all variates as one display. The advantage of this kind of visualisation is an overview of the dataset can be presented directly. However, if the data size is too big, for the limited size of computer of monitor, results obtained by these methods will be unreadable. Typical approaches belonging to this type include Scatterplot matrix, Hyperbox, Parallel Coordinates, and Grand Tour Methods.

Scatterplot matrix

The scatterplot matrix has been an extensively used MDMV visualisation technique in the statistics community. Assuming an n-dimensional dataset, a scatterplot matrix is an arrangement of $(n^2 - n)/2$ pairs of two dimensional plots in which rows and columns of the matrix share common scales. Each plot in a scatterplot matrix is identified by its row and column numbers in the matrix. Dependencies between variables can be obtained by scanning a row (or column) and visualising how one variable is plotted against all others.

Scatterplot matrices provide simple representations of discrete data. An advantage is that the different dimensions are treated identically; but a decision is expected from the user how the data must be structured for presentation purposes. Despite its popularity in statistics MDMV visualisation applications, the original inventor of this method is unknown (Cleveland 1993).

Hyperbox

A hyperbox is a 2-dimensional depiction of an n-dimensional box (Alpern and Carter 1991). An n-dimensional hyperbox is made of n^2 lines and $n(n-1)/2$ faces. For each

line in a hyperbox, there are $n-1$ other lines with the same length and orientation. The length and slope of the line are arbitrary, and both of them can be mapped to the data variables for visualisation. Lines with the same length and orientation form a direction set, each variable is mapped to one direction. Each face of the hyperbox can be used to plot data of two variables such as a scatterplot or a line plot. To support data analysis, variables can be selected by cutting the hyperbox along each direction set.

Hyperbox is a more powerful tool compared to the scatterplot matrix in the sense that it is possible to map variables to both the size and shape of each facet. It also gives scientists the option to emphasize some of the more important variables. The design of the hyperbox requires practice to understand it. Furthermore, because of the unusual aspect ratio (which is defined as the height of data rectangle divided by the width) presented on some facet, some plots may not be able to convey the right information.

Parallel Coordinates

In a parallel coordinates system (Inselberg and Dimsdale 1987; Inselberg, Reif et al. 1987; Inselberg and Dimsdale 1990), the axes of a multi-dimensional space are defined as parallel vertical lines separated by a distance d. A point in Cartesian coordinates corresponds to a polyline in parallel coordinates.

It is claimed that, under certain conditions, parallel coordinates can allow visualisation of three dimensional time series data better than Cartesian coordinates (Inselberg and Dimsdale 1990). Parallel coordinates can also be used to study correlations among variables in MDMV data analysis. One of more promising applications of parallel coordinates in MDMV visualisation is that, by noting the locations of the intersection points, an approximation of the relationships between each pair of variables can be revealed. The problem with this technique is the limited space available for each parallel axis. The display can rapidly darken with even a modest amount of data.

2.2.5.1.2 *Dimensionality reduction*

In the visualisation of MDMV dataset, dimension reduction may be necessary to produce a k-dimensional data set from a given n-dimensional one, where usually n is very large and k should be much smaller than n. Some commonly used dimensionality reduction techniques include Principal Component Analysis (PCA), Multidimensional Scaling (MDS), Self-Organizing Maps (SOM), BLOB and H-BLOB algorithm, and HyperCell.

Principal Component Analysis

Principal Component Analysis (PCA) is a linear transformation that transforms the data to a new coordinate system such that the greatest variance by any projection of the data lies on the first coordinate (called the first principal component), the second greatest variance on the second coordinate, and so on. (Anderson and Anderson 1984; Smith 2002)

PCA can be used for dimensionality reduction in a dataset while retaining those characteristics of the dataset that contribute most to its variance, by keeping lower-order principal components and ignoring higher-order ones. Such low-order components often contain the "most important" aspects of the data. But this is not necessarily the case, depending on the application. PCA is a popular technique in pattern recognition and image compression.

Multidimensional Scaling

Multidimensional Scaling (MDS) (Kruskal and Wish 1978; Bentley and Ward 1996; Wong and Bergeron 1997) is a non-linear method for projecting n-Dimensional data to a reduced number of dimensions. An MDS algorithm starts with a matrix of item-item

similarities, and then assigns a location of each item in a low-dimensional space, suitable for graphing or 3D visualisation.

N-D data points can, for example, be represented as 2-D display points. The MDS algorithm attempts to make the 2-D display points accurately reflect the relationships that exist between the corresponding n-D points by iteratively evaluating the level of *Stress* in the configuration (high stress means the 2-D relationships are poorly correlated with the n-D relationships) and moving the 2-D points in a direction of reduced stress.

Self-Organizing Map

Self-Organizing Map (SOM) (Kohonen 1990; Kohonen, Oja et al. 1996) was first described by the Finnish Professor Teuvo Kohonen and is thus sometimes referred to as a Kohonen map. SOM is an effective visualisation approach of high-dimensional data. It converts complex, nonlinear statistical relationships between high-dimensional data items into simple geometric relationships on a low-dimensional (typically two-dimensional) display. SOM compresses information while preserving the most important topological and metric relationships of the primary data items on the display,

In the basic SOM algorithm, an N-dimensional reference vector is associated with each cell in the two-dimensional lattice or "map". After random initialization, the reference vectors are updated during a training phase by making repeated passes over the input data set. As each input record is encountered, the reference vector with the smallest Euclidean distance (i.e. the reference vector most similar to current input vector) is allowed to adjust or "learn" such that it more closely represents the input vector.

SOM and MDS are iterative refinement/optimization processes that attempt to adjust weights or positions until a certain criteria is met (for example, the distances or similarities between points in 2-D is a good approximation of the N-D

distances/similarities). Variations in the starting conditions and distance or similarity measures can have significant impact on the results of these methods.

The resulting display coordinates obtained through dimensionality reduction, unlike in the raw data-driven techniques, have no semantic meaning. Instead they can be viewed as supplemental dimensions to the original data set. PCA assumes that the majority of the variation in a data set will be well embodied in the first few principal components, which is not always the case. MDS and SOM, like all iterative optimization procedures, are not guaranteed to be optimal, and the results are generally not unique.

BLOB and H-BLOB Algorithm

BLOB and H-BLOB algorithms (Gross, Sprenger et al. 1997; Sprenger, Brunella et al. 2000) cluster large data sets in Euclidian space, in which data objects can be represented as n-dimensional vectors. The vector representation enables one to calculate simplified representations of complex data sub-regions at interactive rates. The results of BLOB and H-BLOB algorithms can be visualised in 2D or 3D space.

BLOB and H-BLOB algorithms use implicit surfaces for visualising data clusters. The authors of the algorithms pointed out that the majority of algorithms and systems treating cluster visualisation are limited to drawing a simple shape for each data object, with the actual clustering by the perceptual system of the user. The previous work on BLOB was an attempt to explicitly represent clusters by exhibiting them in an enclosing surface, but this and other previous work was restricted to visualising results of partitioning cluster algorithms, rather than hierarchical ones. H-BLOB discovers and visualises hierarchical clustering structures (cluster trees) in a two-staged approach. In the first one, called the analytical clustering step, an agglomerative hierarchical algorithm computes a cluster-tree by partitioning data objects into a nested sequence of subsets. The second stage involves the computation of a single enclosing shape for each cluster in combination with the visualisation process. The enclosing shape for the cluster

is a BLOB implicit surface that approximates the outline of the included data objects as closely as possible. A separate surrounding surface is computed for each cluster at each hierarchy level.

HyperCell

HyperCell (Santos and Brodlie 2002) is a dimension reduction method for the visualisation of multidimensional scalar functions. The basic concept is to represent the function by means of dynamic orthogonal low-dimensional (1D, 2D, or 3D) subspaces, called Cells.

Initially the user defines an N-dimensional region of interest, in which the data can be visualised. Then the user interactively creates cells by selecting up to three dimensions from the function domain. A cell can be visualised using a standard visualisation algorithm such as isosurface or volume rendering. To comprehend the function as a whole, several individual dynamic cells need to be investigated to build up a mental image of it.

The author argued that the visualisation of the multidimensional function through several three-dimensional dynamic subspaces reduced the overall complexity of the problem, since the human mind is not trained to create a mental image of complex functions defined in N-space ($N \geq 4$).

2.2.5.1.3 Approaches show subset of a dataset

Approaches to visualising MDMV datasets by showing subsets of the dataset are usually achieved with two methods: one is to use multiple views of the data, each communicating a subset of the dimensions, e.g. HyperSlice; the other is to embed or

combine data dimensions to form composite spatial dimensions, which include approaches like Hierarchical Axis, Dimension Stacking, and Worlds within Worlds.

HyperSlice

HyperSlice is a method for the visualisation of scalar functions of many variables (van Wijk and van Liere 1993). The central concept of hyperSlice is the representation of a multi-dimensional function as a matrix of orthogonal two-dimensional slices.

HyperSlice defines a focal point of interest $C = (c_1, c_2, \cdots, c_n)$ and a set of scalar widths w_i, where $i = 1, 2, \cdots, n$. Only data within the range $R = [c_i - w_i/2,\ c_i + w_i/2]$ are displayed in the panel matrix. The rest of the data only appears if the user steers the focal point near it. Like the coordinate system used in the scatterplot matrix, a hyperSlice panel is identified by a horizontal and a vertical coordinate. For an off-diagonal panel i, j such that $i \neq j$, the color or grey shade shows the value of the scalar function that results from fixing the values of all variables except i and j to the values of the focal point, while varying i and j over their ranges in R. The diagonal panels show a graph of the scalar function versus one variable which changes over the range in R.

The most important improvement of hyperSlice over the traditional scatterplot matrix is the concept of interactively navigating in the data around a user defined focal point. The user can change the focal point by interacting with any of the panels.

Hierarchical Axis

The conventional way to describe a three dimensional Euclidean space is by using three orthogonal axes. In hierarchical axis (Mihalisin, Gawlinski et al. 1990; Mihalisin, Timlin et al. 1991a; Mihalisin, Timlin et al. 1991b), axes are laid out horizontally in a

hierarchical fashion. Different metrics are used for each independent variable. Hierarchical axis technique maps 'n' independent variable dimensions on to a single hierarchical horizontal axis and plots a single dependent variable on the vertical axis.

The hierarchical axis technique can plot as many as twenty variables in one screen. For data with a larger number of records, i.e., larger than the number of columns of pixels on the display screen, a technique called *subspace zooming* is introduced. A display of multivariate data involves a series of panels, where the number of panels is equal to the number of variates. Each panel displays data from two hierarchical axes, ordered from the slowest to the fastest. This can be considered as a tree structure with the panel showing the slowest axis as the root. The other panels are nodes. A subspace is a sub-tree of the root. A series of panels is a path of the tree. Only the root panel is static, and only one path is shown at a time. The panels of the other paths are hidden until the user interactively clicks the specific data of any non-terminal panel to select another subspace (sub-tree).

The hierarchical axis approach is based on visual statistical analysis of either discrete variables or continuous variables that have been sampled on, or binned to, a regular n-dimensional lattice. It was been shown that this approach worked for such data visualisation tasks as the location of maxima, minima, saddle points, and other features, as well as for visually fitting multivariate data and the visual determination of dominant and weak or irrelevant variables.

Dimension Stacking

Dimension Stacking (LeBlanc, Ward et al. 1990) is a variant of the hierarchical axis technique where each element of the fastest axis is a one dimensional histogram. In dimension stacking, each element is a two dimensional xy-plot. If the data has an odd number of variables, a dummy variate is added. The values of a dependent variable can be plotted as color/grey intensity in each of the squares. Otherwise, each of the two

dimensional plots can be a simple scatterplot. It is possible to interactively adjust what ranges of values each dimension takes and the form in which the dimensions are displayed. A major advantage of dimension stacking over hierarchical axis is that no extra functions or rules, such as 'sum', is needed to plot the data.

Worlds within Worlds

The Worlds within Worlds technique (Feiner and Beshers 1990a; Feiner and Beshers 1990b) visualises multi-dimensional data by nesting dimensions together with a maximum of three variables being shown at each level, to generate an interactive hierarchy of displays. The slowest three axes are represented only by a display of three orthogonal axes. A three dimensional power glove is used interactively to define a position in the space defined by these three axes. A new set of these axes appears at this point. The glove can then be used to pick a point in this space. This continues until all variables are defined. At the lowest level the final variable can be displayed as a surface in the innermost world.

To use this technique properly, users have to know what they are looking for as most of the information is not visible in the initial display. This interactive process tends to be difficult and tedious because there are too many possible combinations of variate mappings.

Table 2.2 summarises the advantageous and limitations of each method mentioned in this section. In the next section, approaches for the visualisation of four-dimensional spatial-temporal datasets, which is the commonest multi-dimensional medical image dataset, are described.

Table 2.2: Summary of visualisation methods for MDMV datasets

Method	Advantageous/Features	Limitations
Show all dimensions and all variates as one display	An overview of the dataset is presented directly.	Displayed results may be unreadable if the data size is big.
Scatterplot matrix	Different dimensions are treated identically.	Not suitable for continuous data
Hyperbox	Variables can be mapped to both the size and shape of each facet of the hyperbox; Some variables can be emphasized and others can be de-emphasizzed.	Difficult to understand; The unusual aspect ration may not be able to convey the right information.
Parallel coordinate	Able to study correlations among variables in MDMV data analysis.	Limited space available for each parallel axis.
Dimensionality reduction	Visualisation methods for three- (or less) dimensional dataset can be applied to view MDMV dataset.	Resulted display coordinates generally have no semantic meaning.
Principle component analysis	Linear transformation; Able to retain characteristics of a dataset that contribute most to its variance.	Can not be used in the case that the original coordinates of a dataset is orthogonal to each other.
Multidimensional scaling	Iterative optimization	Non-linear transformation; Sensitive to the start condition and distance / similarity measure.
Self-organizing map	Iterative optimization; Preserving the most important topological and metric relationships of the primary data items in the display.	Non-linear transformation; Sensitive to the start condition and distance / similarity measure.
BLOB and H-BLOB	Cluster large datasets in Euclidian space	Limited to drawing a simple shape for each data object, and the actual clustering being done by the user's perceptual system.
Hypercell	Suitable for the visualisation of multi-dimensional scalar functions.	To comprehend the function as a whole, one needs to investigate several individual dynamic cells to build up a mental image of it.

Show subset of a dataset	Using multi-view of data, each communicating a subset of the dataset; Embedding or combining data dimensions to form composite spatial dimensions.	Absence of an overview of data
Hyperslice	Interactively navigating in the data around a user defined focal point.	
Hierarchical axis	N independent variables are mapped to a single hierarchical horizontal axis.	Different matrix are used for each independent variable.
Dimension stacking	No extra function or rule is needed to plot the data; Interactively adjust what ranges of value each dimension takes and the form in which the dimensions are displayed.	
World within world	Interactive hierarchy display	Interactive process tends to be difficult and tedious.

2.2.5.2 Visualisation of Spatial-temporal Datasets

Studying dynamic aspects of physiological change in the human body is critical for the advances of medical research. State-of-art medical imaging instruments allow accurate measurement of physiological processes in spatial and temporal domains, which could provide scientists with a new view of how conditions develop and change over time and lead to improved diagnosis or treatment. However, an increasingly challenging problem scientists facing is how to effectively explore and understand the resulting spatial-temporal data, or time-varying volume data, which is large in space and time. Currently, radiologists interested in temporal information from some imaging modalities must manually compare 2D images acquired at different times on a slice-by-slice basis. Such comparisons are difficult and time consuming; thus, not frequently done, particularly when the volumes are not aligned or the quantity of images is very large. Furthermore, 2D slices provide little information about 3D structure or rates of change.

Existing research on information animation has regarded animation as providing one more dimension; enabling 4D graphs by adding motions to 3D graphs. Some researchers even argue that the effect of animation is more than the fourth dimension: motions produce certain cognitive effects and appropriate use of motions empowers users in exploratory data analysis (Nakakoji, Takashima et al. 2001). Nevertheless, animation is the commonest approach for the visualisation of spatial-temporal data.

The task of rendering 4D spatial-temporal data is by nature very time consuming, because multiple volumes must be acquired, processed and rendered at interactive rates. How to improve the rendering speed and reduce a dataset's storage requirement without removing fine features in the data is central to animation visualisation research for spatial-temporal data. Considering the substantial temporal coherence characteristic of time-varying volume data, which means, a great percentage of voxel values do not change, or change very slowly over time, different algorithms are developed for fast rendering: Dobashi (Dobashi, Cingoski et al. 1998) proposed a rendering method by using orthonormal wavelets to encode time coherency; Ma (Ma, Smith et al. 1998) described a method using quantisation of scalar values to reduce the space required to store the volume, octrees to encode spatial coherence and differencing to exploit time coherence; Shen (Shen and Johnson 1994) used differencing in order to detect changes between successive volumes, that is to say, the first volume in the series is fully rendered by ray-casting and subsequently the image is updated by casting rays only from pixels that corresponding to changed areas in the volume; Silver (D.Silver and Wang 1998) identifies features of interest and tracks them in time; Anagnostou (Anagnostou, Atherton et al. 2000) presented a fast rendering approach based on the Shear-Warp factorisation, where reduction in storage space is achieved by detecting the changed areas within each volume and compressing them. Time-coherence is exploited by detecting and rendering the changes in every volume, and spatial-coherence is exploited by utilising a data structure that allows easy volume updates and stores information about the empty space within each volume.

Beside traditional animation displays, some researchers combine animation with techniques generally used for flow visualisation to present spatial-temporal medical image datasets (Tory, Rober et al. 2001). This method is more suitable where expectations of how activity should flow are clear, a flow simulation model can be used to calculate a flow vector; otherwise, it is not obvious that the derived flow vector will provide useful information.

2.2.5.3 Visualisation of Multi-variate Dataset

From functional view, a dataset with m variates can be treated in two ways: as a single function associating the independent variables with different combinations of values of these m variates, shown as:

$$(s_1, s_2, \cdots, s_m) = f(x_1, x_2, \cdots, x_n) \tag{2.6}$$

or as m functions associating the independent variables with individual values of these m variates, which can be presented as:

$$\begin{aligned} s_1 &= f(x_1, x_2, \cdots, x_n) \\ s_2 &= f(x_1, x_2, \cdots, x_n) \\ &\cdots \\ s_m &= f(x_1, x_2, \cdots, x_n) \end{aligned} \tag{2.7}$$

Consequently, all approaches suitable for the visualisation of uni-variate datasets can be applied to multi-variate datasets by using them simultaneously to each variate and presented as individual images. Turning to medical domains, as mentioned at the beginning of section 2.2.5, multi-variate medical image data is usual obtained by fusing data from different modalities; naturally, it is feasible to visualise each variate corresponding to different physiological properties in different displays concurrently, while the individual presentation of variates weaken their correspondence established by fusing.

Apart from the approaches to visualise each variate simultaneously, *Glyph* is another powerful and widely used technique for the visualisation of multi-variate datasets. Glyphs (also referred to as icons) are graphical entities that convey one or more data values via attributes such as shape, size, color, and position.

A glyph consists of a graphical entity with p components, each of which may have r geometric attributes and s appearance attributes. Typical geometric attributes include shape, size, orientation, position, and direction/magnitude of motion, and appearance attributes contain color, texture, and transparency. Attributes can be discrete or continuous, scalar or vector, and may or may not have a distance metric, ordering relation, or absolute zero. The process of creating a glyph thus becomes mapping one or more data variables for a data entry to one or more geometric and/or appearance attributes of one or more components of a graphical entity. A variety of glyphs have been proposed and used in visualisation, such as, profiles, starts, stick figure icons, trees, faces, arrows, polygons, etc.

Once a glyph has been designed and generated from a data entry, it must be placed at a location in display space (2D or 3D). The position attribute can be very effective in communicating data attributes or improving the detection of similarities, differences, clustering, outliers, or relations in the data. Ward (Ward 2002) presented an excellent survey on glyph placement strategies, and also concluded some general guidelines for selecting a placement strategy.

As pointed out by Ward (Ward 2002), although it is a popular method for conveying information visually, glyphs are not without limitations in the communication of multivariate data. Most, if not all, mappings introduce biases in the process of interpreting relationships between dimensions. There are also limitations based on the media being used to communicate the information. Screen space and resolution are limited, and displaying too many glyphs at once can lead to either overlaps (which can

hinder accurate discernment of individual dimensions) or very small glyphs (though, dense packing can form texture patterns for global analysis). Finally, a glyph is not a global technique; glyphs are spread discretely on images, so the images appear cluttered.

Up to now, this chapter had reviewed applications of visualisation in different research areas and approaches for medical image visualisation. With the development of science, the application of visualisation had been extended from data illustration and description to become an important tool in data exploration and analysis. This new type of visualisation is named exploratory visualisation, which will be reviewed in the next section.

2.3 Exploratory Visualisation

This section is composed of two main parts. First, an overview of exploratory visualisation is presented from two aspects: exploratory visualisation with related researches, and design of exploratory visualisation. Secondly, a particular problem in exploratory visualisation, task typology, which is a focus of the research work presented in this thesis, is described.

2.3.1 Overview of Exploratory Visualisation

Scientists have studied multivariable visualisation since 1782 when Crome used point symbols to show the geographical distribution in Europe of 56 commodities (Collins 1993). As the science progress in various aspects, more and more data of large proportions, with many variates and multiple dimensions occured. Physicians, physicists, mathematicians, and other scientists examined, explored, and analyzed data to gain insight into problems. Data exploration and analysis have become crucial steps in scientific research. Algorithmic analysis can be used to quickly and accurately process

data to identify patterns and outliers, and it is commonly dependent on having a computational model of the phenomena of interest. The problem is that the observer may not know what is exactly required, or may not be able to set fixed parameters and thresholds to effectively guide the algorithmic analysis. Alternatively, using visualisation techniques to explore and understand complex, high-dimensional data is an efficient way to combine human intelligence with the immense brute force computation power available today. Consequently, visualisation has been treated as not only a method for illustration and description, but also a part of the entire data exploration and analysis process (Springmeyer, Blattner et al. 1992; Weibel and Buttenfield 1992).

Exploratory visualisation enables the user to test scenarios and investigate possibilities. The user may change various parameter values of a visualisation system that in turn will alter the appearance of the result. Furthermore, the user may generate additional windows that contain the visual result of the new parameters so that different ideas can be compared side-by-side (Roberts 2004A).

2.3.1.1 Exploratory Visualisation and Related Researches

Although with different emphasis, some research domains are related to exploratory visualisation, which include Exploratory Data Analysis (EDA) and Data Mining (DM).

Exploratory Data Analysis (EDA) was defined by John Tukey (Tukey 1977). Although EDA emerged from statistics, it is not a set of specific techniques, but more a philosophy of how data analysis should be carried out. As Tukey saw it, EDA was a return to the original goals of statistics, i.e. detecting and describing patterns, trends, and relationships in data.

The concept of EDA is strongly associated with the use of graphical representation of data. Most EDA techniques are graphical in nature with a few quantitative techniques

(Andrienko and Andrienko 2006). The reason for the heavy reliance on graphics is that by its nature, the main role of EDA is to explore, and graphics gives the analysts opportunity to do so. Moreover, Tukey's exploratory data analysis signified a new era of scientific data visualisation (Wong and Bergeron 1997). It shows how to visually decode/explore information from the data.

Data Mining (DM), also known as Knowledge Discovery in Databases (KDD), has been defined as "The nontrivial extraction of implicit, previously unknown, and potentially useful information from data" (Frawley, Piatetsky-Shapiro et al. 1992). It is a recent topic in computer science but applies many older computational techniques from machine learning and statistics to visualisation techniques. Unlike data analysis, data mining is not based or focused on an existing model, which is to be tested or whose parameters are to be optimized.

The application of visualisation techniques in the context of data mining falls into two categories: one uses exploratory visualisation techniques to support a knowledge extraction goal or a specific mining task; the other utilises visualisation to display the results of a mining algorithm, such as a clustering process or a classifier, and thus enhances the user comprehension of the results (Ferreira de Oliveira and Levkowitz 2003).

2.3.1.2 Design of Exploratory Visualisation

The objective of visualisation design is to match data for specific applications to the most appropriate visualisation techniques. There are many visual design guidelines and a basic principle could be Shneiderman's visual information seeking Mantra: "overview first, zoom and filter, then details-on-demand" (Shneiderman 1996). While this is only a starting point in trying to design an exploratory visualisation system, efforts have been

made to study exploratory visualisation design. In the following, some typical work in this field is mentioned.

Bertin (Bertin 1983) was among the first to take an extensive and systematic approach to visualziation. Through a detailed semiotic analysis, Bertin developed a taxonomy of graphic displays and a set of principles for graphics design. As a pioneer, his work has provoded many great insights and is very useful in practice. Mackinlay (Mackinlay 1986) described an automated graphical presentation design method for relational information based on similar ideas as Bertin's, in which the system chooses the "optimal" visualisation techniques. Wilkinson (Wilkinson 1999) described a system with seven orthogonal components and described a set of grammatical rules for defining graphics. By orthogonal, Wilkinson meant there were seven graphical component sets whose elements were aspects of the general system and that every combination of aspects in the product of all these sets was meaningful. Wikinson's rules are proposed particularly for the development and application of statistical graphics.

In order to address usability issues in more detail, some visualisation design techiniques include user objectives (or tasks) exploration. The first effort to analyse user objectives is made by Bertin, who proposed a typology about possible analysis tasks based on two notions: ''question types'' and ''reading levels''(Bertin 1983). Wehrend and Lewis (Wehrend and Lewis 1990) proposed a scheme for classifying visualisation problems and developed a "catalog" for users to look up and share visualisation techniques for specified data types and tasks. The methodology presented by Roberston (Robertson 1991) includes the context of use and allows users to choose the best visualisation of the data with objective, directed display design methods, or to match representation to the intrinsic characteristics of data and goals for its interpretation. Zhang (Zhang 1996) developed a general theoretical framework for RIDs (Relational Information Displays), which included four components: dimensional representations, a representational taxonomy, a task taxonomy, and a mapping principle for the relation between

representations and tasks. Espinosa and his colleagues (Espinosa, Hendrickson et al. 1999) stated that the study of a user's tasks should yield usable information for visualisation design and developed a methodology for designers to consider user needs when developing visualisation systems.

2.3.2 Task Typology for Exploratory Visualisation

As mentioned by Qian et al (Qian, Wachowicz et al. 1997), a generalized view of the process of data analysis includes three steps. Initially an analyst has an information need. This need can be described by stating what is known (or given) and what is to be found. In order to find the needed information, the analyst plans a sequence of operations to be applied to the data. Finally, she/he tries to perform these operations using the available tools. At the same time, the preceding review about exploratory visualisation design demonstrated that many researchers take task analysis as an essential part to be considered in design process. Various approaches are available to explore possible tasks in data analysis and visualisation, and different task taxonomies have been suggested. Generally speaking, a task typology cannot be right or wrong: any classification is right to the extent of its serving the purpose for which it was devised. In the following, some main work in the task typology domain is reviewed.

2.3.2.1 Bertin's Task Typology and Improvements Based on This Typology

As a pioneer, Bertin (Bertin 1983) proposed a typology about possible analysis tasks based on two notions: "question types" and "reading levels":

> *"- there are as many Types of Questions as components in the information;*
>
> *- for each type there are Three Level of Reading: the elementary level, the intermediate level, and the overall level;*

- any question can be defined by its types and level."

Bertin also pointed out that "*their analysis permits knowing in advance the totality of the questions which any given information can generate*" (Bertin 1983). The advantage of Bertin's task typology is that it directly relates tasks to components of data. Such a feature is very convenient for a tool or application developer: having a particular data set, the developer can easily anticipate the questions that may potentially arise and care about appropriate support for finding answers to them. Bertin's typology was introduced for arbitrary data, other researchers improved this typology and made it more suitable for different environment.

Koussoulakou et al (Koussoulakou and Kraak 1992) pointed out that, for spatial-temporal data, the concept of the three reading levels defined by Bertin can be utilised for the temporal component in the same manner as it is done for the spatial component. By applying the three reading levels independently to both spatial and temporal dimensions, Koussoulakou classified nine kinds of questions about spatial-temporal data.

Peuquet (Peuquet 1994) also specifically considers spatial-temporal data. In order to include a time-based representation, Peuquet expended the dual spatial representational framework into a Triad framework in which information is stored relating to Where (the location-based view), What (the object-based view), and When (the time-based view). Accordingly, the Triad framework permits the user to pose three basic kinds of questions: *When+Where->What*; *When+What->Where*; *Where+What->When*.

Blok (Blok 2000) distinguished questions related to describe a variety of phenomena in the spatial-temporal environment into four main categories by two orthogonal dimensions: one dimension is used to describe the length of time series, the other dimension divide exploratory tasks into "identification" and "comparison". Although Blok's framework does not aim to predict all the questions that may arise, it proposed a new concept to reflect the difference between identification and comparison, which was

not enclosed by Bertin's typology. Within the same question type and reading level an analyst may need to examine a single element (set) or to compare or relate two or more elements (sets).

2.3.2.2 Task Typologies Other Than Bertin's Work

Considering that Bertin's theory involve the static presentation of information, Shneiderman (Shneiderman 1996) proposed a Task by data Type Taxonomy (TTT) for dynamic display. In TTT, data are classified into seven types: one-, two-, three-dimensional data, temporal and multi-dimensional data, and tree and network data. Furthermore, seven tasks are defined: overview, zoom, filter, details-on-demand, relate, history, and extracts.

Qian et al (Qian, Wachowicz et al. 1997) described a taxonomy of operations using a set-based information model that is application and data model independent. Such operations integrate both GIS functionality and visualisation tasks at the operational level.

Zhou (Zhou and Feiner 1998) introduce a visual task taxonomy that interfaces high-level presentation intents with low-level visual techniques. In this approach, visual tasks describe presentation intents through their visual accomplishments, and suggest desired visual techniques through their visual implications. Each visual task is described by two parts: an act and a set of arguments to act on.

2.3.2.3 Task Typology Research in Sankt-Augustin

The research group lead by Andrienko in Sankt-Augustin, Germany, have designed and developed software tools and systems for visualisation for more than ten years. Their

work is mainly concentrated on spatial-temporal geographic data. Significant achievements have been made in that group. This section will focus on their progress in the development of task typology for exploratory visualisation.

The first classification of analytical tasks developed by this group depends on which aspect of a spatial phenomenon varies with the time and what kind of view is required with respect to time. (Andrienko, Andrienko et al. 2000) claimed that exploratory analysis tasks can be classified according to two dimensions. One dimension reflects which temporal characteristic is in the focus of exploration: existence of spatial objects, location of spatial objects, shape and size of spatial objects, or thematic data associated with those objects. The other dimension concerns whether an analyst is interested to see the state of the data at some moment of time (snapshot), or how data changed at a moment '$t2$' as compared to some another moment '$t1$', or what happened during the interval $[t1, t2]$.

Later, they combined their research result with Bertin's theory (and its developments) and proposed a cubic data exploratory task typology for spatial-temporal data (Andrienko, Andrienko et al. 2003). Recently the task model was further refined and presented in the book "Exploratory analysis of spatial and temporal data"(Andrienko and Andrienko 2006). More details about this task typology will be introduced in Chapter 5 of this thesis.

In summary, this chapter reviewed the literature on visualisation. The research progress presented in this chapter and background depicted in chapter one constitute a basis for the research work conducted by the author of this thesis. The other chapters of this thesis will concentrate on the achievements made by the author on the visualisation of multi-dimensional medical image datasets.

Chapter 3 ROI Location for Brain EIT Images by Statistical Processing

As pointed out in section 1.2, the first objective of this research is to propose a method to define ROI (Regions of Interest) in functional brain EIT images. The relevant literature review presented in section 1.1.3.3 shows that there are only limited data available on the approaches to ROI definition in EIT images. Alternatively, ROI locations for other type of neuroimages have been widely researched for many years. Statistically based algorithms have significant advantages in the processing of brain medical images. So this chapter starts with an introduction on statistical processing for functional medical images. Within this introduction, a particular approach - SPM (Statistical Parametric Mapping) stands out: SPM has been applied worldwide and almost become a standard for the processing of fMRI data. The second section of this chapter presents a survey of SPM. Then a theoretical analysis about the feasibility of using SPM to process EIT data is conducted and a scheme to process EIT data in SPM is proposed. Next, two types of experiments are carried out. Finally, some conclusions are shown at the end of this chapter.

3.1 Introduction to Statistical Processing for Functional Medical Images

Statistical processing has been an important method and been widely applied to different aspects of medical imaging, such as, reconstruction, registration, and segmentation. Statistical methods for dealing with random events and processes can be used to model the mechanisms that cause image degradation. During functional imaging of the brain, or neuroimaging, the induced changes of regional neural activity are very subtle, repeat observations and statistical methods are generally required for reliable detection. Functional neuroimaging data is seldom viewed directly, instead it is subject to elaborate statistical processing first (Nielsen and Hansen 2000).

As a pioneer, Duffy and his colleagues (Duffy, Bartels et al. 1981) proposed significance probability mapping to analyse topographic maps of brain electrical activity imaged by EEG. In the late 1980s and early 1990s, research of functional brain images was mainly done with PET. Since the middle of 1990s, most researchers moved their attention from PET to fMRI. Consequently, several statistical packages have been developed for the analysis of fMRI images. Gold et al (Gold, Christian et al. 1998) presented an excellent review about fMRI statistical software packages, which included: AFNI 2.01 (Analysis of Functional NeuroImages) (Cox 1996), SPM96 (Statistical Parametric Mapping) (Friston, Frith et al. 1991), STIMULATE 5.0 (Strupp 1996), Yale (Skudlarski, Lacadie et al. 1995), MEDIMAX 2.01 (Infographics Group 1995), FIASCO (Functional Imaging Analysis Software-Computational Olio) (Eddy, Fitzgerald et al. 1996), MEDx 2.0 (Sensor Systems Inc. 1996), and FIT (Functional Imaging Toolkit) (Arnholt 1997). It is clear that each package contains many useful features; but they are neither comprehensive nor interchangeable. The choice of which package to adopt would basically depend on the interests and goals of each user. Gold also pointed out that SPM had been widely used for PET analysis and also became a popular choice for fMRI

analysis (at that time, fMRI just began to take over PET as a main method for brain functional imaging).

The SPM suite and associated theory was originally developed by Karl Friston. SPM'94 was the first major revision of the SPM software. Later versions, including SPM'95, SPM'96, SPM'99, and SPM2, are based on SPM'94, and represent the ongoing theoretical advances and technical improvements. The latest version of SPM is SPM5, which was released in December 2005. The research in SPM is still active. SPM has been applied worldwide and almost become the standard for the processing of fMRI data. In the next section, more details about SPM are given.

3.2 Overview of Statistical Parametric Mapping

Statistical Parametric Mapping (SPM) refers to the construction of spatially extended statistical processes to test hypotheses about regionally specific effects (Friston, Frith et al. 1991). SPM is generally used to identify functionally specialized brain regions and is the most prevalent approach to characterizing functional anatomy and disease-related changes.

With SPM, the analysis of functional neuroimaging data involves many steps that can be broadly divided into three parts:

- Spatial processing
- Estimating parameters of a statistical model
- Making inferences about those parameter estimates with their associated statistics

In the past, SPM has come to refer to the conjoint use of General Linear Model (GLM) and Gaussian Random Field (GRF) theory to analyse and make classical inferences

about spatially extended data through statistical parametric maps. GLM theory is used to estimate parameters that could explain data in exactly the same way as in conventional analysis of discrete data. GRF theory is used to resolve the multiple comparison problem that ensues when making inferences over a volume of the brain. (Friston 2002)

In the following subsections, the statistic theory for SPM is introduced first. The three parts of SPM are described from statistic estimation, statistical inference, to spatial processing. This review is mainly based on the SPM course notes provided by the Wellcome Department of Imaging Neuroscience (Course_Notes 1997), the Human Brain Function book (Richard, Friston et al. 1997), the SPM99 User Manual (Veltman and Hutton 2001), and the SPM theory introduction provided on the Cambridge University Imaging Website (Brett 1999).

3.2.1 Statistic Theory for SPM

From the statistical perspective, SPM includes two main parts: *Parameter Estimation* and *Hypothesis Inference* (or *Test*). Through parameter estimation, a statistical model is established for every voxel. Then all these models are combined together to construct a spatially extended statistical process. Based on this spatially extended statistical process, some statistical variants can be formed and hypothesis tests will be performed on the distribution probability of these variants.

3.2.1.1 Parameter Estimation

In SPM, the same model form is applied to every voxel simultaneously, with different parameters for each voxel. The observed values of a voxel under experimental conditions are considered as a response variable, and the experimental conditions are described with a series of explanatory variables. The General Linear Model (GLM) is

used to express the response variable in terms of a linear combination of the explanatory variables plus an error term. Subsequently, parameters in the linear model can be achieved by least squares estimates.

Underlying the GLM is an assumption that the error term is normally distributed. With this assumption, the least square estimates for parameters in the general linear models are the maximum likelihood and the best linear unbiased estimates; in addition, the estimated parameters are normally distributed as well. From this it follows that linear components of the estimated parameters can be assessed by comparing with a t (or F) distribution. Consequently, a three dimensional statistical image, or 'map', formed of thousands of correlated t or F statistics is obtained. This map is named a statistical parametric map.

3.2.1.2 Hypothesis Inference

The statistical image obtained from parameter estimation contains a large number of voxels so that it is not directly interpretable. It is obvious that performing a statistical test at each and every voxel engenders a large false-positive rate using conventional and unadjusted thresholds to declare an activation as significant. Hence, a null hypothesis that no activation accounting for the experimental conditions appeared at each voxel is made. Under this null hypothesis, the statistical image can be transformed and considered as a Gaussian Random Field (GRF).

In Gaussian Random Field, a series of statistical variables based on different inference levels can be constructed. By testing the statistical probability of these variables, the 'unlikeness' of these statistical variables is interpreted as regionally specific effects, attributable to the experimental context.

3.2.2 Statistical Estimation

Statistical estimation is the foundation of statistical inference. In this section, three main aspects in statistical estimation are described, which include an introduction on the GLM, an explanation of Design Matrix in the GLM model, and how to define the statistical variables for the construction of GRF. At the end of this section, the underlying assumption of GLM is analysed.

3.2.2.1 The General Linear Model

For a response variable x_{ij} ($i = 1, 2, \cdots I$ indexes the observations (scan); $j = 1, 2, \cdots J$ indexes the voxels), g_{ik} ($k = 1, 2, \cdots K$) are explanatory variables relating to the conditions under which the observation i was made. General Linear Model explains the response variable in terms of a linear combination of the explanatory variables, plus an error term:

$$x_{ij} = g_{i1}\beta_{1j} + g_{i2}\beta_{2j} + \cdots + g_{iK}\beta_{Kj} + \varepsilon_{ij} \tag{3.1}$$

Where β_{kj} presents the k th unknown parameters for voxel j;

ε_{ij} denotes the errors which are assumed independent and identically distributed normally.

For a selected voxel:

$$\begin{pmatrix} x_1 \\ x_2 \\ \vdots \\ x_I \end{pmatrix} = \begin{pmatrix} g_{11} & g_{12} & \cdots & g_{1k} \\ g_{21} & g_{22} & \cdots & g_{2k} \\ \vdots & \vdots & \ddots & \vdots \\ g_{I1} & g_{I2} & \cdots & g_{IK} \end{pmatrix} \begin{pmatrix} \beta_1 \\ \beta_2 \\ \vdots \\ \beta_K \end{pmatrix} + \begin{pmatrix} \varepsilon_1 \\ \varepsilon_2 \\ \vdots \\ \varepsilon_I \end{pmatrix} \tag{3.2}$$

Equation (3.2) can be written in matrix form:

$$X = G\underline{\beta} + \underline{\varepsilon} \tag{3.3}$$

Where X has one column for each voxel j and one row for each scan i;

G is a *Design Matrix* composed of coefficients g_{ik}, the Design Matrix has one row for each scan and one column for every effect in the model;

$\underline{\beta}$ presents the parameter matrix where $\underline{\beta_j}$ is a column vector of parameter for voxel j;

$\underline{\varepsilon}$ is a matrix of normal distributed error terms.

Least Squares Estimates of $\underline{\beta}$ can be calculated by:

$$\underline{\hat{\beta}} = (G^T G)^{-1} G^{-1} X \tag{3.4}$$

3.2.2.2 The Design Matrix

Design Matrix G contains both covariates and indicator variants reflecting the experimental design. In PET and fMRI images, covariates generally present global CBF (Cerebral Blood Flow), time, plasma prolactin level, etc; indicator variables usually mention the level of factor (e.g. condition, subject, session, etc) under which the response variable is measured.

Each column of G has an associated unknown parameter in the vectors $\hat{\beta}_j$. Some of these parameters will be of interest (e.g. In PET and fMRI imaging, the effect of a particular sensormoter or cognitive condition, or the regression coefficient of regional CBF on reaction time); the remaining parameters will be of no interest and refer to confounding effects.

3.2.2.3 Statistical Variables to Construct the GRF

With the assumption that the error term ε in General Linear Model is normally distributed:

$$\varepsilon \sim N(0,\sigma^2) \tag{3.5}$$

The parameter estimates are normally distributed as well:

$$\underline{\hat{\beta}} \sim N(\underline{\beta},\sigma^2(G^TG)^{-1}) \tag{3.6}$$

From this it follows that for $\underline{c}$ a column vector of K weights, $\underline{c}^T\underline{\hat{\beta}}$, which is a linear compounds of the parameter estimates, is normally distributed as well:

$$\underline{c}^T\underline{\hat{\beta}} \sim N(\underline{c}^T\underline{\beta},\sigma^2\underline{c}^T(G^TG)^{-1}\underline{c}) \tag{3.7}$$

The residual variance σ^2 is estimated by the residual mean square, which is χ^2 distributed:

$$\hat{\sigma}^2 \sim \sigma^2\frac{\chi^2_{I-P}}{I-P} \tag{3.8}$$

Where $P = rank(G)$.

Furthermore, $\hat{\beta}$ and $\hat{\sigma}^2$ are independent (Fisher's law). Thus, a pre-specified hypothesis concerning linear compounds of the linear compounds of the model parameters $\underline{c}^T\underline{\hat{\beta}}$ can be assessed using:

$$\frac{\underline{c}^T\underline{\hat{\beta}}-\underline{c}^T\underline{\beta}}{\sqrt{\hat{\sigma}^2\underline{c}^T(G^TG)^{-1}\underline{c}}} \sim t_{I-p} \tag{3.9}$$

That is, the hypothesis $H:\underline{c}^T\underline{\beta} = d$ can be assessed by comparing

$$T = (c^T\hat{\beta}-\alpha)/(\sqrt{\hat{\sigma}^2c^T(G^TG)^{-1}c}) \tag{3.10}$$

with a Student's t-distribution having $(I-P)$ degrees of freedom.

3.2.2.4 Parametric Assumptions

Underlying the general linear model is an assumption that the error term is normally distributed. There are a number of reasons for being confident that the data obtained with imaging devices (particularly PET) conform to Gaussian distributions:

The image reconstruction process in PET, back projection, can be thought of in terms of convolving the underlying distribution of radiodecay events with itself many times. The underlying distribution is approximately Poisson and by central limit theory the univariate distribution of intensity values in the back projected image will be Gaussian.

This argument does not however allow for non Gaussian behaviour of the physiological component in functional images (although there is no reason to suppose they are not Gaussian); however a reasonable argument can be made that the univariate behaviour of the final measurements will be Gaussian. This is because of explicit and implicit convolutions of the original distributions in the early parts of data processing [e.g. ramp and Hanning filtering in frequency space (i.e. convolving in Cartesian space) during reconstruction and Gaussian smoothing of images as a pre-processing step].

3.2.3 Statistical Inference

3.2.3.1 The Gaussian Random Field

Gaussian Random Field (GRF) theory deals with the multiple comparisons problem in the context of continuous, spatially extended statistical fields. It provides a method of correcting the p-value that takes into account that neighbouring voxels are not independent by virtue of continuity in the original data.

There are two assumptions underlying the use of the GRF correction:

1. The error fields (but not necessarily the data) are a reasonable lattice approximation to an underlying random field with a multivariate Gaussian distribution.
2. These fields are continuous, with a twice-differentiable autocorrelation function.

The only ways in which these assumptions can be violated is if:

1. The data are not smoothed, (with or without sub-sampling of the data to preserve resolution), violating the reasonable lattice assumption.
2. The statistical model is mis-specified so that the errors are not normally distributed.

3.2.3.2 Inference level

To make inferences about regionally specific effects, the SPM is thresholded, using some height and spatial extent thresholds that are specified by the user. Some statistical variables and their distribution probability p are constructed in the Gaussian random field. These p-values are based on the probability of obtaining c, or more, clusters with k, or more, voxels, above a threshold u in a statistical parametrical map. The p-values can be derived that refer to different inference levels:

1. Set-level inferences

Set-level inferences assume that the number of clusters comprising an observed activation profile is highly unlikely to have occurred by chance in the Gaussian random field and is a statement about the activation profile, as characterized by its constituent regions.

2. Cluster-level inferences

Cluster-level inferences are a special case of set-level inferences, that are obtained when the number of clusters $c = 1$.

3. Voxel-level inferences.

Voxel-level inferences are special cases of cluster-level inferences that result when the cluster can be small (i.e. $k = 0$). Voxel-level tests permit individual voxels to be identified as significant, whereas cluster and set-level inferences only allow clusters or sets of clusters to be declared significant.

Using a theoretical power analysis (Poline, Friston et al. 1995) of distributed activations, set-level inferences are generally more powerful than cluster-level inferences and that cluster-level inferences are generally more powerful than voxel-level inferences. The price paid for this increased sensitivity is reduced localizing power.

3.2.4 Spatial Processing

In SPM, the analysis of neuroimaging data generally starts with a series of spatial transformations. These transformations aim to reduce the artificial variance components in the voxel time-series that are induced by movement or shape differences among a series of scans.

The spatial processing usually starts with a realignment to 'undo' the effects of subject movement during the scanning session. After realignment the data is then transformed using linear or non-linear warps into a standard anatomical space. Finally, the data is usually spatially smoothed before entering the analysis process.

3.2.4.1 Realignment

Realignment in SPM is usually performed in two steps:

- First, estimating six parameters of an affine 'rigid-body' transformation that minimizes the (sum of squared) differences between each successive scan and a reference scan (usually the first or the average of all scans in the time series).
- Then, applying the transformation by re-sampling the data using tri-linear, sinc or cubic spline interpolation.

For most imaging modalities this procedure is sufficient to realign scans to, in some instances, a hundred microns or so (Friston, Ashburner et al. 1995). However, in fMRI, even after perfect realignment, movement-related signals can still persist. This calls for a further step in which the data are adjusted for residual movement-related effects.

3.2.4.2 Spatial Normalization

After realigning the data, a mean image of the series, or some other co-registered (e.g. a T1-weighted MRI) image, is used to estimate the warping parameters that map it onto a template that already conforms to a standard anatomical space.

This estimation can use a variety of models for the mapping, including:

- A 12-parameter affine transformation, where the parameters constitute a spatial transformation matrix.
- Low frequency basis spatial functions (usually a discrete cosine set or polynomials), where the parameters are the coefficients of the basis functions employed.
- A vector field specifying the mapping for each control point.

3.2.4.3 Smooth

The motivations for smoothing the data are threefold:

- Potentially increase signal to noise ratio
- Inter-subject averaging
- Increase validity of SPM

In SPM, smoothing is done by convolving the images with a 3D Gaussian Kernel.

With previous spatial processing, realignment and normalisation do not change voxel values but simply relocate them, while after smoothing each voxel effectively becomes the result of applying a weighted region of interest.

3.3 Statistical Processing for ROI location in Brain EIT Images

As shown in section 1.3.3, identification of ROI (Regions of Interest) is a challenge for EIT visualisation. The preceding description reveals that SPM is a leading statistical analysis package to analyse neuroimages and locate regions in the brain which are activated during measurements. As brain EIT imaging can also create neuroimages, it seems plausible to apply SPM to identifying ROI in brain EIT images. While the SPM method and software are only designed for PET/SPECT and fMRI neuroimages, there has been very little research effort to combine SPM method with brain EIT image analysis. In this section, the methodology to process brain EIT data with SPM is proposed. Experimental results and further discussion are presented in the next section.

3.3.1 Scheme of Processing Brain EIT Data with SPM

As mentioned in section 3.2, to some extent, SPM can be considered as a combination of General Linear Model (GLM) and Gaussian Random Field (GRF). The underlying principle of GLM is an assumption that:

- The error term in the GLM is normally distributed.

Similarly, there are two hypotheses underlying the use of GRF correctly and the only way in which these assumptions can be violated is if:

- The data is not smoothed.
- The statistical model is mis-specified so that the errors are not normally distributed.

Based on these criteria, the following conclusions can be drawn: to investigate if it is reasonable to use SPM to process image data, two examinations must be performed - the first is to prove that the data is smoothed; the second is to correctly specify the statistical model and then test if the error term in the GLM is normally distributed.

For brain EIT imaging data, it is assumed that it is smoothed. Different from other tomography approaches, the initial reconstruction result of 3D brain EIT imaging is a 3D volume dataset instead of a stack of 2D slices. In order to get the sliced data, the initial reconstructed data is interpolated and rasterized, which makes the final EIT image data smoothed. At the same time, the spatial smoothing function provided in the spatial normalization step of SPM processing can be used as a backup method to ensure the smoothness of EIT imaging data.

Friston (Friston, Holmes et al. 1995) pointed out that data obtained with image devices are commonly uniform to Gaussian distribution. Even if the original physiological measurements were not Gaussian, after the explicit and implicit convolutions during

reconstruction and smoothing of image as a pre-processing step, they will be (nearly). From another point of view, according to the Central Limit Theorem, which points out if an error such as ε is a sum of errors from several sources, no matter what the probability distribution of the separate errors may be, their sum ε will have a distribution that will tend more and more to the normal distribution as the number of components increase. Thus there is a tendency for errors that occur in many real situations to be normally distributed. Therefore, it is sensible to conclude that the voxels in brain EIT image data are normally distributed. Furthermore, if the experimental effects in EIT imaging are correctly specified, the error term in the GLM should also be normally distributed.

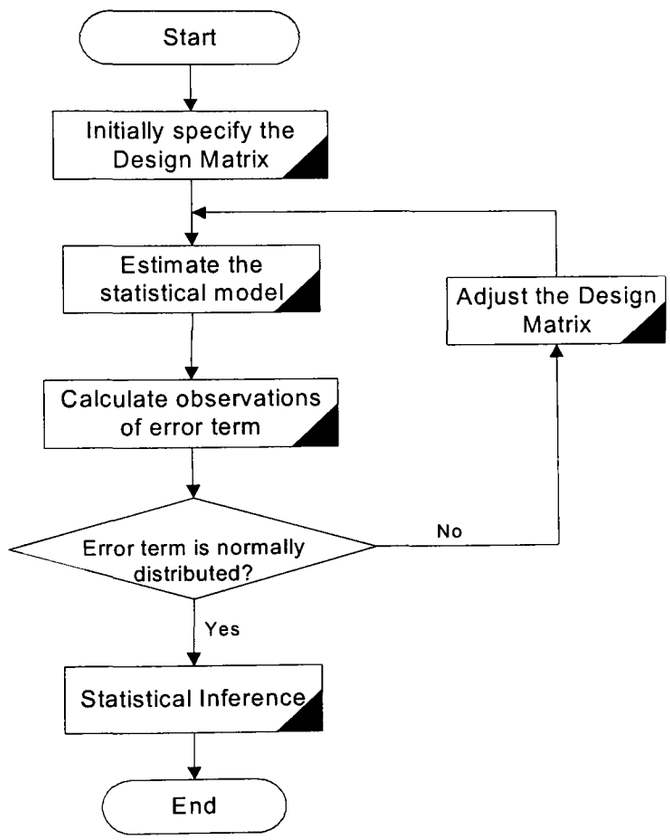

Figure 3.1 Scheme for the processing of EIT data

The previous theoretical analysis demonstrates that, it is possible for EIT imaging data to satisfy the underlying assumptions of GLM and GRF. So it is reasonable to use SPM to process EIT imaging data, and a scheme is proposed to illustrate how to process brain

EIT data with SPM (see figure 3.1). Before testing the practicality of this scheme with some experiments, some points which should be particularly considered in the processing are mentioned below.

3.3.2 Mode Selection

In SPM, although the same statistical theory is utilised for the processing of PET/SPECT data and fMRI data, different analysis modes are provided for them, because of the different features included in these two types of data. Therefore, to process a new type of neuroimages in SPM, the primary step is to decide which analysis mode should be adopted or be employed as a basis.

Generally, PET analysis is a little simpler than fMRI analysis. For PET, the observations (voxel values), are nearly independent, (which means that signal generated for the voxel value for one scan has more or less decayed to negligible levels by the time of next scan), for the relevant long time interval. However, the time spacing between fMRI scans within a scan session is often very short; in this case the signal that generated one scan may still be presented at the time of the next, so temporal autocorrelation occurs. To counter this, SPM provides a temporal smoothing function, which swamps the unknown autocorrelation with a known one, and so allows accurate adjustment of the statistical thresholds.

Furthermore, the "PET mode" is more flexible: it makes no assumptions about the data. The "fMRI mode" assumes that background voxels have intensity below a set percentage of the maximum intensity and global normalization is required.

From another point of view, "fMRI mode" can access to the hemodynamic modelling function based on Balloon Model. The authors of SPM concluded that a Balloon Model was sufficient to account for the nonlinear behaviours of the dynamic changes in

deoxyhemoglobin content during brain activation observed in real time series (Glaser, Friston et al. 2003), and adopted this model in SPM software. The Balloon Model was proposed in (Buxton, Wong et al. 1998). Calculations based on this model show pronounced transients in the deoxyhemoglobin content and the Blood Oxygenation Level Dependent (BOLD) signal measured with functional MRI. Figure 3.2 illustrates the variety of time courses that can be produced by the Balloon Model.

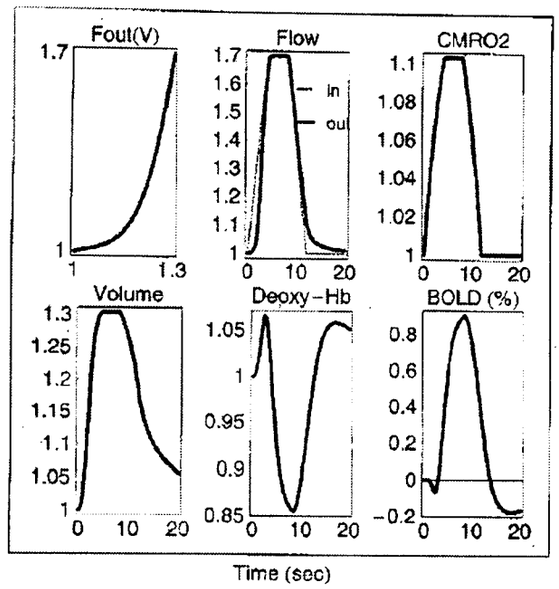

Figure 3.2 Variety of time course calculated by Balloon Model.

Considering the flexibility, the "PET mode" is chosen for the processing of brain EIT data. In the experiments described in section 3.4, two types of EIT data will be used: one is simulated brain EIT data, and the other is previously published human brain EIT data that (Tidswell, Gibson et al. 2001b), obtained from adult subjects during visual stimulation. For a voxel in simulated data, the impedance value at each sample point is specified precisely. There is no interaction between values at different time points. And the observations can be treated as independent. The time spacing between the selected human EIT data is 25 seconds. And with such a relatively long time interval, it is reasonable to treat these EIT observations independently. Therefore, temporal smoothing is not necessary for the experimental data. EIT can, in principle, record thousands of images per second, but modern brain EIT imaging instruments only need tenths of a

second to acquire an image. In that case, any temporal smoothing should be performed as pre-processing.

Considering the hemodynamic model, fMRI measures BOLD signal caused by dynamic changes in both blood oxygenation and blood volume during brain function, while EIT measures brain impedance changes. During visual stimulation, brain impedance changes are mainly caused by blood volume and flow increasing in the low time resolution collection environment (Tidswell, Gibson et al. 2001b). It is sensible to conclude that blood volume change instead of the BOLD signal should be used in EIT analysis. This means it may not be suitable to apply the hemodynamic modelling function provided by SPM to EIT data directly. From this point of view, the inaccessibility of PET mode to this function is not a disadvantage for the processing of brain EIT data.

After choosing the analysis mode, subsequent steps for the processing of neuroimage data with SPM are: spatially normalising the data; specifying the Design Matrix and other parameters. Then, the statistical model is estimated and statistical inference is carried out.

3.3.3 Spatial Processing for EIT Data

As mentioned in section 3.2.4, processing in SPM usually starts with a series of spatial transformations which aim to reduce artefactual variance components in the time-series. These variances are generally induced by head movements of the subject among a series of scans or shape differences among scans for different subjects. In EIT imaging, the electrodes are fixed directly to the skin of the body part to be imaged, they move with the subject; and images are normally reconstructed onto a dimensionally stationary mathematical model, hence no image realignment is required. In practice, skin may move over the underlining structure, which leads to errors in image reconstruction, but this cannot be corrected by image realignment.

Even without movement, EIT images may be spatially distorted, either due to out of plane impedance changes in 2D image reconstruction (Rabbani, Hassan et al. 1996) or mismatches between the model used for the forward solution, and real shape (Jain, Isaacson et al. 1997; Bagshaw, Liston et al. 2003). Electrode position, the conductivity and dimensions of distinct layers, e.g. the skull (Liston, Bayford et al. 2004), can all contribute to such errors. Some of these are compensated for by the use of different imaging methods; others may be reduced by improving the forward model. Nevertheless, such compensation is beyond the scope of SPM.

3.3.4 Testing the Distribution of Error Terms

According to equation 3.3, the error term in General Linear Model can be expressed as:

$$\varepsilon = X - G\beta \tag{3.11}$$

After parameter estimation, errors of each voxel at each sample point, i.e. observations of the error term, can be calculated.

To test if a sample of data came from a normally distributed population, there are generally two methods: one is graphical assessment by plotting residuals; the other is using some statistics to provide a numerical measurement. In practical regression situations a detailed examination of the corresponding residuals plots is usually informative, and the plots will almost certainly reveal any violation of assumptions serious enough to require corrective action (Draper and Smith 1981). While the effectiveness of graphical assessment is ensured by large sample size, The Chi-square 'goodness-of-fit' test is the most frequently used statistic approach to examine if a sample of data came from a population with a specific distribution. An attractive feature of chi-square test is that it can be applied to any univariate distribution for which you can calculate the cumulative distribution function. The Chi-square test requires a sufficient sample size, usually more than 30, in order for the approximation to be valid.

The Chi-square test is adopted in the experiments described in section 3.4 to test the distribution of error term. In the following, an overview of how to use the Chi-square test in this thesis is presented.

For every voxel, observations of the error term are sorted and divided into K groups. Each group i has a maximum value MA_i and a minimum value MI_i, and $MA_{i-1} = MI_i$.

To test the null hypothesis $H_0 : P_i = p_i$, the test statistic TS in Chi-square test is:

$$TS = \sum_{i=1}^{K} \frac{(N_i - e_i)^2}{e_i} \tag{3.12}$$

Where $i = 1,...,K$ indexes the group

$N_i = nP_i$ is the observed frequency for group i, n is the sample size

$e_i = np_i$ is the expected frequency for group i, n is the sample size.

In this thesis, Chi-square test is used to examing whether the error term conforms to normal distribution, so the expected frequency for group i is:

$$p_i = \int_{MI_i}^{MA_i} \frac{1}{\sqrt{2\pi\sigma^2}} \exp(-\frac{(x-\mu)^2}{2\sigma^2})dx \tag{3.13}$$

Where μ is the mean of the error distribution

σ^2 is the variance of the error distribution

Mean μ and variance σ^2 of the error term can be obtained with Maximum Likelihood Estimation.

The degrees of freedom df of the Chi-square distribution, which approximates the test statistic TS, can be calculated with:

$$df = K - 1 \tag{3.14}$$

Let $\chi^2_{K-1,\alpha}$ denote a Chi-square random variable having $(K-1)$ degrees of freedom which will exceed this value with probability α , then the approximated significance level α test of the null hypothesis H_0 against the alternative H_1 is as follows:

$$\begin{cases} Reject\ H_0 & if\ TS \geq \chi^2_{K-1,\alpha} \\ Do\ not\ reject\ H_0 & otherwise \end{cases} \tag{3.15}$$

3.4 Experiments and Discussions

In order to verify the feasibility of processing brain EIT data with SPM, two types of experiments are carried out and described in the following sections: the first is implemented with simulated EIT data, and the second is performed with human EIT data under visual stimulation. Discussion based on each set of experimental results follows.

3.4.1 Experiment with Simulated EIT Data

EIT researchers usually use three types of data: simulated data, phantom data and human data. During the collection of human or even phantom data, there are always some unpredictable factors that degrade image quality. With the intention of making the data more controllable and to facilitate the evaluation of experiment results, simulated data was used at the first step of the experiments. In the following, the procedure to create simulated EIT data is described first, then how the simulated data are analysed in SPM according to the scheme proposed in section 3.3.1 is depicted.

3.4.1.1 Creation of simulated EIT Data

As pointed out in section 1.1.2, in brain EIT imaging, functional impedance changes over a sample time of minutes may be caused by cells swelling or blood volume and

flow increase. The simulated datasets are created to imitate the conductivity change caused by the blood volume and flow increasing. Obviously, during practical imaging, there is always noise included. In order to model those noise effects, three types of simulated datasets are generated.

Type I – Noise-free Dataset

This type of dataset aims to model an ideal situation: which is how the impedance changes over time is precisely known, and no noise is induced by the imaging equipment.

The size of the simulated dataset is 200×200×200×36 (x, y, z, t), which means there are 36 sample time points, and a volume dataset with size 200×200×200 (mm) is generated corresponding to each sample time point. The time interval is one second during the first three sample time points, and changes to one third of a second afterwards. Coordinates of these datasets are defined as (referring to human head): x increases from left to right, y increases from posterior to anterior, and z increases from inferior to superior. x, y, and z values are changed from -100 to 100 (mm). The zero point (0, 0, 0) is defined as the centre of brain.

In the simulated datasets, the human brain is simplified as a sphere with constant impedance value. The blood volume and flow increasing region, which is the Region of Interest (ROI) in the simulated data, is also defined as a sphere. This ROI is centred at point (0, -40, 0), and is 40mm in diameter (see figure 3.3(a)). A function is used to express the impedance change ratio in the ROI:

$$t\_course = 1 + (3 \times t - 0.55 \times t^2 + 0.025 \times t^3)/100 \tag{3.16}$$

Figure 3.3(b) is a plot of this function. As mentioned in section 1.1.2, blood volume and flow give changes in the local brain impedance by a few percent. In the simulated dataset, the impedance change ratio is less than five percent.

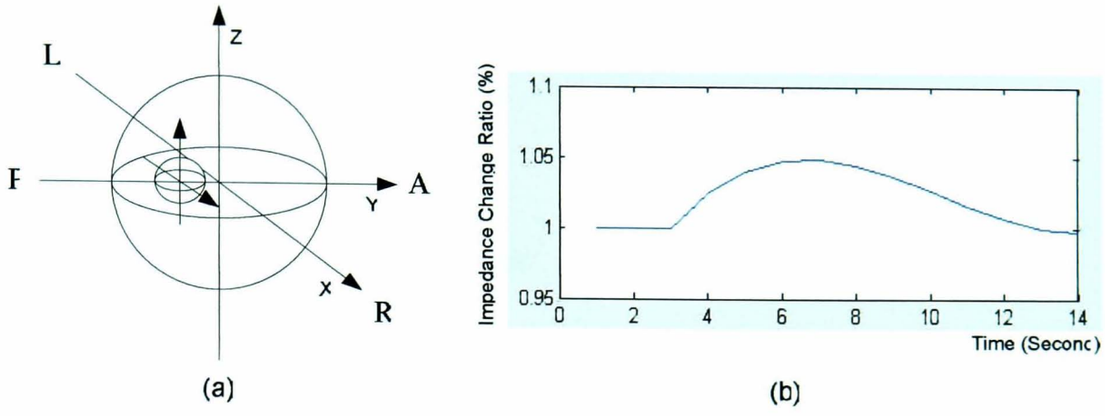

Figure 3.3 ROI in the simulated datasets

(a) Scheme of the impedance change area; (b) Plot of the impedance change ratio in ROI

As described in section 1.1.2, the EIT reconstruction approach includes two steps: the solution of forward problem and the solution of inverse problem. To create a simulated dataset, first the boundary voltages are calculated by solving forward problem. Then a volume imaging dataset is reconstructed from these boundary voltages with TSVD (Truncated Singular Value Decomposition) reconstruction algorithm. The solid line in the flow chart in figure 3.4 illustrates the procedure to produce a noise-free type dataset.

Type II – True-noise Dataset

In practice, it is almost impossible to precisely describe impedance changes happening in human brain. And usually, only a outline of impedance change can be deduced. In order to simulate this situation, the second type of dataset, the true-noise dataset, is created by adding some noise before the solution of forward problem (see point A in figure 3.4). The other parts for true-noise dataset are same as the noise-free dataset.

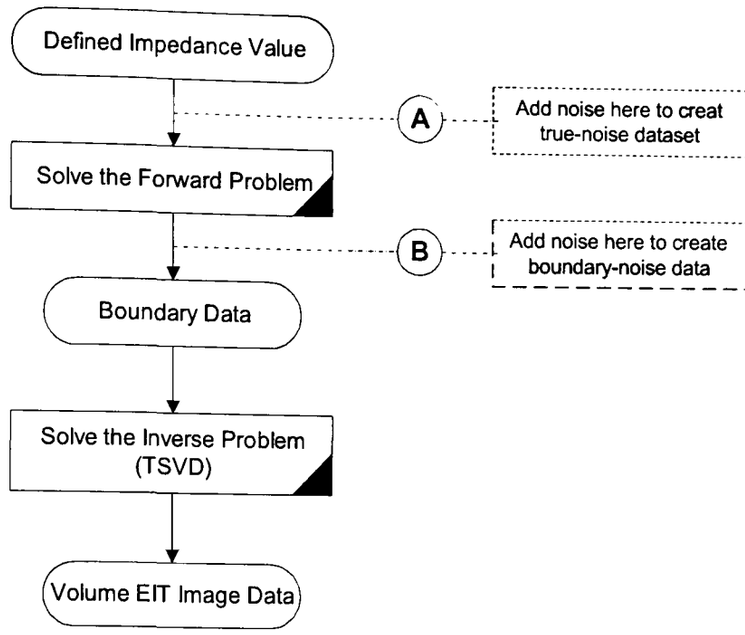

Figure 3.4 Procedure to create simulated EIT data

Type III – Boundary-noise Dataset

In addition to the unpredictability of the impedance change value, there is another noise source in practical measurements: the noise induced by imaging equipment. In order to imitate this environment, A third type of dataset: boundary-noise dataset was produced, this uses a similar procedure as the creation of true-noise dataset, but more noise is added after the solution of forward problem (see point B in figure 3.4).

Table 3.1: Scheme of the simulated datasets with 14 time sample points

Dataset No.	Noise type	Noise ratio
Dataset 1	Noise free	--
Dataset 2	True noise	10%
Dataset 3	True noise	20%
Dataset 4	Boundary noise	2%
Dataset 5	Boundary noise	5%

Adjusting the noise ratio, different datasets can be produced. Table 3.1 presents an overview of the datasets used in the experiments described in this section. Figure 3.5 illustrates a two-dimensional time series display of selected transverse planes (where $z = 0$) in these datasets.

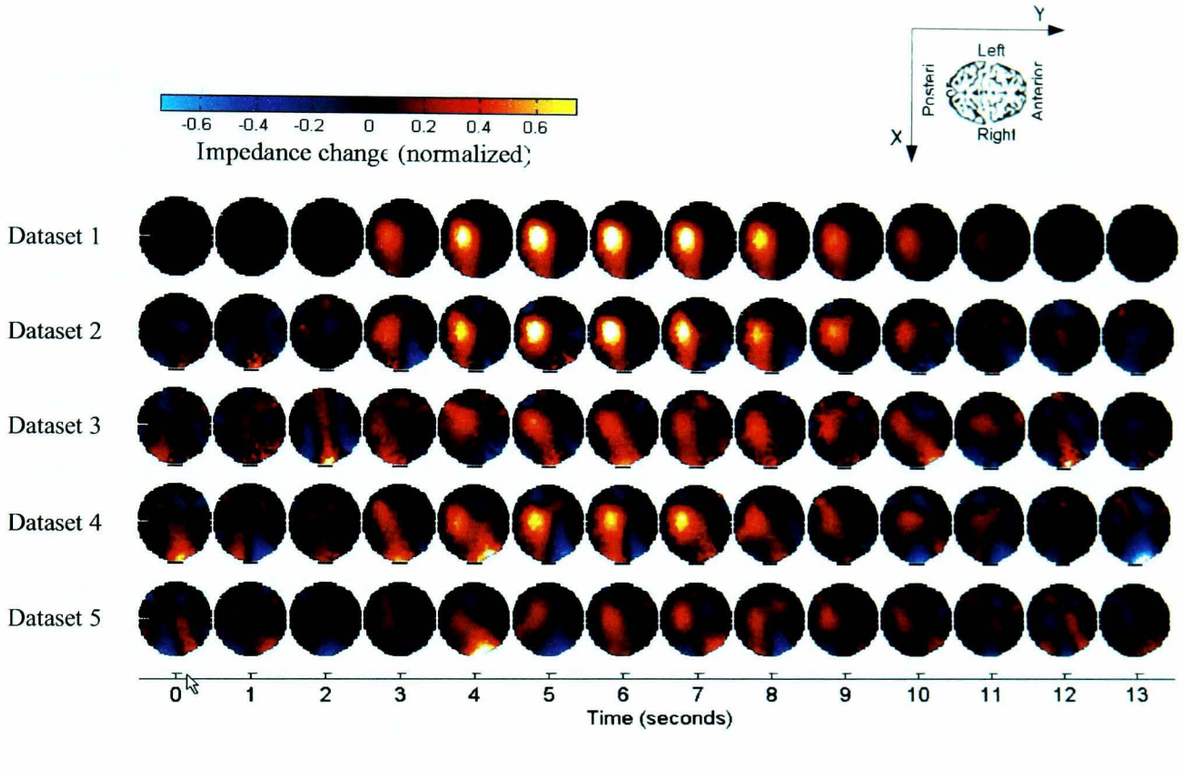

Figure 3.5 2D time series display of transverse planes (z=0) in the simulated datasets

Observing the time series display corresponding to the first dataset, it is easy to find a global maximum. This is a single local maximum in this dataset. The area around this maximum position shows where the blood volume and flow increases, which is the ROI in this dataset. In the second and the fourth datasets, although not as easy as the first dataset, it is not difficult to find out the ROI. While in the third and the fifth datasets, especially in the fifth dataset, there is more than one local maximum. It would be difficult to decide which one is the ROI if the information on how these datasets were created was unavailable.

3.4.1.2 Design Matrix Specification

With the decision to select PET mode and not to use spatial normalization for brain EIT data (see the details in section 3.3.2 and section 3.3.3), the construction of a Design Matrix is a key step for each EIT dataset to be analysed with SPM.

In SPM, both PET and fMRI modes provide different choices to form any Design Matrix, these are classified according to factors considered in the analysis, such as conditions, subjects, and sessions. In the estimated datasets, only one subject is considered and no experiment condition change is included. Therefore, the second design type in PET mode - "Single-subject: covariates only" – is selected as a framework for a Design Matrix, where the conductivity change and scan time are defined as covariates in the initial Design Matrix. Other main parameters used in the experiments were set as shown in table 3.2. The meaning of each parameter included in this table can be briefly explained as: the *threshold* in analysis setup is used to exclude voxels whose value is less than the threshold from statistical analysis; *Global calculation* stands for the method adopted to calculate the global impedance change during the imaging procedure; *Mask with other contrast* represents if any other contrast is used simultaneously in this statistical inference step; the *threshold* in the result setup is used to compare with probability of the statistic; *extend threshold* is used to determine that, when a cluster is identified as significant, how many voxels must be included in it; *Visualisation overlays* defines how the SPM analysis results are displayed.

Table 3.2: Parameters setting for the test of simulated EIT datasets

Analysis Setup ...		
	Threshold	-Inf
	Global calculation ...	Mean voxel value
Results Setup ...		
	Mask with other contrast(s)	no
	Threshold (T or p value)	0.01
	& extent threshold (voxels)	1
	Visualisation overlays...	sections

3.4.1.3 Testing the Distribution of Error Terms

With a specified Design Matrix, the statistical model is estimated. Error terms are then calculated according to equation (3.11). In this subsection, results of using Chi-square test to examine the distribution of error terms are given.

To make sure that there are at least 80% of the observed frequency N_i exceed 5 in the test, the 36 observations of error terms are divided into 7 groups, thus the degrees of freedom in the test is: $df = 7 - 1 = 6$. For significance level $\alpha = 0.005$, $\chi^2_{6,0.005} = 18.55$.

Using the methods mentioned in section 3.3.4, the test statistic TS is calculated for every voxel in each dataset, and then compared with $\chi^2_{6,0.005}$. Table 3.3 presents an overview of the test results. The second column in table 3.3 is total number of voxels being statistically estimated in SPM. The third column describes the number of voxel whose TS is greater than $\chi^2_{6,0.005}$, which equals to 18.55, and so whose normal distribution assumption is rejected. The last column displays the rejected ratio in this dataset. As the results show, all the reject ratios are less than 2%. Consequently, it is sensible to draw a conclusion that the error terms are normally distributed in the specified GLM.

Table 3.3: An overview of Chi-square test results

Dataset No.	Total Voxel Number	Voxel Number ($TS \geq \chi^2_{6,0.005}$)	Percentage
Dataset 1	193046	2461	1.27%
Dataset 2	229816	3976	1.73%
Dataset 3	232771	3586	1.54%
Dataset 4	210479	3389	1.61%
Dataset 5	229586	3753	1.63%

According to the scheme defined in section 3.3.1, once the error terms are normally distributed, it is not necessary to refine the initial Design Matrix. Then the next step should be statistical inference.

3.4.1.4 Statistical Inference Results and Discussion

SPM provides different methods to display inference results. The one chosen in this thesis is to overlay the results on orthogonal sections of processed image data. Figure 3.6 shows the statistical analysis results. In each result, except the one for dataset 1, there is a closed zone highlighted by SPM, which seems to cover the same region as defined for impedance variation. To test if it is true, the centroid of the highlighted zone and the specified impedance variation area are compared.

Table 3.4: Analysis of centroids in results set I

Dataset No.	Central Voxel	Variation	Percentage
Dataset 1	-	-	-
Dataset 2	(-7,-35,-2)	(-7,5,-2)	3.5%
Dataset 3	(-5,-42,-4)	(-5,-2,-4)	2.5%
Dataset 4	(-4,-37,1)	(-4,3,1)	2%
Dataset 5	(-2,-41,2)	(-2,-1,2)	1%

As defined in section 3.4.1.1, the centroid of the impedance change region locates at point (0, -40,0). The central voxel (rounded centroid position) for each highlighted zone is calculated and listed in the second column of table 3.4; the third column in this table presents variation between the calculated central voxel and the centroid of the defined impedance change region. Dividing the variation by 200 (because x, y and z coordinate all change from –100 to 100 in the simulated data), the variation percentage is obtained. The last column in table 3.4 shows the biggest variation percentage among three coordinates. Typically confidence level can be set as 95%. In these tests, all the

percentage variations are less than 5%. So it is reasonable to draw a conclusion that SPM correctly located the centroid of the changed impedance region.

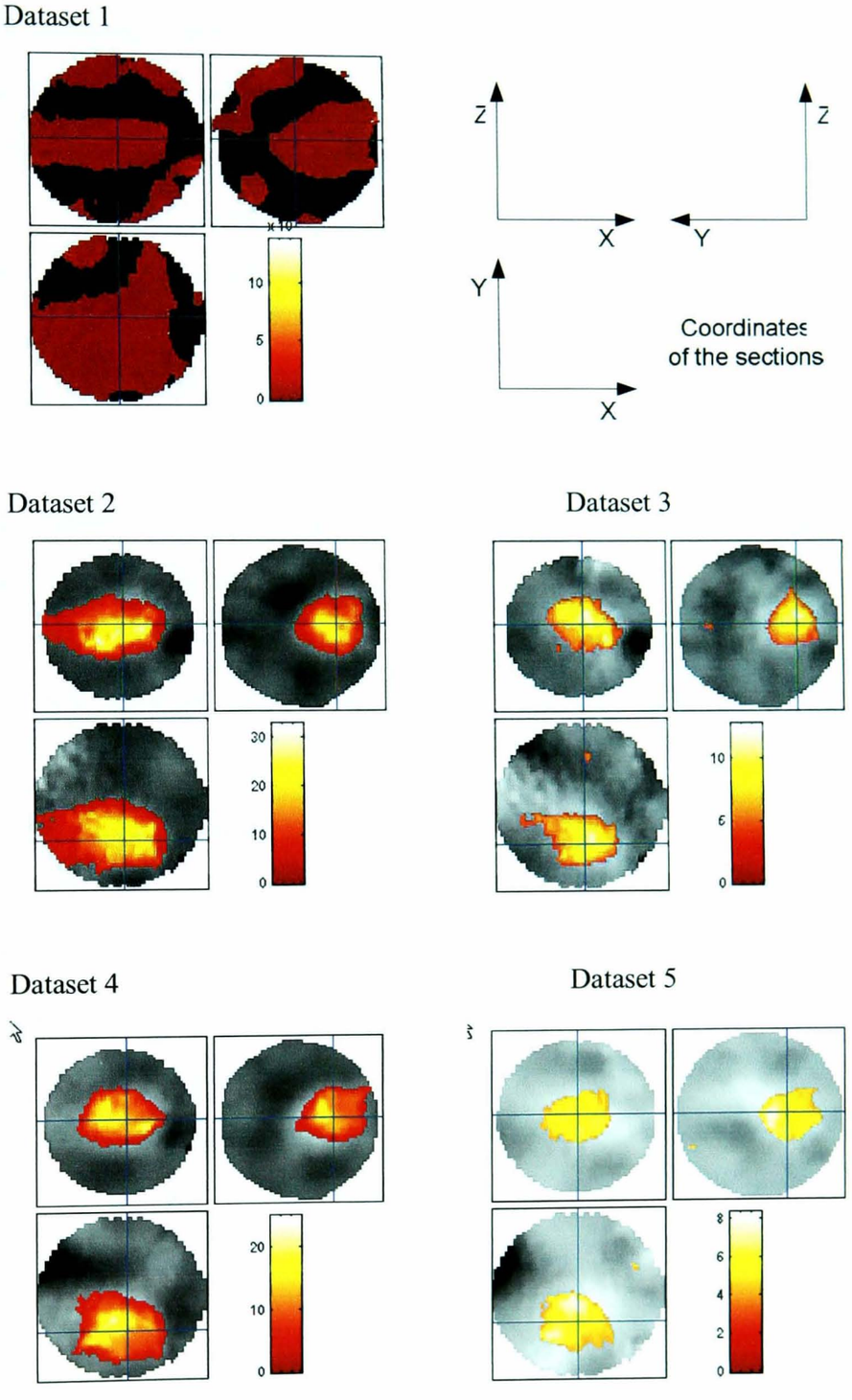

Figure 3.6 Statistical processing results set I

As mentioned in section 3.4.1.1, the specified impedance change region in each simulated dataset is identical, however areas marked by SPM varies among the datasets.

A possible reason is the smoothing effect included in EIT reconstruction processing, which blurs the sharp change at the edge of impedance variation region. Voxels in this blurred area have same impedance change tendency as voxels in the specified region, while their changing amplitudes are smaller. At a specified probability threshold, some voxels in the blurred area are marked as statistically significant conforming to the defined function. If there is some noise added in, some voxels in the blurred area, which have similar or smaller amplitude to the amplitude of noise, will not be included in the highlighted zone again, no matter how low the probability threshold is.

In our experiments, same probability threshold, which was 0.01, was used for each dataset. This made the area of marked zone change a lot: the higher amplitude of the noise, the smaller the highlighted zone. How to choose a suitable probability threshold for different datasets is an important topic that needs to be investigated in future work.

Besides the probability threshold, there is another threshold used in SPM analysis: voxel value threshold. By using the value threshold, voxels whose value are less than this threshold will not be included in the statistical calculation. In the preceding tests, the voxel value threshold was set as "-Inf" (see table 3.2), which means all the voxels in the simulated dataset are included in the statistical analysis. If the previous explanation about the change of highlighted area in the test results is correct, adjusting the value threshold hopefully can enclose the highlighted region in the first dataset. Therefore, another set of tests were conducted by specifying the value threshold to "ten percent of the maximum value". Figure 3.7 shows the updated test results.

Comparing the two result sets, it is easy to find out that the most significant change occurred in the first dataset: a well defined area was marked by SPM in the second set of test. No obvious changes happen to results corresponding to other datasets. The central voxel (rounded centroid position) of each highlighted region in the second set of test is

listed in table 3.5. Similar to the first set of experiments, the percentage variations for all centroids are less than 5%.

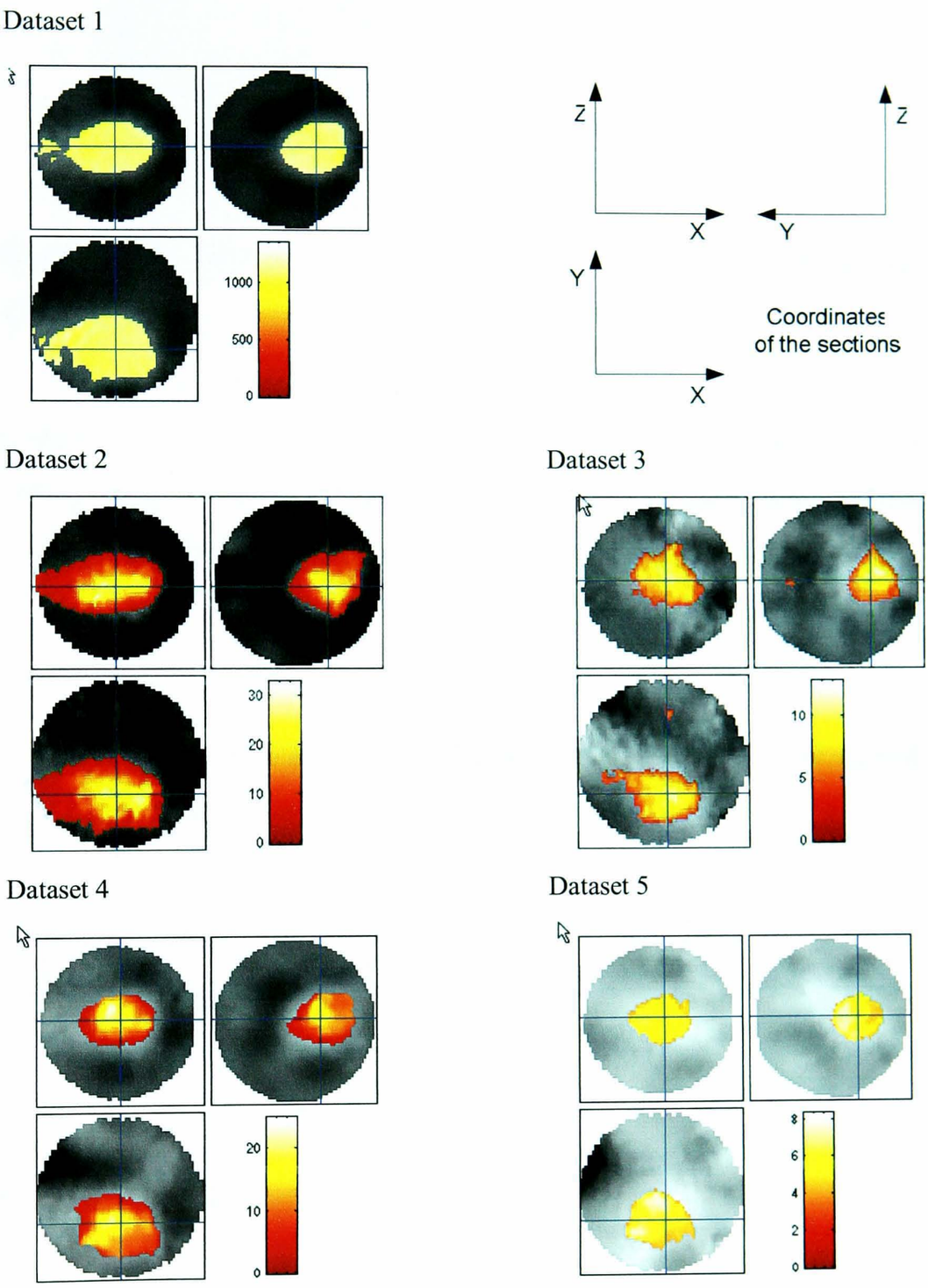

Figure 3.7 Statistical processing results set II

Table 3.5: Analysis of centroids in results set 2

Dataset No.	Centrol Voxel	Variation	Percent
Dataset 1	(-37,9,1)	(3,9,1)	4.5%
Dataset 2	(-39,-8,0)	(1,-8,0)	4%
Dataset 3	(-42,-6,-3)	(-2,-6,-3)	3%
Dataset 4	(-37,-3,2)	(3,-3,2)	1.5%
Dataset 5	(-42,-3,0)	(-2,-3,0)	1.5%

3.4.2 Experiment with Human Visual Stimulation Reconstructed EIT Images

The preceding section demonstrated with simulated datasets that it is reasonable to utilize SPM to analyze brain EIT images according to the proposed scheme. In this section, a further verification is conducted by using SPM to analyze human brain EIT data.

3.4.2.1 Introduction to the Human Visual Stimulation Reconstructed EIT Images

Before the analysis of human brain EIT data with SPM, the procedure about how the boundary impedance data is obtained and the image data is reconstructed are depicted below.

3.4.2.1.1 Boundary Impedance Data Acquisition

The used human brain EIT data was obtained with a modified HP4284A impedance analyzer from subjects during visual stimulation. This data was previously published and more details can be found in Tidswell's paper (Tidswell, Gibson et al. 2001b). In the

following, a simple introduction on how the boundary impedance data was collected is given.

The visual stimulation experiment lasted 6min and 15sec with a scalp impedance dataset acquired every 25sec. This allowed 15 EIT image datasets to be acquired. The visual stimulus was presented for 75sec in each experiment through the observation of a 0.6° checkerboard oscillating at 8Hz on a black and white monitor placed 70cm in front of the subject. Baseline conditions before and after the stimulus were darkness. 14 subjects took part in this experiment, while one recording was rejected from further analysis due to excess noise from movement artefact.

3.4.2.1.2 Image Reconstruction

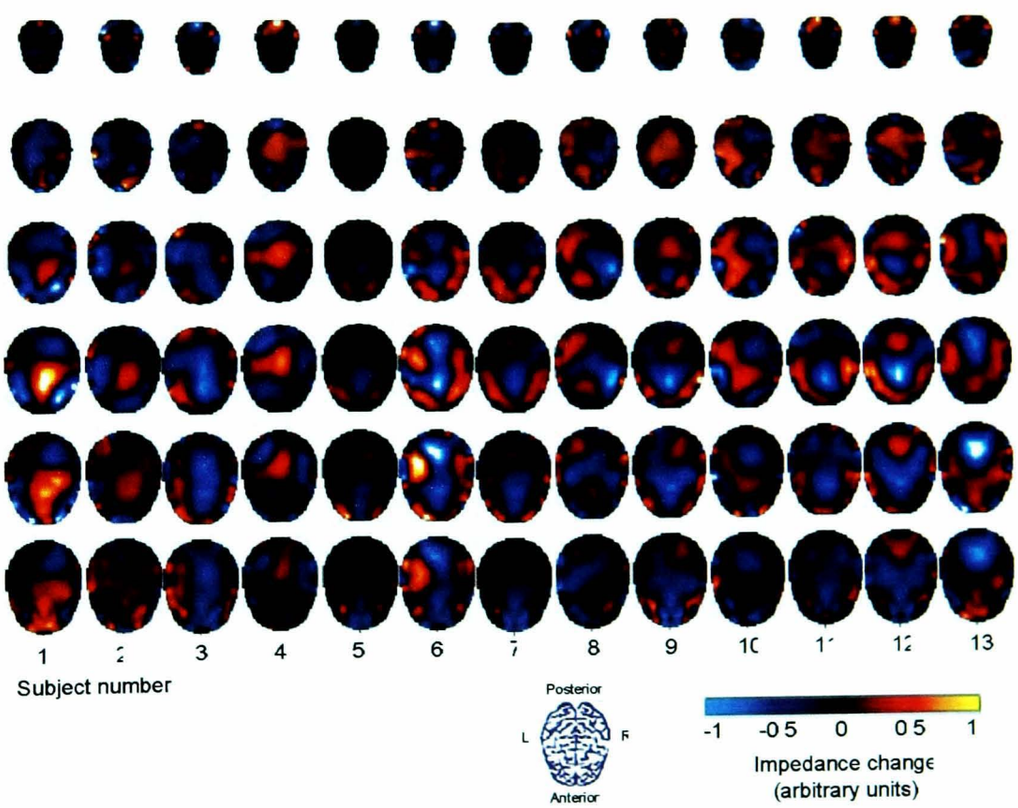

Fig 3.8 Re-reconstructed human brain EIT images for the ninth frame of 13 subjects

In the original paper, Tidswell (Tidswell, Gibson et al. 2001b) reconstructed EIT images from the acquired boundary impedance data with human head modelled as a

homogeneous sphere. With the technology development, advanced reconstruction algorithms for EIT imaging of brain function have been proposed, e.g., reconstruction algorithm with human head modelled as a concentric sphere (Liston 2004), reconstruction algorithm with human head modelled as an anatomically realistic mesh (Bayford, Gibson et al. 2001; Bagshaw, Liston et al. 2003), and nonlinear reconstruction algorithm (Horesh, Bayford et al. 2004; Yerworth, Horesh et al. 2004). The EIT images used in this analysis were obtained by re-reconstructing the boundary impedance datasets collected by Tidswell with human head modelled as an anatomically realistic mesh. Figure 3.8 illustrates the re-reconstructed images for the ninth frame of 13 subjects.

3.4.2.2 Hemodynamic Model and Design Matrix for the Human Brain EIT Images

Principally, during visual stimulation, the visual cortex is active and so more blood is needed in that area. An increase of regional Cerebral Blood Volume (rCBV) will decrease cortical impedance because blood has a lower impedance than the surrounding cortex (Ranck 1963; Geddes and Baker 1967). Ideally, EIT should be able to reveal these impedance changes in that area. However, according to Tidswell's analysis based on the originally reconstructed images, only in 9 out of 13 subjects, significant impedance changes (which means the impedance changes roughly coincide with the experimental condition changes) were seen in areas near the visual cortex. And impedance changes in 4 out of the 9 subjects are increased, which cannot be explained by blood volume increase (Tidswell, Gibson et al. 2001b). Although the algorithm used in re-reconstructed generally performs better than the original one, no significantly improved conclusion can be drawn based on the re-reconstructed images.

Several factors affect the accuracy of EIT imaging: the noise introduced by the imaging instrument; the inaccurate modelling of the head; temporal blurring of the impedance

response in the images, and so on. Generally, statistical analysis methods are good at dealing with random events and processes, they are ideal to be used to model the mechanisms that cause image degradation and enable a more reliable detection of changes in brain. Based on the positive results obtained by processing simulated brain EIT images in SPM, further analyse is conducted to analysis these human brain EIT datasets with SPM.

Following the methodology proposed in section 3.3, PET mode is adopted in this analysis. Although PET mode is not accessible for the hemodynamic modelling function for BOLD signal measured with fMRI, the blood volume function calculated by Balloon Model can be enclosed in PET analysis mode as a covariate in the Design Matrix. As a contrast, another Design Matrix is applied in the experiment, which uses stimulus function instead of the blood volume function as a covariate. In the following, experiments using Design Matrix including stimulus function is mentioned as experiment series I, and the experiments using Design Matrix including blood volume function is named experiment series II. Other main parameters used in the experiments were set as shown in table 3.6.

Table 3.6: Parameters setting for the test of human brain EIT datasets

Analysis Setup ...		
	Threshold	-Inf
	Global calculation ...	Mean voxel value
Results Setup ...		
	Mask with other contrast(s)	no
	Threshold (T or p value)	0.1
	& extent threshold (voxels)	1
	Visualisation overlays...	sections

After the definition of Design Matrix, statistic estimation can be carried on within SPM. According to the scheme suggested in section 3.3.1, before the statistical inference, error terms should be calculated and test on their distributions should be executed, and the Design Matrix should be adjusted if necessary. While, within the human brain EIT

datasets, only 15 sample values are available for each error term. This sample size is too small for any method to effectively test if a population confirms to a certain distribution. Therefore, the distribution tests for error terms have to be ignored, and statistic inference is conducted directly after statistic estimation.

3.4.2.3 Statistical Inference Results and Discussion

As for the simulated data, the inference results of human brain EIT data are displayed by overlaying them on orthogonal sections of the processed data. Figure 3.9 illustrates the results, where the human brain EIT images are presented in greyscale in three orthogonal planes and the areas highlighted by SPM are superimposed in colour.

From the experimental results, it can be observed that, when using stimulus function as a covariate, four out of thirteen subjects (subject number 1, 2, 6, 10) appear to have explainable impedance change near the visual cortex area; and when using blood volume function as a covariate, seven out of thirteen subjects (subject number 1, 2, 4, 6, 9, 10, 13) appear to have explainable impedance change near the visual cortex area. Tidswell (Tidswell, Gibson et al. 2001b) once described that, in five out of thirteen subjects, explainable impedance changes were seen.

Tidswell's conclusion was drawn only based on individual observation of time-series images. In our experiments, explainable impedance change areas were deduced basing on a statistical criterion, as mentioned above, the threshold probability is fixed as 0.1 for all subject and both series of experiments. Comparing with experiment series I, sensible ROIs are revealed for more subjects (subject number 4, 9, 13) in experiment series II. Turning to the subjects whose ROIs have been detected in both series of experiments (subject number 1, 2, 6, 10), the regions highlighted in experiment series II are generally more significant, referring to the functional area definition of human brain (see figure 3.8). As a whole, it is reasonable to conclude that, with properly defined Design Matrix,

SPM is suitable to reveal ROIs in human brain EIT images. Furthermore, it seems correct to use balloon hemodynamic change model to simulate the impedance change during brain function activity.

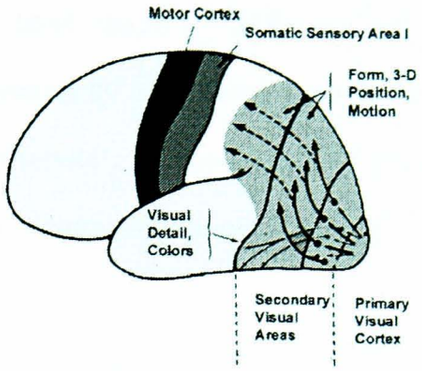

Figure 3.8 Functional area of human brain

It is also noticed that, in datasets for six subjects (subject number 3, 5, 7, 8, 11, 12), there are no regions near visual cortex, or even no regions in the whole brain, have been marked as explainable ROIs in both experiment series. Even for the explainable ROIs highlighted in the seven subjects, there are some differences between those ROIs and the visual cortex in human brain. Many factors may account for this failure. First of all, the data adopted in our experiments is not up-to-date. Those data was measured by HP 4282A analyzer, which is not an instrument specially designed for brain EIT imaging and can only obtain an image every 25sec. According to the hemodynamic model (balloon model), the blood volume change caused by normal function in the brain almost comes back to baseline in 20sec. So, the low temporal resolution will affect the efficiency of blood volume function used in the Design Matrix. While, unfortunately, these data are the only available human brain EIT data for this research. However, there is no reason to say that the EIT imaging did not detect activations occurred in the visual cortex during the visual stimulation experiment.

Secondly, although the data used in the experiments are re-reconstructed with a relatively new algorithm, the quality of the new EIT images is still not very satisfactory. The reason is twofold. On the one side, the collected boundary impedance data is rough,

as mentioned in the Chinese old saying, "Even the smartest housewife cannot cook without rice". On the other side, although the new reconstruction algorithm models human head as an anatomically realistic mesh instead of a homogenous sphere, it does not consider the difference head shape of different individuals. So, if the measured impedance change were produced by impedance changes in the expected site of cortical activity, the inaccurate reconstruction algorithm, electrode positioning errors, system errors of the instrument, and measurement noise, can all cause errors of localisation in the final images.

Thirdly, instead of the assumption that visual stimulus will increase rCBV in visual cortex and therefore decrease the impedance value in that area, the patterns of human cortical impedance changes under visual stimulus may be complex; perhaps there are multiple impedance changes due to cell swelling, increased rCBV and decreased rCBV within and away from the functionally stimulated cortex. Considering the low spatial resolution, EIT images represent a combination of multiple changes. Consequently, these multiple changes might not be independently localized; or other functions, which can precisely describe these situations, should be included in the Design Matrix.

Subject Number	Results with experimental condition used as a covariate	Results with blood volume function used as a covariate
1	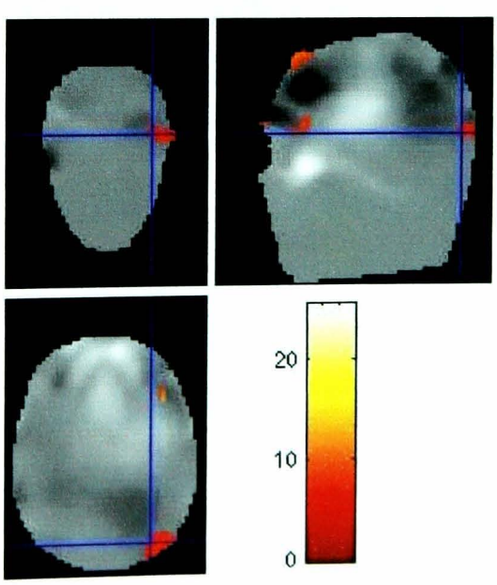	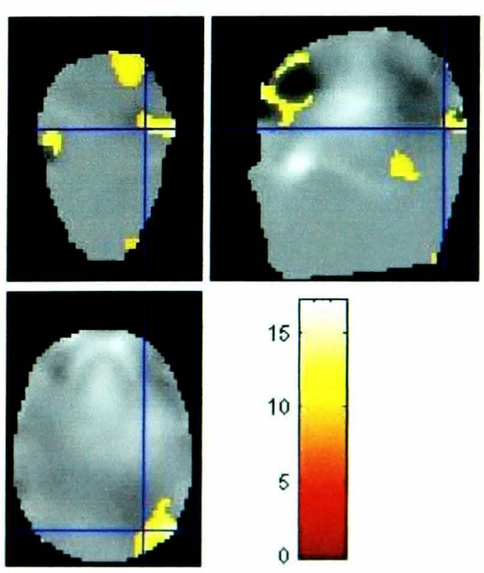

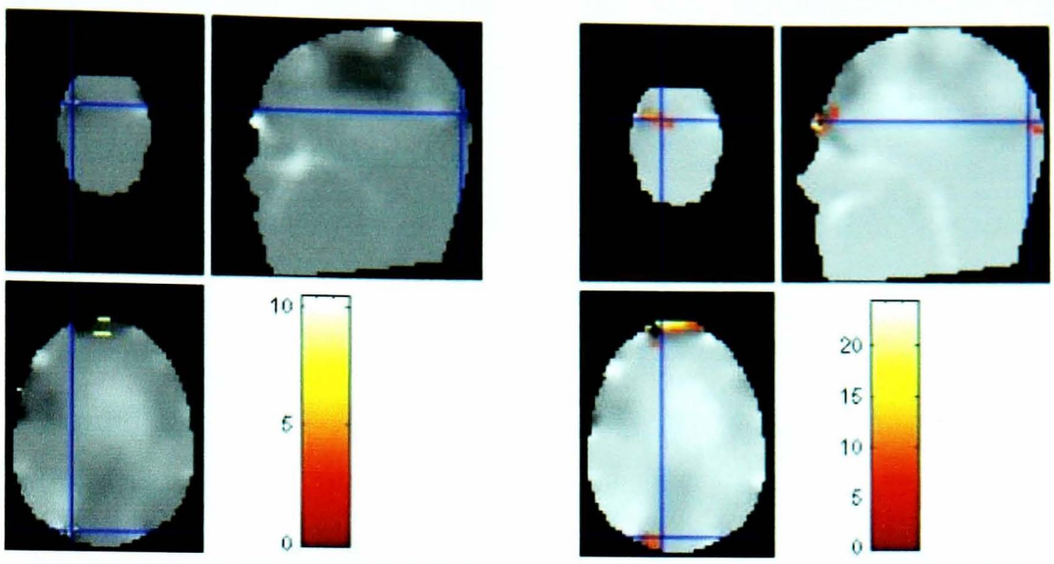

2

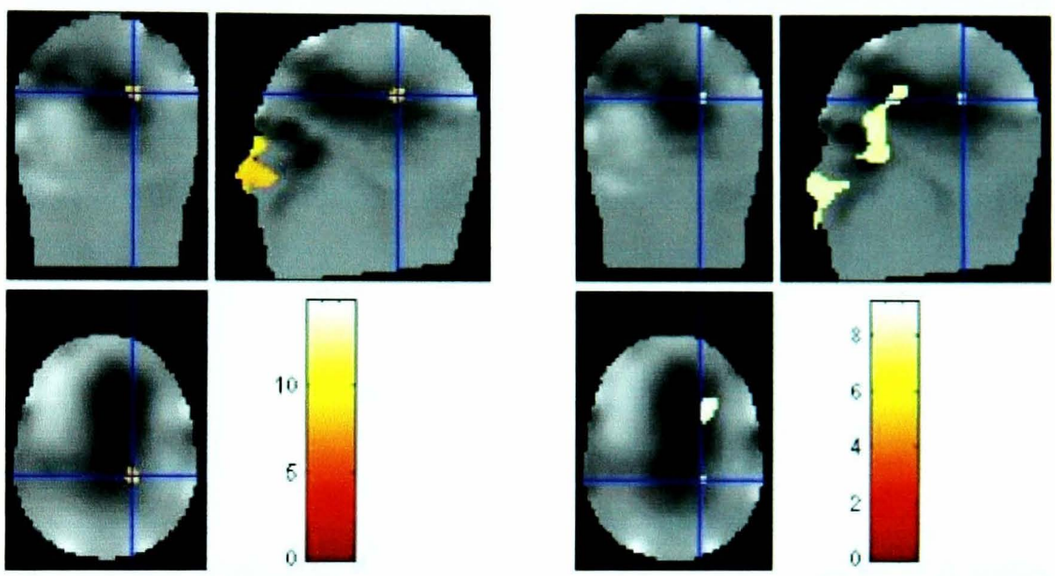

3

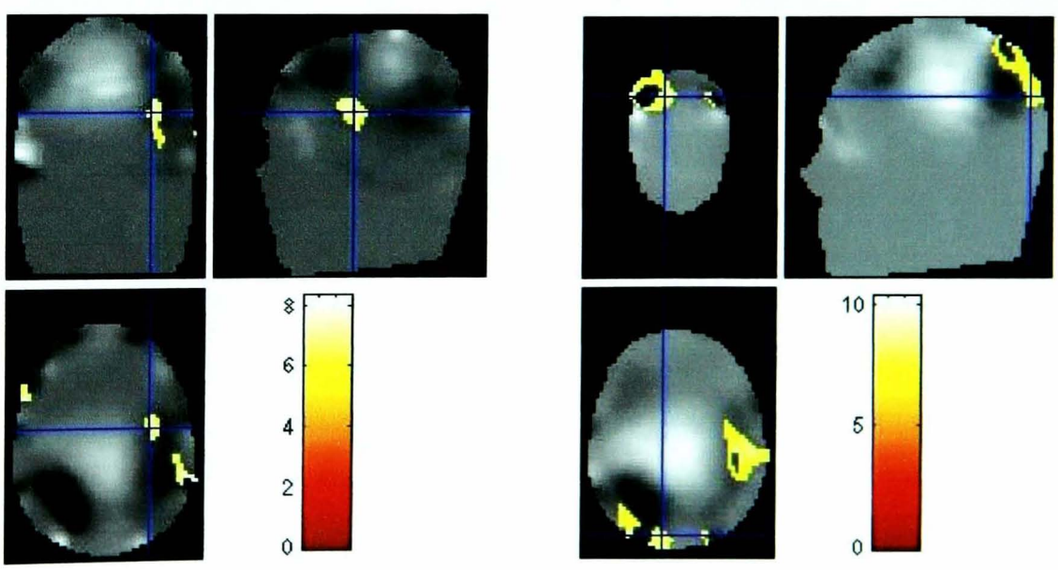

4

5

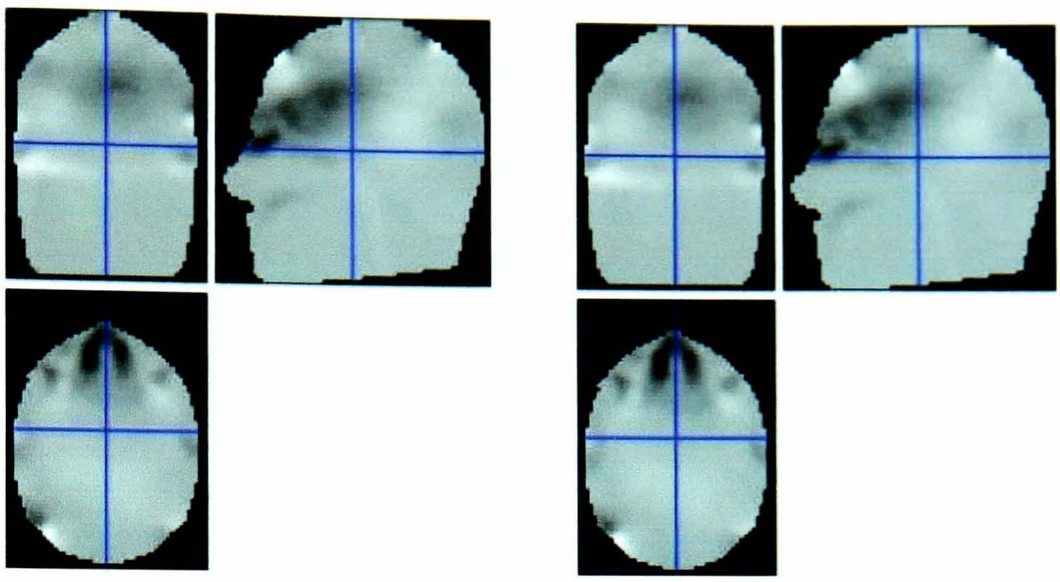

6

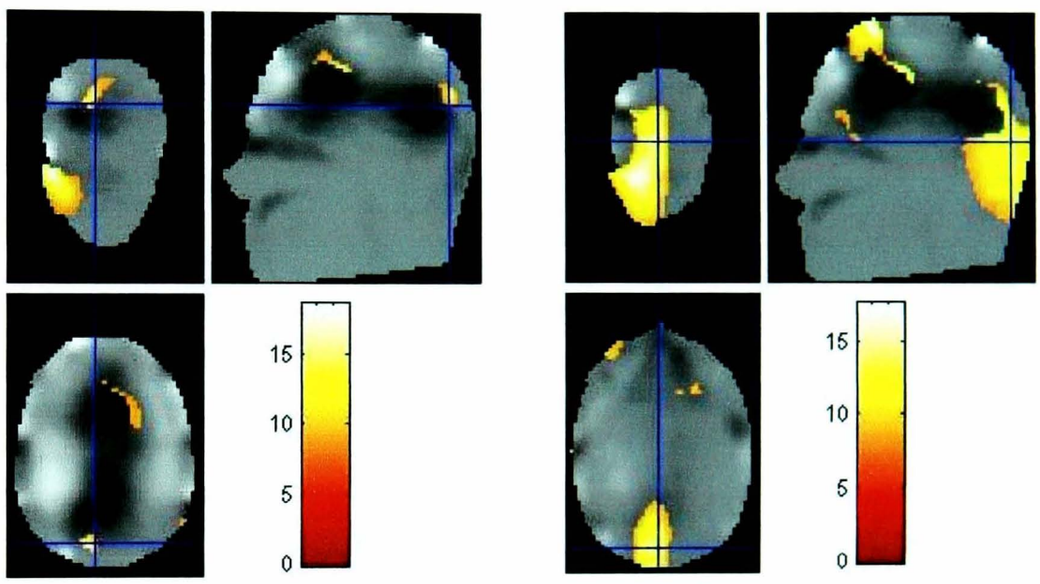

7

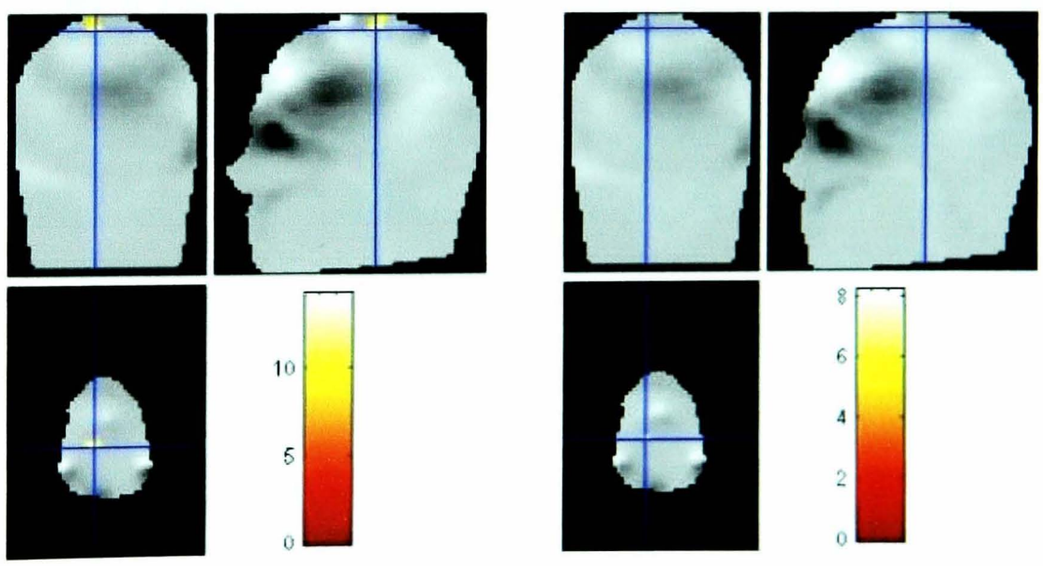

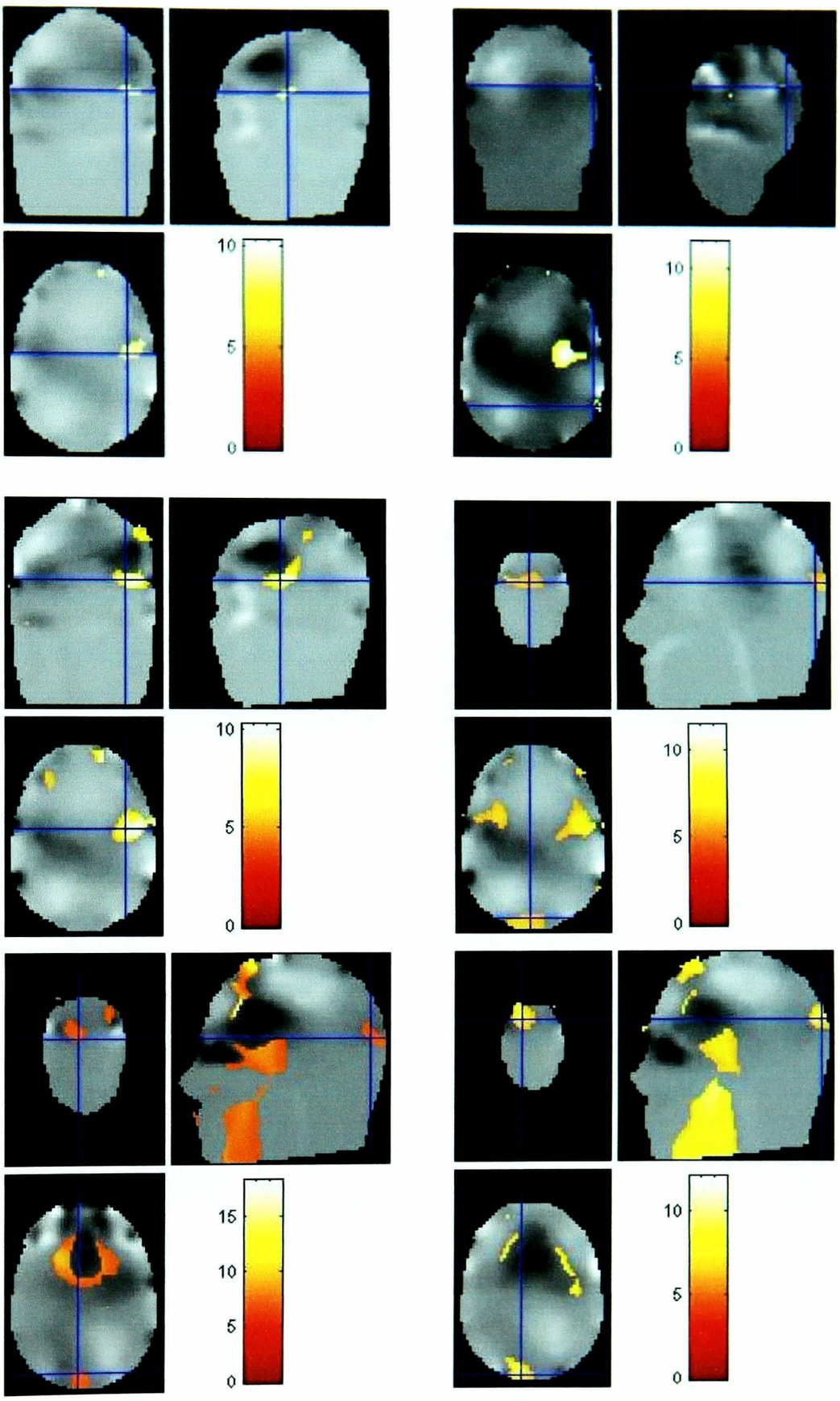
8
10
5
0
9
10
5
0
10
15
10
5
0
10
5
0

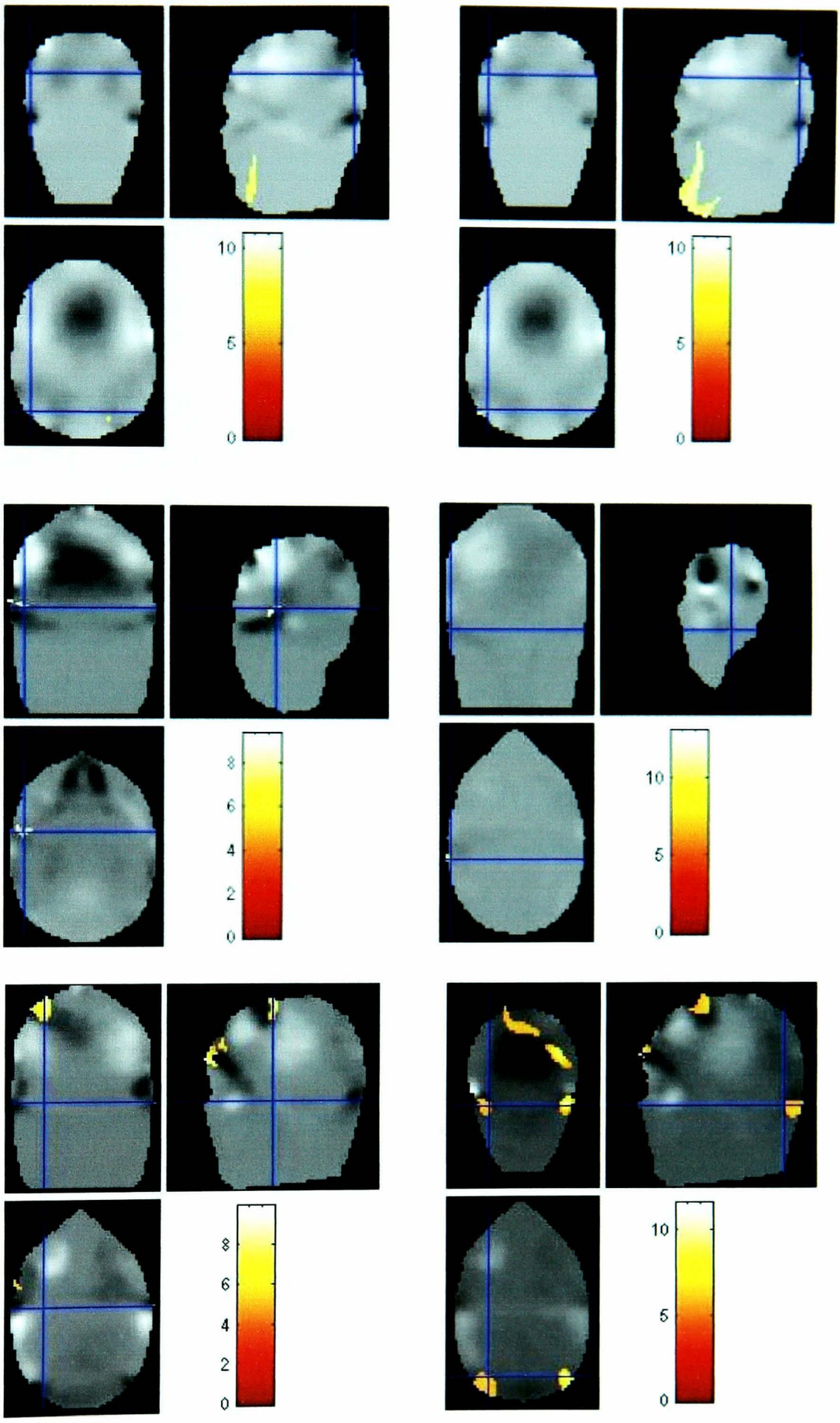

Figure 3.9 Statistical processing results for human brain EIT datasets

3.5 Conclusion

This chapter aimed to achieve the first objective of this research: to propose a method to define ROI in functional brain EIT images. An introduction of statistical processing for functional medical images and SPM techniques is presented first. Then a new scheme for the processing of four-dimensional temporal-spatial brain EIT data with SPM to detect ROI in the data is proposed based on a theoretical analysis in section 3.3. To evaluate the feasibility of this scheme, two types of experiments are carried out: one is implemented with simulated EIT data, and the other is performed with human brain EIT data under visual stimulation. The experimental results demonstrated two facts: SPM is able to localise the expected ROI correctly; it is reasonable to use balloon hemodynamic change model to simulate the impedance change during brain function activity.

Chapter 4 Registration of Brain EIT Images with Anatomical Brain Data

4.1 Introduction

Image registration is a fundamental task in image processing used to overlay two (or more) images taken, for example, at different times, from different viewpoints, and/or by different sensors. Medical image registration has been widely studied and utilized in four main kinds of applications: combining information obtained from different imaging modalities; aligning temporal sequences of images for monitoring changes in size, shape, or image intensity over time intervals that might range from a few seconds to several months or even years; relating preoperative images and surgical plans to the physical reality of the patient in the operating room during image-guided surgery or in the treatment suite during radiotherapy; and relating images from different subjects to a standard atlas for cohort studies (Hill, Batchelor et al. 2001).

As described in section 1.1.2, EIT imaging is a relatively new medical imaging method with high temporal resolution and poor spatial resolution. Little anatomical information is included in EIT imaging dataset. Clinicians usually have abundant knowledge about human morphology; the understanding of EIT images could be enhanced by visualising EIT imaging data in an anatomical context. Therefore, to develop a registration scheme

to combine human morphology information with brain EIT images is the second objective of this research. The work presented in this chapter aims to achieve this objective.

Following this introduction, the next section of this chapter is an overview of medical image registration; then a scheme for the registration of brain EIT images with an anatomical brain dataset is proposed; next, experiments are described and discussion based on the experimental results is conducted; finally, a conclusion of this chapter is drawn.

4.2 Overview of Medical Image Registration

Generally, medical image registration is realized in three steps: first, a number of features are selected from the images and correspondence is established between them; then a transformation function is determined; finally, with the estimated transformation function, one image is transformed and resampled to align with the other one. Over the years, a broad range of registration techniques have been developed, which can be categorized with respect to various criteria. A criterion, which is adopted in this overview, is the features that algorithms are based on. Features used in registration can be sorted into two main groups: *geometric features* and *voxel intensity*. Consequently, registration algorithms can be classified into geometric feature based registration methods or voxel intensity based registration methods.

4.2.1 Geometric Feature Based Registration Methods

The most widely used geometric features in registration are points and surfaces, though lines and extreme points identified using differential geometric operators are also used. Landmark-based, or point-based, registration involves identifying corresponding points

in the images to be aligned, registering the points and inferring the image transformation from the transformation determined from the points. Landmark-based registration is versatile in the sense that it, at least in theory, can be applied to any image, no matter what the object or subject is. The difficulty of this kind of method is the identification of corresponding landmarks, which is a segmentation procedure technically, and usually requires some user interaction.

In surface-based registration, the surfaces are commonly represented by a set of points, contours drawn on a series of slices, or many triangular patches. The registration transformation is determined by iteratively transforming one surface or each point on one surface until the best match is found by some criteria. 'Head-and-hat' algorithm (Levin, Pelizzari et al. 1988; Pelizzari, Chen et al. 1989) and Iterative Closest Point (ICP) algorithm (Besl and McKay 1992) are two most famous surface-based registration approaches. Surface-based registration uses more of the available data than landmark identification, and supposes to be more robust and accurate. However, this kind of algorithm is sensitive to starting positions, and maybe prone to choose wrong solutions or local minima.

Deformable model based registration is another type of geometric feature based registration approach. 2D deformable models, i.e., deformable curves, appear in literature as *snakes* or *active contours*; 3D deformable models are sometimes referred to as *nets*. Deformable model based registration makes use of energy to describe the distortion in images. The registration is achieved by locating the minimum energy state in an iterative fashion. To ease the physical modelling, the data structure of deformable models is often represented using localized functions such as splines, instead of a point set. Deformable models are best suited to find local curved transformations between images, and less so for finding (global) rigid or affine transformations. Deformable models are in theory very well suited for inter-subject and atlas registration. A drawback

of deformable models is that they often need a good initial position in order to properly converge, which is generally realised by (rigid) pre-registration of the images involved.

4.2.2 Voxel Intensity Based Registration Methods

Voxel intensity based registration methods calculate the registration transformation directly from the voxel intensity values in the images rather than from geometrical structures derived from the images. The first and most important step in this kind of registration is to measure voxel similarity between the images. With the similarity measure, an optimization algorithm is used iteratively to find the transformation that maximizes or minimizes the value of the measure, as appropriate.

SSD (Sum of Squared intensity Difference) and SAD (Sum of Absolute Difference) are two commonly used similarity measures in the earliest voxel intensity based registration methods. The SSD and SAD measures make the implicit assumption that after registration, the images differ only by Gaussian noise. During the registration process, alignment is adjusted until the smallest SSD or SAD is found. CC (Correlation Coefficient) is a basic statistical similarity measure for registration. CC-based registration assumes that there is a linear relationship between the intensity values in the images. During the registration course, one image is moved with respect to the other until the largest value of the correlation coefficient is found. SSD, SAD, and CC all can just be used to measure voxel similarity between images from same modality.

PIU (Partitioned Intensity Uniformity), which was proposed by Woods et al. (Woods, Mazziotta et al. 1993), is the first successful application of a voxel similarity based algorithm to the registration of images from different modalities, although it has never been widely applied for registration other than MRI–PET images. PIU algorithm assumes that "all pixels with a particular MR pixel value represent the same tissue type so that values of corresponding PET pixels should also be similar to each other". It

partitions the MRI image into 256 separate bins based on the intensity value of the MRI voxels, and then seeks to maximize the uniformity of the PET voxel values within each bin.

By thinking of registration of images as attempting to maximize their shared information, measure of information can be used as a registration metric. A typical example of this kind of metric is MI (Mutual Information), which was originally introduced by Shannon (Shannon 1948) and proposed for intermodality medical image registration by researchers in Leuven, Belgium (Collignon, Maes et al. 1995; Maes, Collignon et al. 1997)) and MIT in the USA (Viola 1995; Wells, Viola et al. 1996) simultaneously and independently. MI can qualitatively be thought of as a measure of how well one image explains the other, and is maximized at the optimal alignment. MI measure is broadly used in various image registration problems. Particularly, in multimodality medical registration, MI technique has become a standard reference (Zitova and Flusser 2003).

4.3 A Scheme for the Registration of Brain EIT Images with an Anatomical Brain Dataset

As pointed out at the beginning of section 4.2, image registration starts from feature selection. However, as a prerequisite, the images to be registered should be decided initially. Therefore, before the discussion on feature selection and registration scheme, the first part of this section aims to pick up a suitable anatomical brain atlas for EIT images.

4.3.1 The Anatomical Brain Atlas

The motivation of registering EIT images with another imaging dataset is to deal with the absence of anatomical information in EIT imaging. There are two questions which require answering in the selection of the anatomical image dataset. First, which modality should the dataset be imaged from? Secondly, with a selected imaging modality, which dataset should be adopted in the registration?

In section 1.1, various anatomical medical imaging modalities have been introduced. Among those modalities, both CT and MRI can provide good structure information of human body with millimetre resolution. Furthermore, images obtained from CT scan include high quality information about bones, but not suitable for tissue visualisation. However, different tissues can be identified more clearly in images obtained from MRI imaging than those from CT, although MRI images are less sensitive to changes inside bones. Human brain is composed within the skull of different tissues, such as, grey matter, white matter and CSF (Cerebral Spinal fluid) functional activities revealed by brain EIT imaging generally appear in the tissues. Therefore it is more suitable to choose MRI images as an anatomical context in the visualisation of brain EIT images.

Beside millions of clinical MRI images stored in different hospitals all over the world, there are various MRI datasets that have been applied as reference data on different occasions, such as, MRI dataset for the Digital Human, Montreal BrainWeb reference datasets. In this research, a high-quality high-resolution Montreal BrainWeb reference dataset is adopted as the MRI brain atlas. The advantages of Montreal BrainWeb reference dataset over other MRI reference data is that, this MRI dataset is created by simulation, so it avoids the distortion which is usually found in MRI imaging (Collins and Zijdenbos 1998). Montreal BrainWeb reference datasets have been widely used as a standard reference data ("ground truth") for anatomical brain mapping and quantitative brain image analysis methods. From another point of view, once the modality of the

anatomical atlas is decided, the selection of particular atlas dataset has limited effect on the registration scheme. That is to say, same scheme can be used to register brain EIT images with different MRI reference dataset with minor adjustments.

Currently, the BrainWeb contains simulated brain MRI data based on two anatomical models: a normal one and the one with multiple sclerosis. For both of these, full 3D volume data have been simulated using three sequences (T1-, T2-, and PD(Proton Density)- weighted) and a variety of slice thicknesses, noise levels, and levels of intensity non-uniformity. The dataset applied to this research is from its normal brain model, with parameters set as: Modality = T1, Intensity Non-Uniformity = 20%, Noise = 3%, Phantom_name = normal, Slice_thickness = 1mm, and Protocol = ICBM.

4.3.2 Feature Selection

As described in section 4.2, features used in medical image registration can be grouped into two kinds: geometric features and voxel intensity. Different features are suitable for different situations. Generally, geometric feature based registration methods are recommended when the local structural information is more significant than the information carried by the image intensity. They allow registering images of completely different nature and can handle complex between image distortions. On the other side, voxel intensity based registration methods use the full image context instead of relatively sparse extracted information throughout the process. They are theoretically more flexible and can avoid the difficulty to detect the respective features. Furthermore, MI (Mutual Information) technique, which is specific voxel intensity based registration method, has become a standard reference in multimodal medical registration.

Considering the significance of MI technique in multimodality medical registration, it is attractive to apply MI technique in the registration of brain EIT images and MRI reference dataset. Mutual information measures the statistical dependency between two

datasets. It can be thought of as a measure of how well one image explains the other, and is maximized at the optimal alignment. Because of the low spatial resolution in EIT images, currently, it is almost impossible to "explain" the anatomical information included in MRI images with the functional impedance information included in EIT images, and vice versa. That is to say, it is very difficult to register EIT and MRI with MI technique by optimizing the statistical dependency between their voxel intensities. Other voxel similarity measures like SSD, SAD, and CC assume that images differ only by Gaussian noise or a linear relationship between the intensity values in the images. They cannot be used to measure the voxel similarity between images from different modalities. In brief, voxel intensity is not a suitable feature for the registration of brain EIT images and MRI reference dataset. Therefore, geometric features will be used in this registration.

Voxel intensities in EIT image represent the impedance change or absolute impedance value with a poor spatial resolution. It is very difficult to use those intensities as a registration feature directly. Moreover, it is hard to select any geometric meaningful features inside the brain in an EIT image and find out their correspondences in a MRI image. However, there is some geometric information that can be traced on the brain surface in EIT images. As mentioned in section 1.1.2, EIT imaging for human brain is conducted with electrodes attached to scalp (as shown in figure 1.3). Currently, thirty-one electrodes are used in brain EIT imaging (as illustrated in figure 4.1). Twenty-seven of the thirty-one electrodes, which will be called *twenty-seven system electrodes* later, are located according to the international 10-20 system for EEG electrode placement (Binnie, Rowan et al. 1982). The fundamental of the 10-20 system is the positions of *four basic fiducial points*: nasion, inion, left preaurical point, and right preaurical point. The other four in the thirty-one electrodes, which will be called *four additional electrodes*, are added to optimize current distribution in the brain: two of them are placed on the mastoid bones behind each ear, and the other two are placed over the base of the occiput. The positions of those thirty-one electrodes and the four basic fiducial

points are projected on the surface of the head mesh used in the reconstruction algorithm. EIT reconstruction produces volumetric impedance data wrapped by the head mesh. The impedance value at each voxel in an EIT image dataset is obtained by rasterising the corresponding volumetric impedance data. There is a direct mapping between the coordinates used in the head mesh and the reconstructed image dataset: the axes in the two coordinates have same directions but different units. So, with the positions of the thirty-five landmarks on the head mesh, it is relatively easy to identify the position of those landmarks in EIT images. Then, the next question is whether it is possible to identify positions corresponding to the thirty-five point features in MRI images.

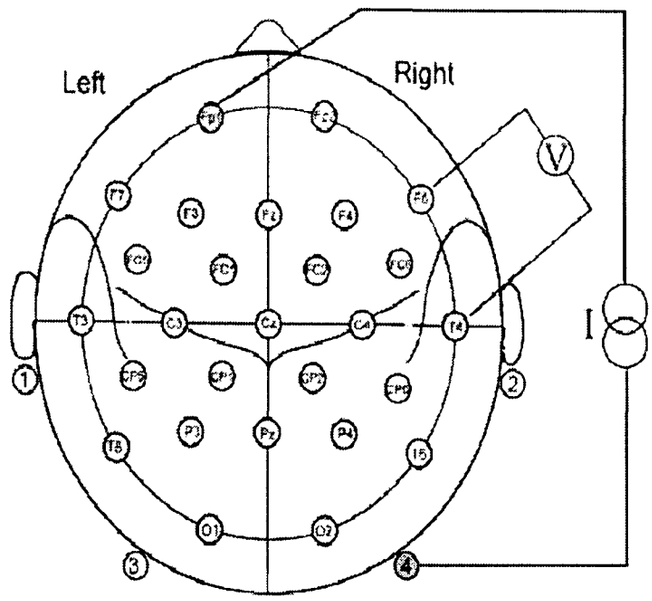

Figure 4.1 Electrode distribution in brain EIT imaging

Viewed from above the head. The electrodes taken from the International 10-20 system are labelled according to that system. The four additional electrode positions are labelled with 1-4 separately.

Among the thirty-five point features, the four additional electrodes and the four basic fiducial points for the 10-20 system, have clearly defined anatomical location. Considering the rich anatomical information included in MRI images, it is possible to identify these eight features in MRI images. After the recognition of the four basic

fiducial points, corresponding positions for the twenty-seven system electrodes can be located in MRI images consequently according to the rules of the 10-20 system.

In summary, registration of EIT images and MRI atlas can be conducted based on landmark features. The potential landmark features for this registration include the thirty-one electrode positions used in brain EIT imaging and the four basic fiducial points in the 10-20 system.

4.3.3 The Registration Scheme

After the decision of features to be employed in the registration of EIT images and MRI reference dataset, this section intends to propose a scheme for this registration.

According to the approaches to locate the point features in MRI image, the set of those points $P = \{p_i : (i = 1, \cdots 35)\}$ can be grouped into two subsets: points in subset $P_A = \{p_A^m : (m = 1, \cdots 8)\}$, which include the four basic fiducial points in 10-20 system and positions used for the four additional electrodes in the EIT imaging, can be segmented out from MRI images; anatomical location corresponding to points in subset $P_B = \{p_B^n : (n = 1, \cdots, 27)\}$, which include the twenty-seven system electrodes, have not been obviously defined, and positions of those points have to be calculated according to the rules in the 10-20 system. Considering this difference existed in the point features, a two-level landmark-based registration scheme is proposed and illustrated in figure 4.2.

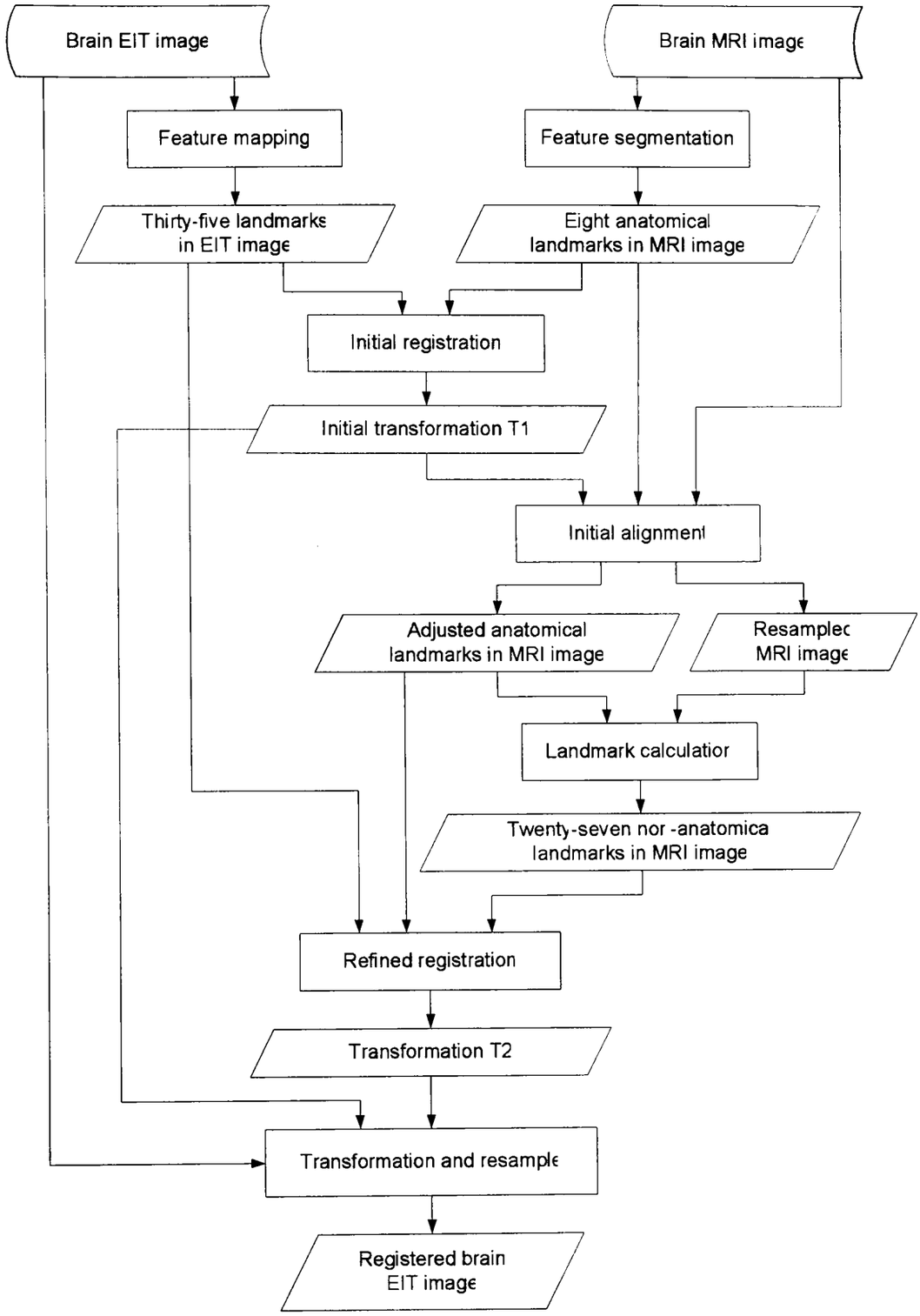

Figure 4.2 The landmark-based registration scheme

The main processes in this scheme are *initial registration* and *refined registration*. As a preparation, the positions of the thirty-five landmarks $P_{eit} = \{P_{eit,A}, P_{eit,B}\}$ in the EIT image are located by mapping their corresponding positions in the head mesh used for

reconstruction to the volumetric image space, and positions for eight landmarks in subset $P_{mri,\ A}$ are manually segmented in the MRI image. The initial registration is based on the eight pairs of landmarks in $P_{eit,\ A}$ and $P_{mri,\ A}$. An affine transformation T_1 is determined by the least-squares method in this registration. With the transformation T_1, the MRI image I_{mri} and the landmark subset $P_{mri,\ A}$ are transformed and resampled to align with the EIT image:

$$\begin{cases} P_{mri,A}{}' = T_1(P_{mri,A}) \\ I_{mri}{}' = T_1(I_{mri}) \end{cases} \tag{4.1}$$

Based on the resampled MRI image $I_{mri}{}'$ and the landmark subset $P_{mri,\ A}{}'$, the other landmark subset $P_{mri,\ B}{}'$ in the MRI image are calculated according to rules in the international 10-20 system. Up to this point, thirty-five landmarks have been identified in both EIT image and MRI image. Therefore, the refined registration is carried out with the thirty-five pairs of landmarks in P_{eit} and $P_{mri}{}' = \{P_{mri,A}{}', P_{mri,B}{}'\}$, and affine transformation T_2 is calculated by the least-squares method.

After the initial registration and refined registration, the brain EIT image I_{eit} is transformed with T_1 and T_2 and resample to align with the reference MRI image in the final step of this scheme:

$$I_{eit}{}' = T_1^{-1}T_2(I_{eit}) \tag{4.2}$$

4.4 Experiments and Discussions

In order to demonstrate the registration scheme proposed in the preceding section, some experiments have been conducted and are described below.

4.4.1 Datasets Used in the Experiment

The EIT dataset registered in the experiment is selected from the human brain EIT dataset used in section 3.4.2, where details on how data were collected have been described. Figure 4.3 presents three orthogonal slices in the EIT dataset. As mentioned in section 4.3.1, a Montreal BrainWeb reference dataset will be registered with the brain EIT image to provide anatomical information inside the brain in the visualisation. Figure 4.4 illustrates three orthogonal planes of the selected reference MRI dataset.

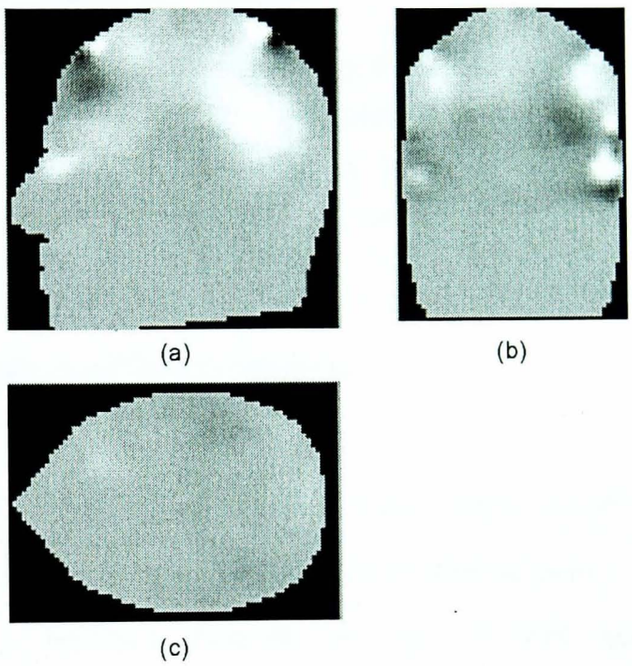

Figure 4.3 Displays of three orthogonal slices in the selected brain EIT dataset

Coordinates in the brain EIT dataset is that: x is from left to right, y is from back to front, and the z axis is from below to upper. Slice (a) is perpendicular to the x axis and crosses nasion and inion; slice (b) and slice (c) are perpendicular to y and z axes separately, and cross left and right preaurical points.

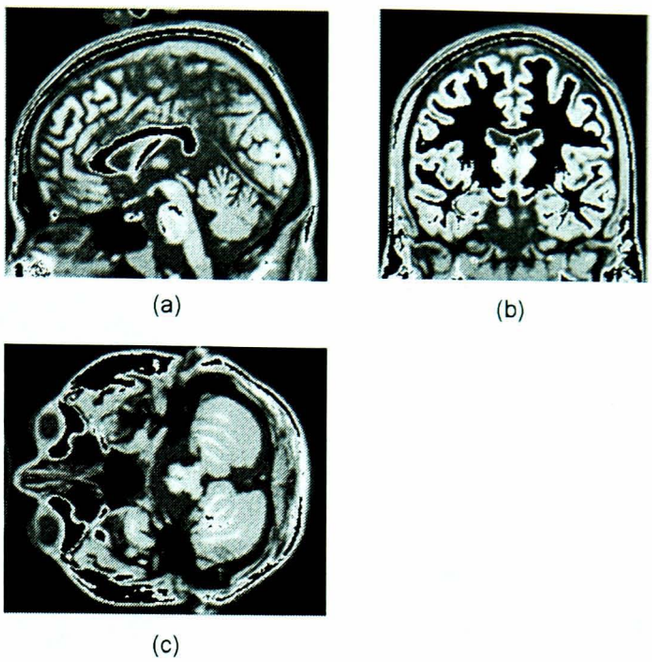

(a) (b)

(c)

Figure 4.4 Displays of three orthogonal planes in the selected Montreal BrainWeb reference dataset

Coordinates in the MRI dataset is same as the EIT dataset, and the three planes are sliced with same criteria used in figure 4.3.

4.4.2 Identification of the Features

As pointed out in section 4.3.2, to reconstruct EIT images, positions of the thirty-one electrodes used in EIT imaging and the four basic fiducial points in the 10-20 system, which compose the thirty-five landmarks for this EIT-MRI registration, have been marked on the head mesh during the reconstruction processing. Figure 4.5(a) illustrates the head mesh with positions for the electrodes coloured in red. Considering the map between coordinates in the head mesh and the reconstructed EIT dataset, it is relatively easy to identify the landmarks in EIT images. Figure 4.5(b) displays the central sagittal plane of the EIT image dataset with landmarks on this plane highlighted in green.

The eight landmarks belonging to subset $P_{mri,A}$, which have clearly defined anatomical location, in the MRI image are segmented manually by the author in this experiment.

Figure 4.6 presents positions of the four basic fiducial points on corresponding MRI slices.

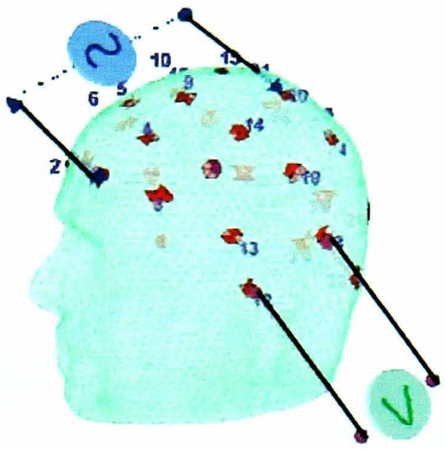

(a) Head mesh used in EIT reconstruction with positions for electrode coloured in red

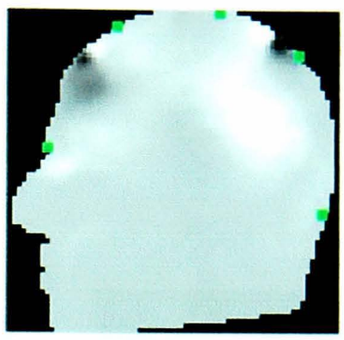

(b) Central sagittal plane in the EIT dataset with landmarks highlighted in greer

Figure 4.5 Landmarks in the EIT image

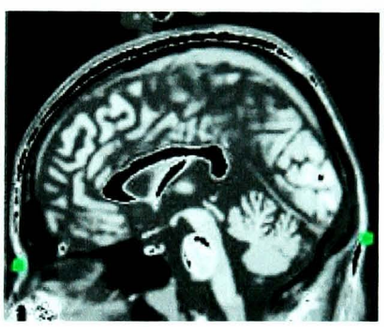

(a) Nasion and inion ir the MRI dataset

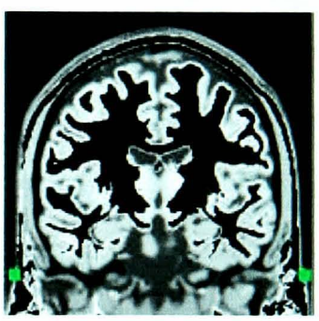

(b) Left and right preaurical points in the MRI dataset

Figure 4.6 Landmarks in MRI dataset

With the eight landmarks identified, the remaining twenty-seven landmarks in the MRI image can be calculated subsequently. However, according to the proposed registration scheme, before this calculation, an initial registration is performed to align the MRI image with the EIT image. And the landmarks in $P_{mri,A}$ is transformed to $P_{mri,A}'$. Figure 4.7 shows the result of the initial registration. Subsequently, the twenty-seven landmarks

are computed based on the transformed landmarks $P'_{mri,A}$ and the resampled MRI images I'_{mri}. Figure 4.8 illustrates landmarks on the central sagittal plane in MRI image.

Up to now, thirty-five pairs of landmarks have been identified in the EIT image dataset and the resampled MRI image dataset. According to the proposed scheme, the next step is to perform the refined registration with these landmark correspondences.

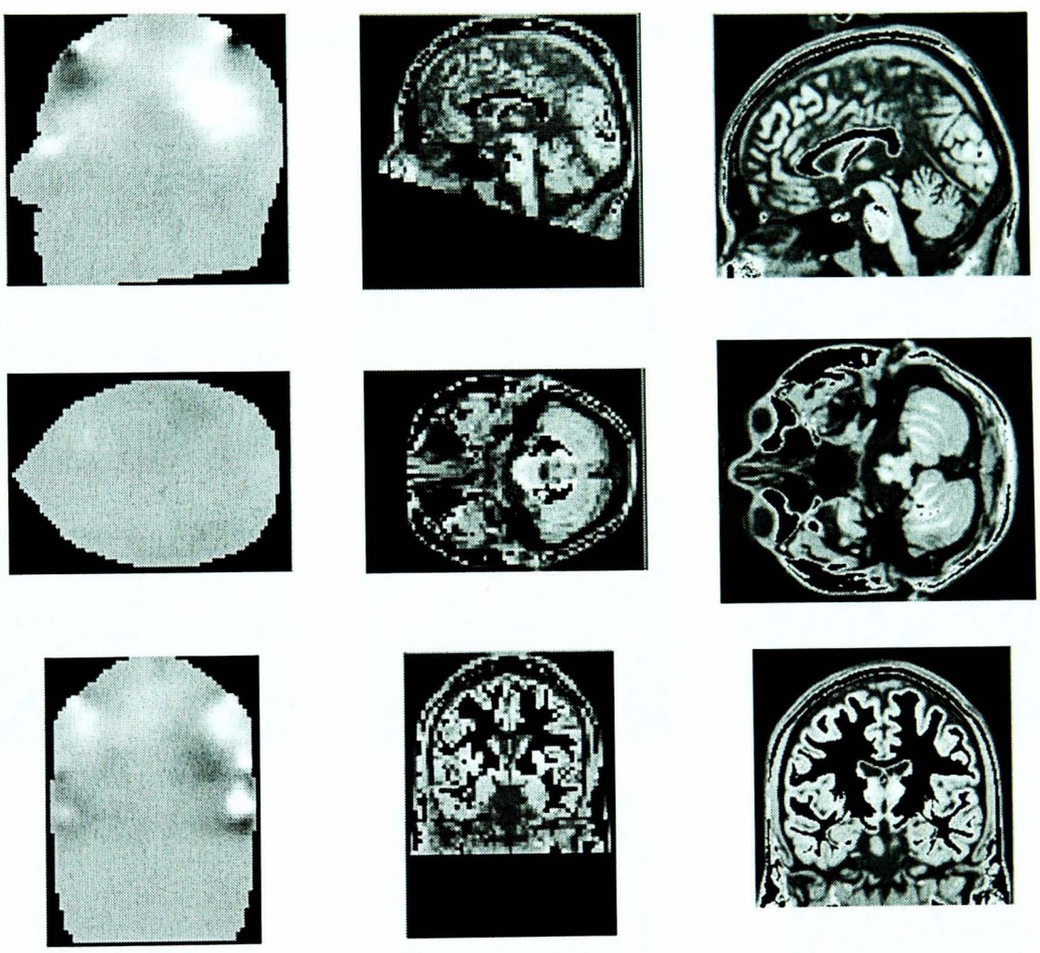

(a) Slices from the EIT dataset

(b) Slices from the MRI dataset after intial registration

(c) Slices from the MRI dataset

Figure 4.7 Demonstration of the initial registration results

Slices in different columns are from different image dataset; Coordinates in those datasets are defined as: x is from left to right, y is from back to front, and z axis is from below to upper. Slices in the first row are perpendicular to x axis and cross nasion and inion; Slices in the second and the last row are perpendicular to y and z axes separately, and cross left and right preaurical points.

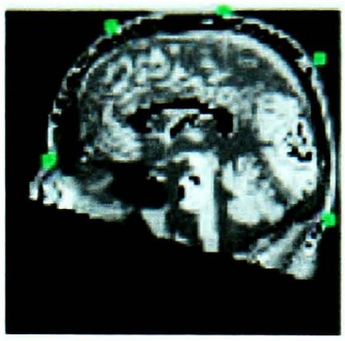

Figure 4.8 Landmarks on the central sagittal plane in the MRI dataset after initial registration

4.4.3 Registration Results and Discussions

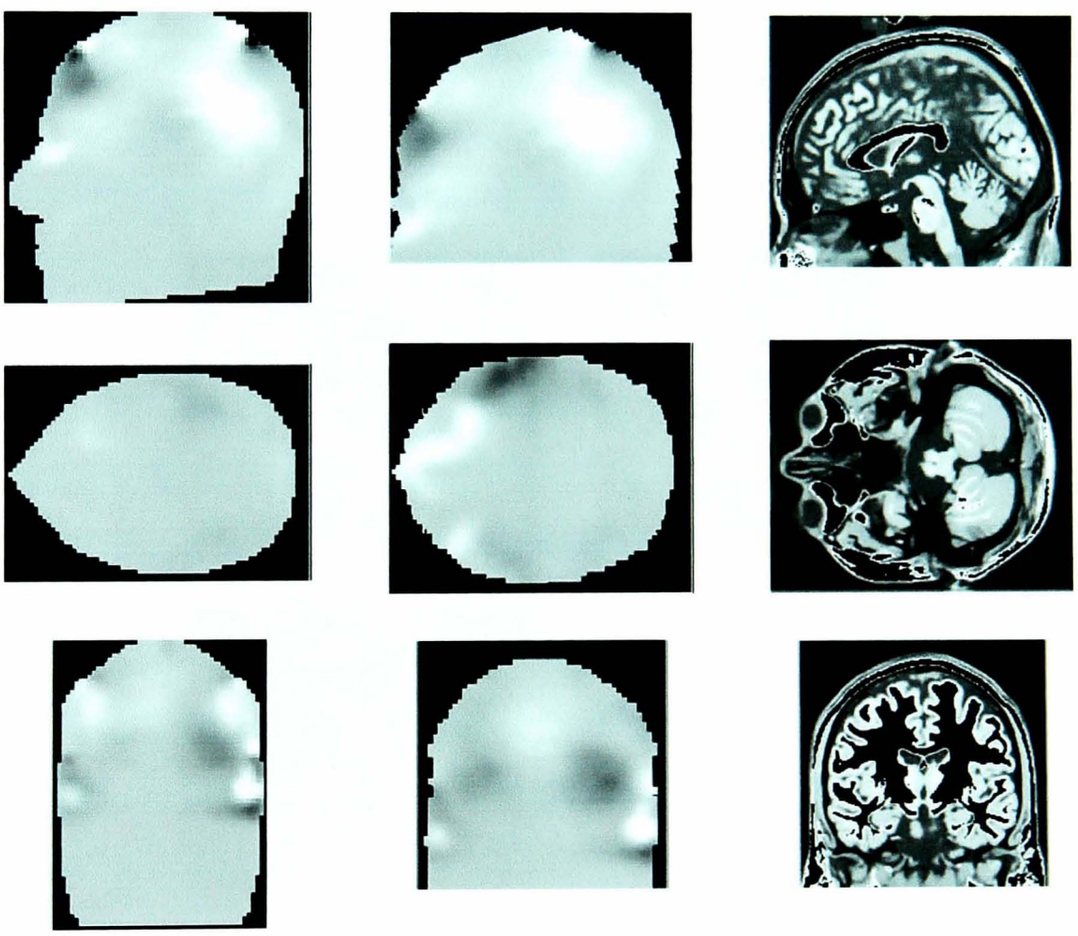

(a) Slices from the EIT dataset

(b) Slices from the registered EIT dataset

(c) Slices from the MRI dataset

Figure 4.9 Demonstration of the final registration results

Slices in different columns are from different image dataset; Coordinates in those datasets defined in the same way as figure 4.8, and the planes are sliced with same criteria used in figure 4.8.

Through the refined registration between the EIT image and the resampled MRI image, transformation T_2 is obtained by the least-squares method. The goal of this registration is to align the EIT image with the reference MRI image instead of the resampled one. Therefore, the final transformation T should be a combination of the transformation T_2 and transformation T_1, which is calculated through the initial registration and is described using the relation between the reference MRI image and the resampled MRI image. Finally, the EIT image is transformed with T and resampled. Figure 4.9 represents the final result of this EIT-MRI registration experiment. Figure 4.10 overlays the brain surface contours in the registered EIT images on the corresponding slices of the reference MRI images, where the red lines stand for the contour in the registered EIT dataset. Visual inspection of the contours overlaid on the MRI slices indicates an encouraging coincident alignment of the brain surfaces in these two datasets.

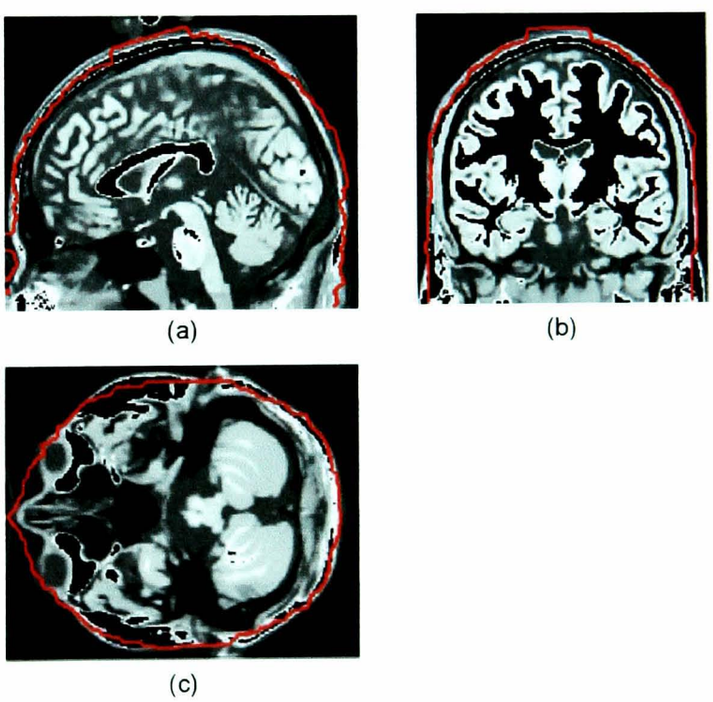

Figure 4.10 Overlay brain contours in EIT images on MRI slices

The three MRI slices appeared in this figure are same as those slices in figure 4.4, the red line stands for the brain contour in the registered EIT dataset .

To access the registration accuracy between the landmarks quantitatively, the Euclidean distances between registered landmark correspondences are calculated. The Root Mean Square (RMS) and Standard Deviation (STD) of these distances were adopted as an indicator for the absolute registration accuracy. Table 5.1 lists the RMS and STD values after the initial registration and the refined registration according to the proposed scheme. As pointed out by Singh et al (Huppertz, Otte et al. 1998) that, with a few reference points the stability of registration will vary from point to point within the brain, depending on the geometrical relationship between the point of interest and the fiducial points. Points in the brain further from the fiducial points will be subject to greater uncertainty than nearer points. The RMS of Euclidean distances between registered landmark correspondences is less than 3mm, however, it is difficult to access the registration accuracy for the other voxel in the dataset, and further assessment of the registration accuracy is beyond the scope of this research.

Table 4.1: Registration accuracy indicated with RMS and STD of Euclidean distances between registered landmark correspondences

Registration Step	RMS (mm)	STD (mm)
Initial registration	3.11	1.38
Refined registration	2.62	1.27

The purpose of registering brain EIT images with anatomical brain data is to make up the absence of anatomical information in EIT imaging and enhance the visualisation of EIT images. With the proposed EIT-MRI registration scheme, a relatively accurate registration is achieved. Subsequently, it is possible to fuse the anatomical and functional information involved in the two kinds of image modalities and visualise it in a single view. Figure 4.12 is a demonstration of this kind of display, where the impedance information in EIT dataset is represented in transparent color and the anatomical information provided by MRI dataset is displayed with grey scale. Besides the fusion of raw EIT image data with anatomical image data, the EIT_MRI registration scheme can

also be combined with the ROI detection process described in chapter 3. This application will be demonstrated in Chapter 5.

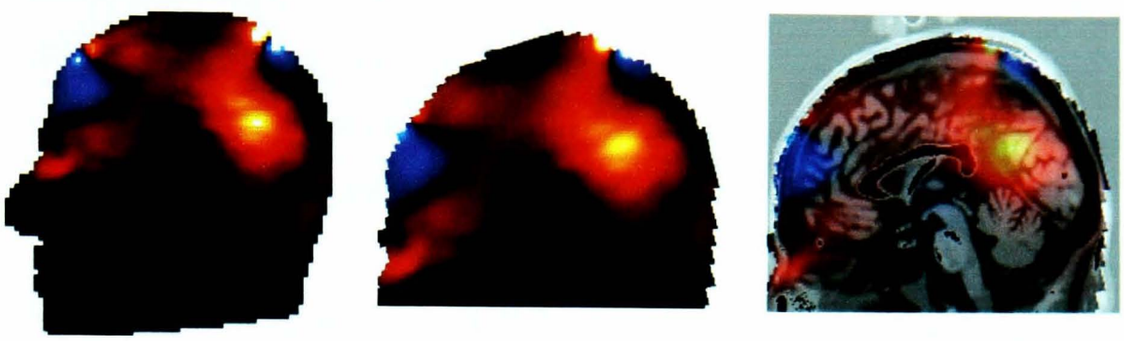

(a) The central sagittal slice in the EIT dataset

(b) The central sagittal slice in the registered EIT image

(c) The registered central sagittal slice fused with anatomical information

Figure 4.11 Visualisation of the fused EIT-MRI information

Medical image registration can be divided into intra- and inter- modality registration. Inter-modality registration usually includes registration between CT and MRI, CT and PET, PET and MRI, X-ray and CT, EEG/MEG and MRI, Ultrasound and MRI, etc (Maintz and Viergever 1998). Little work has been done to register EIT images with images from other modalities. Among all the inter-modality registration, EEG-MRI registration is the most similar one to the registration problem studied in this chapter: both EEG and EIT are measured by attaching electrodes to the scalp and recording boundary properties. EEG-MRI registration has been widely studied for many years, because EEG cannot be uniquely reconstructed, and registration of EEG data with MRI data is an important approach for the source location in EEG imaging.

The most frequently used approach to register EEG and MRI data relies on matching fiducials, such as nasion, inion, and pre-auricular points, determined in both coordinate systems (Toma, Matsuoka et al. 2002; Stefan, Scheler et al. 2004). Other methods match EEG electrodes or electrodes markers visible in the MRI images, or use specifically designed devices to achieve a more precise and reliable identification of fiducials (Singh,

Holliday et al. 1997). As a more precise and practicable alternative, an approach based on matching EEG- and MRI- derived reconstructions of the head or scalp surface has been presented, where the MRI-derived surface is segmented from the MRI image, and the surface for EEG can be derived by one of two methods: digitization of 1000 up to 2000 more or less arbitrarily chosen points on the scalp surface, or spline interpolation of the digitized 3D-electrode coordinates (Brinkmann, O'Brien et al. 1998; Huppertz, Otte et al. 1998; Lamm, Windischberger et al. 2001).

The registration scheme proposed in this chapter is landmark-based. Landmark-based transformations can be calculated fast without iteration. Surface-based registrations are usually performed in an iterative way and are relatively time consuming. From another point of view, in the situation that accuracy had higher priority than speed, surface-based registration is preferred to landmark-based registration. In fact, a surface-based EIT_MRI registration research is being conducted by other researchers at Middlesex University. That research is performed between personal MRI data and brain mesh nets used in EIT image reconstruction instead of EIT brain image data, and aims to create personal brain mesh nets. The main goal of that research is to improve the reconstruction of EIT image rather than the enhancement of EIT image visualisation. Because of the inherent connection between brain mesh nets used in EIT reconstruction and EIT brain images, it is straightforward to apply the registration algorithm developed in that research to the visualisation of EIT images. Furthermore, considering that a good start position will speed up the iterative calculation of the transformation for surface-based registration and improve the registration accuracy, the registration scheme proposed in this chapter can be utilised as a pre-processing step to locate a good start position. Regardless, before the success of that surface-based EIT-MRI registration research, the scheme proposed in this chapter presents an initial solution for EIT-MRI registration. Once a surface-based algorithm is developed to provide a more accurate EIT-MRI registration, the landmark-based scheme still has the speed advantage and can be adopted in the situation where high speed is required.

4.5 Conclusion

This chapter studied the second objective of this research: to provide an anatomical context for EIT image visualisation by registering them with images from anatomical imaging modalities. Because of the poor spatial resolution and the particular property presented by voxel intensities in EIT images, it is almost impossible to employ voxel intensity based registration methods in this application. In this chapter, a landmark-based registration scheme is proposed by making use of the limited geometric information in EIT images, which is inherent from EIT reconstruction processing. Encouraging results have been demonstrated by registering EIT and MRI data according to this scheme and visualising the fused information in one view.

After addressing the first two objectives in this chapter and chapter 3, the next chapter in this thesis will focus on the third objective of this research: to derive a system development methodology for the visualisation of multi-dimensional medical images, and construct a prototype visualisation system for five-dimensional brain EIT datasets.

Chapter 5 Task-based Visualisation System Development for Multi-dimensional Medical Data

5.1 Introduction

In section 2.2.5, general visualisation approaches for MDMV (Multi-Dimensional Multi-Variate) data have been reviewed. Some of those methods attempt to show all dimensions and all variates visually as one display, some try to reduce the dimensionality of dataset before visualisation, whereas others allow the user selecting subsets for display. Due to different features included in data from different research fields, different challenges are raised in the selection of proper visualisation means for specific data. In the following, challenges included in the visualisation of multi-dimensional medical image data are analysed.

5.1.1 Challenges in the Visualisation of Multi-dimensional Medical Image Data

For multi-dimensional medical image data, three typical features should be considered in the visualisation process: first of all, spatial or anatomical information is vital for medical implementations; secondly, dimensions included in medical image dataset are

generally orthogonal to each other; thirdly, it is critical to keep all useful information collected by medical imaging, although they are not always obvious, and sometimes are quite weak and difficult to identify from noise.

With MDMV visualisation methods to show all dimensions and all variates as one display, all dimensions are expressed on a two-dimensional interface, usually with little consideration of the inner natural structure of those dimensions. For example, it is viable to display a 5D EIT imaging dataset (which includes impedance information of a 3D part of a subject obtained during a time interval and under different frequencies simultaneously) with Parallel Coordinates, where the axes of a multidimensional space are defined as parallel vertical lines separated by a distance d, and a point in Cartesian coordinates corresponds to a polyline. With such a display, it is difficult for a clinician to connect those polylines with actual spatial or anatomical information of subjects. Generally, if a visualisation method can not present spatial or anatomical information intuitively or meaningfully, it is not suitable for medical image dataset visualisation. Unfortunately, this is a common problem included in most MDMV visualisation methods showing all dimensions and all variates as one display.

Dimension reduction is always an attractive approach for the processing of multi-dimensional datasets. However, it does not work for all datasets. Take the most famous dimension reduction approach - PCA (Principal Component Analysis) as an example. PCA is a linear transformation that transforms the data to a new coordinate system such that the greatest variance by any projection of the data comes to lie on the first coordinate (called the first principal component), the second greatest variance on the second coordinate, and so on. If the original coordinates are orthogonal to each other, PCA can not create a new coordinate with less dimensions. For example, it is impossible to express the spatial Cartesian coordinate, which is composed by x, y and z axes, with a two-dimensional coordinate without significant loss of information. Dimensions included in medical image datasets, which commonly include space and time, are

usually orthogonal to each other. This fact limits the feasibility of methods based on dimension reduction for medical image dataset visualisation. Furthermore, as with visualisation methods to show all dimensions and all variates as one display, it is difficult to reserve the spatial or anatomical information involved in medical image dataset by visualising it with approaches based on dimension reduction.

Considering the limitations included in methods to visualise high-dimensional dataset by dimension reduction or presenting all dimensions as one display, showing subset of a dataset seems to be the best way to visualise multi-dimensional medical image data. The difficulty in showing subsets is how to define the subset in each display.

5.1.2 Combining Subset Visualisation Approach with Task Exploration

During the research, the author noticed that to accomplish a specific visualisation task, usually, just a subset of a dataset is processed. Furthermore, the subset generally has fewer dimensions compared with the whole dataset. Let us take a 5D EIT imaging dataset as example again. Supposing a visualisation task like:

Question 5_1: "*At a given point position, say* (x_1, y_1, z_1), *how did the impedance change along the time course under different frequencies?*"

To address this requirement, it is sensible to focus on a two-dimensional (time and frequency) subset corresponding to the given point, and present the spatial context of the given point in another display.

As pointed out by Rudolf Arnheim, "The mind is always steered by purpose" (Arnheim 1997), a visualiser does not only look at data but also look for something "interesting". The "interestingness" can be understood as relevance to the major research question that

the visualiser puts to himself/herself, or, in other words, the primary task of data visualisation, the motive for doing the visualisation.

Respecting the fact that, explicitly or implicitly, tasks always exist, and it is possible to reduce visualisation complexity according to user's requirements, the author is convinced that it is reasonable to explicitly consider the potential tasks in the initial stage of system development for multi-dimensional medical image visualisation.

Normally, there are two main sorts of approaches to reveal potential tasks for a visualisation system: one is *practical investigation* with cooperation from people like domain experts; the other is *theoretical generation* according to a task model. Advantages of practical investigation include that the obtained tasks are usually concrete, understandable, and it is relatively easy to discover the most interesting tasks for the analyser/visualiser. However it is not trivial to ensure the completeness of the revealed tasks with this approach. Particularly, in some cases, there is neither abundant experience nor domain experts available. In contrast, completeness of tasks generated theoretically according to a model depends on the integrity of the adopted model. Another advantage of theoretical generation approaches is that some important while not quite obvious tasks, which may be ignored in practical investigation, can be identified through theoretic deduction. Theoretically generated tasks are logically meaningful, in other words, it maybe relatively abstract and not easy to be understood. Automatically, based on these two methods, there is a third way for task exploration: combination of practical investigation and theoretical generation.

As described in the research goal, brain EIT images are adopted in this research as a demonstration of multi-dimensional medical image data. EIT imaging, particularly 5D EIT imaging, is a relatively new medical imaging method, which has not been used clinically up to now. There is limited experience on what kinds of tasks (or questions)

will be put forward for the visualisation of (5D) EIT data. Considering this situation, it is desirable to expose potential tasks for EIT visualisation according to a model.

An introduction of different task typology models has been included in chapter 2. Each model has its own advantages and can be applied in different applications. The work presented in this chapter is based on the new version of Andrienko's task typology model, which synthesised other pioneers' achievements and is the latest model for task typology. This model aims to handle general data, although almost all examples cited by those authors are from the geographic field, particularly spatial-temporal data. Additionally, the functional representation of a dataset, which has been employed since the initial stage of this research to define dimension of a dataset, is utilized in the new version of Andrienko's model.

In the next section, an overview of Andrienko's task typology model is presented. Then a new task typology model is derived by refining Andrienko's model. Next, a methodology to develop a visualisation system based on task exploration is proposed. Subsequently, a prototype system is developed, following the proposed methodology, for the visualisation of 5D brain EIT image data. Finally, a conclusion is drawn at the end of this chapter.

5.2 Overview of Andrienko's Task Typology Model

The first version of Andrienko's task typology was originally proposed in (Andrienko, Andrienko et al. 2000). Later, Andrienko et al. took advantage of Bertin's theory (and its developments) and updated their model in (Andrienko, Andrienko et al. 2003). The second version of this model was mainly for exploratory analysis of spatial-temporal data. In their new book (Andrienko and Andrienko 2006), Andrienko et al. refined the taxonomy a lot. The latest model, which is introduced in the following, can be

summarized as two fundamental formal models and three criteria. Naturally, most of the descriptions are based on Andrienko's book (Andrienko and Andrienko 2006).

5.2.1 Two Fundamental Models

A data model and a task model compose the two fundamental formal models for Andrienko's task typology. The fundamental data model represents a dataset as a function, and the fundamental task model describes a task as a combination of a target and constraints.

5.2.1.1 The Fundamental Data Model

A set of data may be represented by a function that assigns particular values of attributes to various references. So, a dataset may be represented by a formula such as

$$f(x) = y \tag{5.1}$$

In general case, both x and y can be multiple variables. So the above formula can be expressed in a more "detailed" manner:

$$f(x_1, x_2, \cdots, x_m) = (y_1, y_2, \cdots y_n) \tag{5.2}$$

Where f is a function symbol, x_i $(i = 1, 2, \cdots, m)$ is an *independent variable* (which is also mentioned as *reference* in Andrienko's book) defining the context in which the data was obtained, y_j $(j = 1, 2, \cdots, n)$ is a *dependent variable* (which is also called *attributes* in Andrienko's book) representing the results of measurements, observations, calculations etc. obtained in the context defined by independent variables (or references).

For example, there are weather data for main cities in United Kingdom, which include such variables as city_name, date, maximum_temperature, minimum_temperature, wind_speed, and wind_direction. In this dataset, city_name and date are independent

variables (references); the others are dependent variables (attributes). So the functional representation of this dataset is:

$$f(city\_name, date) = (max\_temp, min\_temp, wind\_speed, wind\_direction) \quad (5.3)$$

Another example is spatial-temporal EIT data. These data include five variables: sample_time t, coordinate x, coordinate y, coordinate z, and impedance_value p. In this dataset, sample_time t, coordinate x, coordinate y, and coordinate z are references, and impedance_value p is the only attribute. This dataset can be represented in functional form as:

$$f(x, y, z, t) = p \quad (5.4)$$

These two datasets will be referred to as *the example weather dataset* and *the example EIT dataset* separately throughout this chapter.

The value of each dependent variable (or attribute) is determined only by the independent variables (or references) and has nothing to do with values of other attributes, it is sensible to consider each attribute independently. Therefore, formula (5.2) can be rewritten as a set of functions with only one dependent variable (or attribute) in each of them:

$$\begin{cases} f_1(x_1, x_2, \cdots, x_m) = y_1 \\ f_2(x_1, x_2, \cdots, x_m) = y_2 \\ \cdots \\ f_n(x_1, x_2, \cdots, x_m) = y_n \end{cases} \quad (5.5)$$

Here, the initial function f has been split into n functions $f_1, f_2, \cdots, f_n$. Each of these functions defines values of one of the attributes on the basis of the values of the references. Consequently, the example weather dataset represented in formula (5.3) can be rewritten as:

$$\begin{cases} f_1(city\_name, date) = max\_temp \\ f_2(city\_name, date) = min\_temp \\ f_3(city\_name, date) = wind\_speed \\ f_4(city\_name, date) = wind\_direction \end{cases} \quad (5.6)$$

5.2.1.2 The Fundamental Task Model

A task (or question) can be split into two parts: a *target*, which defines what information needs to be obtained, and the *constraints*, which describe what conditions information related to the target needs to fulfil. So, a task can be expressed as a formula:

$$?\,(target) : (constraints) \tag{5.7}$$

Where the "?" is employed to label the task target; ":" is applied to separate the target part and the constraint part in the expression.

The target and constraints can also be viewed as unknown and known (or specified) information respectively. The goal of a task is to find the initially unknown information corresponding to the specified information. Both the target and constraints can be defined with references, or attributes, or combinations of them, or relations between references/attributes.

For example, a possible visualisation task for the example weather dataset can be:

Question 5_2: "*What is the maximum temperature in London on 27 Sep 2006?*"

According to the task model, this task can be represented as:

$$?\,(max\_temp) : (city\_name = London, date = 27 - Sep - 2006) \tag{5.8}$$

5.2.2 Three Criteria in the Task Typology

There are three partition criteria included in Andrienko's task typology model. To simplify the statement, the author of this thesis labels them *searching level*, *searching mode*, and *searching direction* separately:

- *Searching level* is used to distinguish tasks according to the level of data analysis, which includes elementary level and synoptic level.
- *Searching mode* presents task classification of lookup, comparison, and relation-seeking.

- *Searching direction* contains two options: direct tasks or inverse tasks.

5.2.2.1 Searching Level - elementary level or synoptic level

The idea of searching level was originally proposed by Bertin (Bertin 1983). In Bertin's theory, there are three "level of reading": elementary, intermediate, and overall. These levels indicate whether a question concerns a single data element, a group of elements taken as a whole, or all elements constituting the component. For example, there are three questions for the example EIT dataset:

Question 5_3: "*At a specified position* (x_1, y_1, z_1), *what is the impedance value at the sample time point* t_1*?*"

Question 5_4: "*At a specified position* (x_1, y_1, z_1), *how did the impedance vary during the sample time interval* $[t_1, t_2]$*?*"

Question 5_5: "*At a specified position* (x_1, y_1, z_1), *how did the impedance vary during the whole sample time interval?*"

According to Bertin's definition, in question 5_3, references *position* and *time* are both at elementary reading level; attribute *impedance_value* is at elementary reading level as well. In question 5_4, references *position* is at elementary reading level; reference *time* and attribute *impedance_value* are at intermediate reading level. In question 5_5, references *position* is at elementary reading level; reference *time* and attribute *impedance_value* are at overall reading level.

Considering that intermediate level and overall level have many more commonalities than differences: usually the same tools and analysis procedures can be used in both levels. Andrienko et al. combined these two levels into a single one and named it "*synoptic level*". Along with this explanation, for the above examples, reference *time* is at synoptic level in question 5_4 and 5_5. Andrienko et al. also pointed out that the

notion of elementary level and synoptic level applies only to references and not to attributes. Furthermore, when the number of referential variables is two or more, these multiple references can be addressed on different levels (elementary level or synoptic level) independently of each other.

In summary, elementary level tasks refer to individual elements of reference sets; synoptic level tasks deal with a reference set or its subsets as wholes rather than address their elements. For a dataset with N references, there are 2^N possible combinations of searching levels.

5.2.2.2 Searching Mode - lookup, comparison, or relation-seeking

In the fundamental data model, variables in a dataset are classified into two types: references and attributes. Consequently, relations among different variables of a dataset can be grouped into three types:

R1: Relations between references

R2: Relations between attributes

R3: Relations between references and attributes

Furthermore, questions always concern relations between variables. Let us take question 5_1 "*What is the maximum temperature in London on 27 Sep 2006?*" as an example. In this question, elementary references *city_name* and *date* are given; the target of this question is to find out the corresponding elementary attribute *max_temp*; relation concerned in this question is between references (*city_name* and *date*) and attribute (*max_temp*), which is expressed as f_1 in formula 5.6. For a dataset, two basic questions are expected:

Q1: Given two (or more) elementary (or synoptic) variables, identify what relation exists between them.

Q2: Given one (or some) elementary (or synoptic) variables, and a relation, find other elementary (or synoptic) variables, related in the specific way to the given elementary (or synoptic) variables.

Beside these two basic questions, another kind of question can be formulated in the following form: given a relation, find elementary (or synoptic) variables linked by this relation. However, this formulation can be transformed into the basic question Q2, which in this case is repeated for every elementary (or synoptic) variable in the dataset.

Combining preceding relations and basic questions, six types of tasks can be drafted: *R1-Q1, R1-Q2, R2-Q1, R2-Q2, R3-Q1, and R3-Q2*. It is straightforward to identify that question 5_1 belongs to the task type *R3_Q2*.

For a given dataset, it is assumed that all relations between references and attributes, or, at least, all such relations that of interest to a data analyst, are defined by the data function, if the dataset is represented as a function. Hence, basic question Q1 does not come up when the focus is put on relations between references and attributes (relation R3): there is no sense in asking what kind of relation exists between a given reference and a given attribute. So for relation R3, only question Q2 is reasonable. Andrienko et al named task type *R3_Q2* "*lookup*" tasks. Question 5_1 is a lookup task.

For relations R1 and R2, both question Q1 and Q2 make sense. In these cases, Question Q1 is called "*comparison*" task, and question Q2 is "*relation-seeking*" task. Comparison tasks target to determine what relations exist between two (or more) references or attributes. In a relation-seeking task, a certain relation is specified, and items that are related in the specified way need to be detected. Andrienko et al. mentioned that the fundamental idea of relation-seeking task is to find references such that the corresponding attributes are related in a specific way.

Comparison and relation-seeking tasks do not occur in their basic forms, which do not involve the data function. In other words, no data are needed for answering such questions, because relations between references and between attributes are determined by the general, invariant properties of the respective sets. Such as, with the example EIT dataset, it is not useful to ask a question like:

Question 5_6: "*What is the time difference between the given sample time points* t_1 *and* t_2*?*"

On the contrary, comparison and relation-seeking tasks appear as the basic forms modified by introducing additional targets and additional constrains, so that the data function is involved in at least one constraint. Therefore, a comparison task for the example EIT dataset can be put forward as:

Question 5_7: "*At a given position* (x_1, y_1, z_1)*, what is the time difference between sample time points* t_1 *and* t_2*, where a given impedance value* p_1 *was obtained at* t_1*, and a given impedance value* p_2 *was obtained at* t_2*?*"

The classification of searching mode into lookup, comparison, and relation-seeking can be applied to different searching levels. By separating similarity/difference relations from other possible relations, Andrienko divided synoptic tasks into "*descriptive synoptic*" tasks and "*connectional synoptic*" tasks. That is to say, both descriptive synoptic tasks and connectional synoptic tasks deal with relations relevant to a dataset as a whole or to substantial parts of it, rather than associations between individual elements. The difference of these two synoptic tasks is that description synoptic tasks only consider similarity/difference relations between references or attributes, while connection synoptic tasks handle other relations, such as, correlation, dependency, or structural connection.

5.2.2.3 Searching Direction - direct tasks or inverse tasks

The third partition criterion in Andrienko's task typology is searching direction, which classifies lookup and comparison tasks at different searching levels into direct tasks and inverse tasks. Direct lookup tasks are those where references are specified and the goal is to find the corresponding attributes. In contrast, inverse lookup tasks are tasks where references corresponding to specified attributes need to be found. This also includes tasks where references are partly specified. Comparison tasks targeting relations between attributes are called direct comparison tasks, and comparison tasks where relations between references need to be determined are called inverse comparison tasks.

The preceding example questions 5_1, 5_2, 5_3 and 5_4 are all direct tasks. A possible inverse task for the example weather dataset can be:

Question 5_8: "*In which cities, did the maximum temperature exceed 30 Celsius degree in June 2006*?"

In this question, reference variable *city_name* is the target.

5.3 Application of Andrienko's Model to Medical Data

The original purpose for Andrienko et al. to investigate task typology was to understand what essential criteria are used or should be used in choosing or designing tools for exploratory data analysis. In the study presented in this thesis, Andrienko's task typology model is adapted and applied to reveal potential visualisation tasks and further define subsets to be displayed corresponding to those tasks.

Andrienko at al. claimed that their model can be applied to general datasets. However, the author of this thesis noticed that Andrienko's research work, including work of other pioneers in this area such as Bertin, mainly concentrated on geographic data. No

application of this sort of task typology to the medical field has been found through literature review so far. Data used in different research fields have different features; even for a same dataset, researchers from different domain may have different interests and analyse it from different prospects. To facilitate task exploration for medical data visualisation, a series of refinements to Andrienko's model is conducted in the following subsection. Then a new task typology model is derived from Andrienko's model. Finally, the derived model is employed to the discovery of potential tasks for 5D EIT data visualisation.

5.3.1 Formalise Criteria into Dimensions

As summarised in section 5.2, three criteria are included in Andrienko's task typology model; under certain conditions, tasks classified by one criterion may be further categorized by the other criteria. The final model can be expressed as an unbalanced tree-structure. The author of this thesis noticed that, from the visualisation point of view, it is possible to formalise the task model further and the details are given below.

5.3.1.1 About the Application of Searching Level to Attributes

Regarding searching level in the task typology model, it is acceptable to apply it only to references and not to attributes, while Andrienko et al did not clarify the reason for this in their book. In other words, the phenomenon that "*If one were to try to assign values from an arbitrary set S to a dependent component, it might occur that for many values there are no corresponding references (i.e. these values have never been attained), while for other values there are multiple references (i.e. these values have been attained more than once).*" (Andrienko and Andrienko 2006) is not strong enough to support the conclusion that searching level should not be utilized with attributes.

As the author of this thesis understands, the real reason is that: in a dataset, attributes are not independent; therefore, the classifications of searching level for attributes are not independent from the classifications of searching level for references, which are dependant variables. In algebra and set theory, functions are "many-to-one" mappings. If an attribute is considered at synoptic level, which means a set of attribute values are treated as a whole, there must be one or more corresponding references at synoptic level. That is to say, it is impossible to consider all references in a dataset on elementary level and, at the same time, treat the attribute depending on these references at synoptic level. For instance, in the example EIT dataset, if the *impedance_value* is processed on synoptic level, which means a set of impedance values are analysed as a whole, obviously, this set of impedance values must correspond to a set of *coordinate* values (synoptic level) or/and a set of *sample time* points (synoptic level). In other words, it is impractical to collect a set of impedance values at one spatial position and one time sample point in an EIT imaging. On the contrary, each reference in a dataset can be considered at different searching levels independently.

In conclusion, considering the dependent feature, the notion of elementary and synoptic level should only be applied to references and not to references and attributes simultaneously.

5.3.1.2 Descriptive and Connectional Synoptic Tasks

In Andrienko's model, synoptic tasks are divided into "descriptive synoptic" tasks and "connectional synoptic" tasks. Descriptive tasks process similarity/difference relations between references or attributes and are treated as a description of data; connectional tasks handle all the other possible relations between references or attributes and suppose to gain a deeper understanding of data. From the point of view of the cognitive operations and efforts involved, it may be acceptable to separate similarity/difference relations from other possible relations, "*because cognitive operations and efforts*

involved in these two sorts of tasks are different." (Andrienko and Andrienko 2006) At the same time, Andrienko et al also accepted that, from the formal point of view, connectional tasks can be subsumed under the category of descriptive tasks.

Anyway, a classification cannot be right or wrong. What is important is that it is convenient or inconvenient. It maybe helpful for choosing or designing tools for data analysis aimed at separating the cognitive operations and efforts involved in sorting similarity/difference relations from other relations. Connectional tasks may require quite different tools from descriptive tasks. Visualisation can be treated as a method for data analysis, or a separate research area from analysis. The task typology is used to assist the definition of subsets for the visualisation. It focuses on the feature of subsets, such as dimensions, corresponding to different types of tasks instead of cognitive operations and efforts involved in a relation discovery or description. To make the task model more convenient to apply, this research prefers to treat all potential relations between references and/or attributes equally and not to divide synoptic tasks further.

For lookup tasks at synoptic level, the relations concerning in this kind of tasks are relations between references and attributes. All relations between references and attributes are defined by data function of the dataset. It is awkward to classify a data function into relations like similarity, difference, or correlation. Therefore, it seems unreasonable to put lookup tasks as a subcategory for descriptive synoptic tasks or connectional synoptic tasks. This difficulty further strengthens the decision to treat synoptic tasks as a basic element in the searching level criterion.

5.3.1.3 Rethinking of Relations in Task Typology

A relation may be the target of a task or may be specified as a task constraint. Relations among different variable of a dataset can be grouped into different kinds: data function f relates references to attributes, there are also relations within the reference and

attribute sets. The list of potential relations within the reference and attribute sets can be various. This research focuses on binary relations: relations involving two items. In fact, relations in which more than two items participate can be represented by collections of binary relations.

Comparison tasks target to determine what relations exist between two references or attributes, and data functions must be involved in the tasks. In other words, at least one of the two items included in a comparison should be specified through a direct or inverse lookup task. However, not any combination of references or attributes is meaningful: the components involved must be comparable, which generally acquires the components have coincident or at least overlapping value domains. In this research, only relations between same references or attributes are considered.

The relations that can potentially exist between objects are diverse. For elements of reference or attribute set, the possible relations are determined by the properties of this set. For two elements of any set, relations like same or different always exist. If the set is ordered or at least partly ordered, the corresponding elements can be linked by ordering relations, such as, less than, less than or equal, equal, greater than or equal, greater than. Space is not ordered. However, if a particular coordinate system is introduced into space, it is possible to consider various relations specific to this coordinate system, such as, distances, directions in space.

Relations between subsets of reference or attribute sets, which correspond to synoptic searching level, can be characterised as same or different, overlapping or not overlapping, included or not included. In an ordered set, there may be ordering relations between subsets, for example, relations between time intervals can be before or after. In a set with distances, there may be distance relations between subsets. Beside this, correlation can exist between subsets for different reference and attribute sets, or even for different subset from same reference or attribute set.

5.3.1.4 Searching Direction for Relation-seeking Tasks

In Andrienko's model, searching direction has been used as a subcategory criterion for tasks at different searching level and different searching mode except relation-seeking. Andrienko et al. described the fundamental idea of relation-seeking task as finding references such that the corresponding attributes are related in a specific way. Referring to the definition of searching direction for lookup and comparison tasks, where direct tasks target to find attributes or relations between attributes, and the goal for inverse tasks are references or relations between references, the relation-seeking tasks specified by Andrienko at el. can be grouped as inverse tasks. However, relation-seeking tasks can also target for attributes with corresponding references related in a specified way, and these kinds of relation-seeking tasks can be classified as direct tasks. Let us check two possible tasks in the example weather dataset first:

Question 5_9: "*On 27 Sep 2006, in which cities was maximum temperature higher than London's maximum temperature?*"

Question 5_10: "*In London, for the date when the highest maximum temperature in 2005 was achieved, what was the maximum temperature on the same date in 2006?*"

In question 5_9, the target is *city_name(s)*, which is a reference in the example weather dataset; a relation between *max_temp*, which is an attribute in the example weather dataset, in London and *max_temp(s)* in the targeted cities is specified as a constraint. So question 5_9 is a relation-seeking task. The target for question 5_10 is *max_temp*, which is an attribute in the example weather dataset; a relation between *date*, which is a reference in the example weather dataset, on which the highest *max_temp* in 2005 was achieved and the date corresponding to the targeted *max_temp* is specified as a constraint. Therefore, question 5_10 is a relation-seeking task as well. Following the classification of researching direction for lookup and comparison tasks, question 5_9 and 5_10 can be defined as an inverse and direct task separately.

As we can see, both question 5_9 and question 5_10 are reasonable relation-seeking tasks. Therefore, in this research, the fundamental idea of relation-seeking task proposed by Andrienko et al. will not be adopted. Relation-seeking task will be defined as: finding references or attributes such that the corresponding attributes or references are related in a specific way. With the refined definition, searching direction can be adopted as a subcategory criterion for relation-seeking tasks consequently.

5.3.2 The Derived Task Typology Model for Medical Data Visualisation

After previous refinement, the three criteria in Andrienko's model are formulated: they are independent to each other; tasks classified by one criterion can be further categorized by the other two criteria. It is reasonable to claim that they have been transformed from three general criteria into three dimensions. Consequently, a new task typology model can be derived from Andrienko's model.

The new task typology model includes two fundamental models and three task dimensions. The two fundamental models are same as those models adopted by Andrienko. The three task dimensions are *searching level dimension*, *searching mode dimension*, and *searching direction dimension*. The searching level only includes elementary level and synoptic level: no further division is involved. Because of the independent characteristic, these two levels can be employed to each reference variable in a dataset. Therefore, if there are N references in a dataset, the number of possible values on searching level dimension is 2^N. Searching mode dimension contains three possible values: lookup, comparison, and relation-seeking. Searching direction dimension has two potential values: direct and inverse. The definitions of those values on these two dimensions are inherited from Andrienko's model. With the three dimensions, task typology for a dataset can be illustrated as a cubic grid (see figure 5.1), each voxel in this grid presents a type of task.

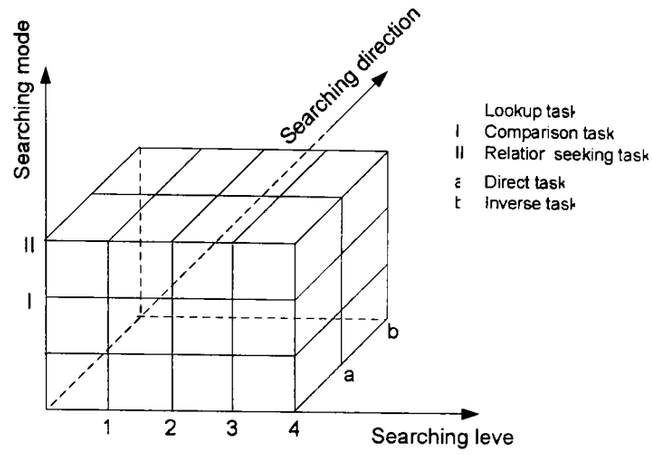

Figure 5.1 Graphical illustration of the refined task model

In this graph, the references number N is set to be 2, so there are $2^N = 2^2 = 4$ possible values for searching level dimension.

Considering relations included in tasks on different searching mode, lookup tasks include one relation: the data function; comparison and relation-seeking tasks contains at least two relations: one is the data function and the other is relations between references or attributes. By treating lookup tasks as atomic task, comparison and relation-seeking tasks can be considered as compound tasks. Any compound task is built up from smaller operations, or subtasks. Usually, four kinds of subtasks can be identified for compound tasks like comparison and relation-seeking tasks:

1. Direct lookup tasks;
2. Inverse lookup tasks;
3. Identify relations existing between two specified elementary (or synoptic) references (or attributes);
4. Find an elementary (or synoptic) reference (or attribute) related to a given elementary (or synoptic) reference (or attribute) with a specified relation.

In general, direct comparison tasks can be compounded with subtasks 1 and 3; inverse comparison tasks can be formed with subtask 2 and 3; direct and inverse relation-seeking tasks can be constituted with subtasks 1, 2 and 4.

5.3.3 Task Exploration for Visualisation of 5D EIT Data

After the proposal of the new task typology model, this section will take 5D EIT data as an example to demonstrate how to apply the proposed model in task exploration for visualisation.

5.3.3.1 Realising the Fundamental Data Model for EIT Data

Following the fundamental data model used in the task typology, 5D EIT data can be presented as:

$$g(x, y, z, t, f) = p \tag{5.9}$$

Where x, y, z present three spatial coordinates, t stands for time, f for frequency, and p describes the impedance values inside the brain. In this function, there are five independent variables (or references). It is reasonable to treat the three spatial coordinates as a whole, because they specify positions in the Cartesian space together. Therefore, if l symbolises the location defined by (x, y, z), formula 5.9 can be rewritten as:

$$g(l, t, f) = p \tag{5.10}$$

With this representation, there are three references and one attribute in a 5D EIT dataset. What should be noticed is that this is just a simplification for task exploration but not a dimension reduction for visualisation.

5.3.3.2 Customizing the Three Dimensions for EIT Data

The values on searching mode and searching direction dimensions are fixed, while possible values on searching level dimensions depend on the number of references in a dataset. When a 5D EIT dataset is represented with formula 5.10, there are three references. Therefore, $2^N = 2^3 = 8$ values exist on the searching level dimension for

this dataset, as listed in table 5.1. In this table, "0" and "1" denote that the corresponding reference is at elementary level and synoptic level separately. Symbols *A~H* stand for eight combinations of the three references on different searching level. For example, symbol *C*, which corresponds to the combination "101" in the table, means reference *location* is on elementary level, reference *time* is on synoptic level, and reference *frequency* is on elementary level.

Table 5.1: Values on searching level dimension for a 5D brain EIT dataset

Reference	A	B	C	D	E	F	G	H
Location	1	1	1	0	1	0	0	0
Time	1	1	0	1	0	1	0	0
Frequency	1	0	1	1	0	0	1	0

With the customization of the three dimensions, task typology for a 5D EIT dataset can be illustrated in a cubic grid form as figure 5.2.

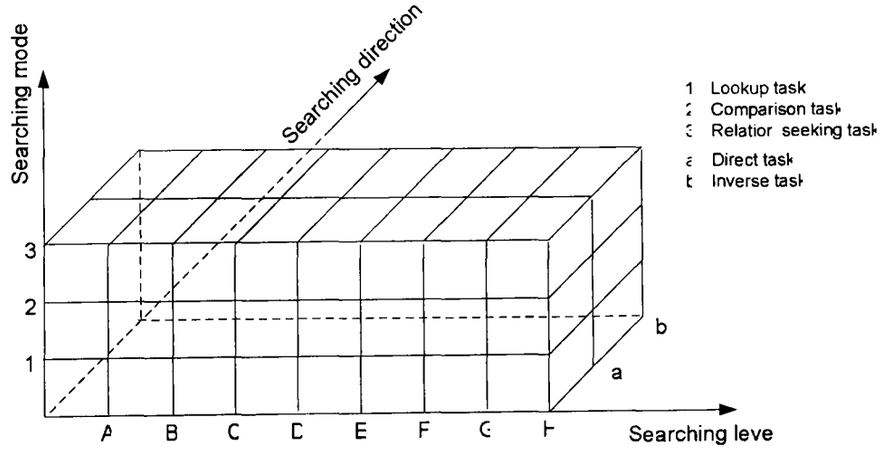

Figure 5.2 Graphical illustration of task typology for a 5D EIT dataset

Up to now, a formalized task typology with three dimensions has been established for 5D EIT data. The next step is to explore potential visualisation tasks according to this typology. Table 5.2 lists the general task formulae for tasks (represented with a series of subtasks for each task type) at different searching modes and different searching

directions. The searching level dimension does not appear in the task type column of this table, because, for a specified searching mode and searching direction, same formula presentation can be used for tasks at different searching levels.

Table 5.2: General task formula for different task type

Task type		General task formula
Lookup	Direct	$?P:(L,T,F)$
	Inverse	$?(L,T,F):P$
Comparison	Direct	$?P_1:(L_1,T_1,F_1)$ $?P_2:(L_2,T_2,F_2)$ $?R_p:(P_1,P_2)$
	Inverse	$?(L_1,T_1,F_1):P_1$ $?(L_2,T_2,F_2):P_2$ $?R_L:(L_1,L_2)$ $?R_T:(T_1,T_2)$ $?R_F:(F_1,F_2)$
Relation-seeking	Direct	$?(L_1,T_1,F_1):P_1$ $?L_2:(R_L,L_1)$ $?T_2:(R_T,T_1)$ $?F_2:(R_F,F_1)$ $?P_2:(L_2,T_2,F_2)$
	Inverse	$?P_1:(L_1,T_1,F_1)$ $?P_2:(R_P,P_1)$ $?(L_2,T_2,F_2):P_2$

In order to save space, details of the deduced questions are presented in Appendix A, and only questions at searching level *G* (synoptic location, synoptic time, and elementary frequency) and *H* (synoptic location, synoptic time, and synoptic frequency) are listed there. These two levels contain the most complex task types for a 5D brain EIT dataset.

5.4 From Task Exploration to Visualisation System Development

With the proposed task typology model, potential visualisation tasks for multi-dimensional medical data can be deduced. It is possible to develop a visualisation system based on the deduced tasks. Three aspects should be considered in the development of a task-based visualisation system: first, how to facilitate the question formulation; secondly, how to choose a method on the basis of the question, the type of data available, and the level of information required, and process the data with the chosen method to find out the answer to the question. Finally there is the issue of how to display the results suitably. More details of this system development methodology are described in the following subsections, with 5D brain EIT data used for demonstration purposes.

5.4.1 Question Formulation

The specification of a task can be carried out in two steps: firstly, defining the task type that a task belongs to, and secondly setting individual features for that task. Making use of the derived task typology model, the type of a task can be defined by setting values corresponding to the three task dimensions: searching level, searching mode and searching direction. As defined in the fundamental task model, a concrete task is constituted with targets and constraints. After the decision of searching direction, targets are specified to be attributes (or relations between attributes) for direct tasks, and references (or relations between references) for inverse tasks. Task constraints can be defined with references, attributes, or relations between references or attributes. Among the three dimensions of the task typology model, searching level significantly affects the setting of constraints. Generally, it is easier to set a constraint with elementary references or attributes than synoptic references or attributes.

Let us take a 5D brain EIT dataset as an example. There are three references and one attribute in this dataset. On elementary searching level, references *location*, *time*, or *frequency* all correspond to point values. It is relatively straight forward to set a constraint by specifying a value for an elementary reference/attribute. For example, by inputting a value in an editable textbox, adjusting a slider, or choosing a position on a displayed image directly. On the synoptic searching level, a synoptic location generally corresponds to a two-dimensional area or a three-dimensional region in a brain; synoptic time or frequency is a one-dimensional time interval or frequency range separately. The simplest way to employ those synoptic references as constraints is to define their boundary values.

Because of the dependent feature, searching level of an attribute can not be specified directly but is dependent on the searching level of the corresponding references. That is to say, only when all the references are on elementary level, attributes used in constraints can be treated as zero dimensional. For example, in a 5D brain EIT dataset, if a task is defined on searching level *A*, which corresponds to elementary location, time and frequency as presented in table 5.1, then a constraint related to impedance can be a zero dimensional value. Similarly, if a task is defined on searching level *E*, which corresponds to an elementary location, synoptic time and synoptic frequency as presented in table 5.1, then a constraint related to impedance must be two dimensional.

5.4.2 Selection of Processing Method

Knowing the questions (or type of questions), one may look at familiar techniques from the perspective of whether they could help one to find answers to those questions. In some cases, there may be a subset of existing tools that cover all potential question types. It may also happen that for some tasks there are no appropriate tools. In that case, the nature of the tasks gives a clue as to what kind of tool would be helpful. This is an important initial step in designing a new tool. Ideally, a visualisation system must

contain a set of tools that could answer any possible visualisation question. This ideal will, probably, never be achieved, but a designer conceiving a system or toolkit for visualisation need to anticipate the potential questions and at least make rational choice concerning which of them to support.

As mentioned in section 5.3.2, four basic subtasks exist in tasks revealed according to the task typology, where the first two subtasks: direct lookup tasks and inverse lookup tasks are the main factors determining the choice of processing methods. For a direct lookup task, attributes appear in the target part; references are used as constraints. It is not difficult to obtain the targeted attributes according to the given references, considering that medical datasets are generally indexed along reference components when they were stored.

Inverse lookup tasks are usually more difficult to process. Many image processing technologies can be considered in efforts to solve certain kind of inverse tasks. For example, thresholding can be described as an inverse task like that: within a given image, find out pixels with grey value greater than a given value. Similarly, edge detection can be mentioned as: in an image, find out pixels whose grey values satisfy some specified feature. Although a large number of image processing methods are available nowadays, some inverse tasks still cannot be addressed properly with existing tools.

As mentioned in the previous section, searching levels of references influence the setting of attributes as a constraint. Furthermore, searching level affects the selection of analysis method for inverse tasks a lot, because it determines the dimension of data involved in the process directly. Let us take some inverse tasks for a 5D EIT dataset as example:

Question 5_10: *For a given impedance value p_1, where, when and under which frequency was it attained?*

In this task, the searching level is elementary for all the three references, and the corresponding searching level for attribute *impedance* is elementary as well. The formulary representation of this question is:

$$? (location, time, frequency) : (impedance = p_1) \quad (5.11)$$

A possible method to answer this question is to conduct a search on the whole dataset. For each step during this searching, a point in the 5D space formed by the dataset is chosen, impedance value corresponding to this point is compared with the given impedance value. In this each step of this process, a zero-dimensional point is analysed.

Question 5_11: *For a given impedance change pattern P_1, where, at which time point, and during which frequency interval was it attained?*

In this task, references location and time are at elementary level, reference frequency is at synoptic level. Therefore, searching level for attribute *impedance* is synoptic. Formula representation for this question is similar as that one for question 5_10:

$$? (location, time, frequency\ interval) : (impedance\ change\ patter = P_1) \quad (5.12)$$

To obtain results for this task, a search can be conducted with each step choosing a combination of an elementary location l, a time point t, and a frequency range F, and comparing impedance pattern corresponding to this combination with the given impedance change pattern. Each of this kind of combination decides a one-dimensional line in the 5D space formed by the dataset.

Commonly, the complexity to resolve a revise task grows with the increase of the dimension of data involved in the process. For potential visualisation tasks of a dataset, dimensions of data involved in the process range from zero to the dimension of the dataset. Most image analysis approaches are performed with data less than four dimensions. With the improvement of medical imaging methods, more and more analyses have to be conducted with multi dimensional data.

For example, with a fMRI imaging dataset obtained under VEP (visual evoked response) test, one of the most interesting tasks is to locate the brain region which is activated under the visual stimulation. From the perspective of task typology model: this four-dimensional MRI dataset has two references (*location* and *time*) and one attribute (the *BOLD signal* collected by a MRI instrument). This task can be rewritten as:

Question 5_12: *During the whole time interval, for a given BOLD signal change pattern, (which is represented with a description of the experiment condition), find out the locations where signal change is similar to the given pattern.*

Searching level of this task is synoptic for location and time, so data involved in this process is four-dimensional. As mentioned in chapter 3, SPM can be utilized to solve this task, where the General Linear Model is used to describe signal change across time at each voxel, and Gaussian Random Field is adopted to adjust the multiple comparison effects among voxels.

VEP tests can also be carried out with EIT imaging, 4D or 5D VEP EIT data can be obtained with dynamic or spectroscopic EIT imaging system separately. For 4D (spatial-temporal) VEP EIT data, tasks similar to question 5_12 can be raised like:

Question 5_13: *During the whole time interval, for a given impedance change pattern, find out the location where impedance change is similar to the given pattern.*

Through the literature review, no existing method has been found to process this task. To fill this gap, the author of this thesis proposed to apply SPM to EIT data. Details about this part of work have been presented in chapter 3.

For 5D (spectral-spatial-temporal) VEP EIT data, tasks like question 5_12 can be put forward in three ways:

Question 5_14: *With a specified frequency, during the whole time interval, for a given impedance change pattern, find out the location where impedance change is similar to the given pattern.*

Question 5_15: *At a specified sample time point, during the whole frequency range, for a given impedance change pattern, find out the location where impedance change is similar to the given pattern.*

Question 5_16: *During the whole time interval and frequency range, for a given impedance change pattern, find out the location where impedance change is similar to the given pattern.*

Searching level included in question 5_14 is elementary for frequency, synoptic for time and location. This corresponds to level G in table 5.1. data involved in the process to answer this question is four-dimensional (spatial-temporal), which is same as question 5_13. The proposed method of applying SPM to EIT can be adopted to answer this question.

For question 5_15, the searching level is elementary for time, synoptic for frequency and location. This corresponds to level F in table 5.1. Data involved in the process of answering this task is 4D as well, but these four dimensions are composed with 3D for location and 1D for frequency instead of time. In principle, methods used in SPM can be applied to analyse some inverse tasks on that level F as well.

Situation involved in question 5_16 is more complex, where the searching level is synoptic for time, frequency, and location. This corresponds to level H in table 5.1. data appeared in the process of answering this question is 5D. Up to now, no suitable method has been found to cope with this kind of inverse task directly. One possible solution is to extend the GLM in SPM from one dimensional to two-dimensional (by considering the effect of time and frequency simultaneously), and then solve the multiple comparison effects with GRF. This work will be left for future. Currently, the 5D data involved in the process to answer question 5_16 are split into a series of 4D spectral-spatial subset under different values on the 5^{th} dimension, (which is normally frequency), and the 4D subsets are handled with SPM.

5.4.3 Task-based Visualisation

The goal of the task-based visualisation system development methodology is to facilitate the visualisation of multi-dimensional data, particularly multi-dimensional medical data. As explained in the first section of this chapter, the motivation of proposing a task-based methodology is twofold. First, among the three kinds of generally used visualisation approaches for MDMV (Multi-Dimensional Multi-Variate) data, subset-based method is most suitable for the visualisation of multi-dimensional medical image data. Secondly, subsets of a multi-dimensional dataset can be reasonably selected according to visualisation tasks. Among the three aspects of the task-based visualisation system development methodology, question formulation and method selection define and locate the subsets properly, and the third part supports the multi-dimensional medical data visualisation with subset-based approaches.

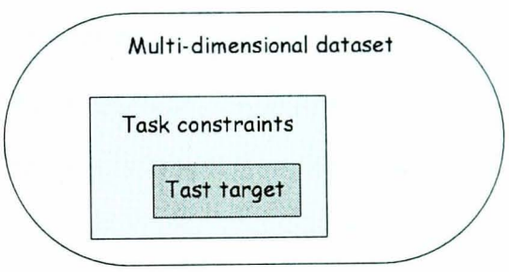

Figure 5.3 Illustration of the relation between a whole dataset and subsets defined by a task

For a specified task, two kinds of subsets (as illustrated in figure 5.3) can be defined for visualisation: One includes data corresponding to the target for a task, which will be mentioned as *target subset* later; the other contains data corresponding to the target and its constraints context defined in the task, which is cited as *target-constraint subset* below. Take question 5_14 as an example, the target subset defined by this question is a three-dimensional brain region. The target-constraint subset related to this question is a four-dimensional dataset including the identified brain region, the whole time interval, and impedance information corresponding to this region during the whole time interval at the given frequency.

The dimension of a target-constraint subset is equal to the dimension of the data involved in the process to answer the question, and is normally bigger than the dimension of the corresponding target subset. As reviewed in chapter 2, various algorithms are available for the visualisation of data with three or less dimensions, and animation is a powerful approach to provide information on an extra dimension. It is acceptable to display a four-dimensional medical dataset in one view. Therefore, a principle for subset selection can be proposed as: for *target subset* and *target-constraint subset* corresponding to a task, if the dimension of the target-constraint subset is not more than four, then the target-constraint subset should be utilized preferentially in the subset-based visualisation; otherwise, the target subset is adopted if its dimension is less than the dimension of the target-constraint subset. Beside the presentation of the selected subset, other information in the data is important for further understanding of a task. So navigation is an essential feature for a subset-based visualisation system. Let us take question 5_14 as an example again. The target subset and the target-constraint subset are three dimensional and four-dimensional correspondingly. According to the proposed principle, with such a visualisation task, it is desirable to display the target-constraint subset in one view, and the other information in the dataset can be inspected through navigation.

5.5 The Prototype Visualisation System – EIT5DVis

To demonstrate the proposed system development methodology for multi-dimensional medical data, a prototype system named "EIT5DVis" is developed for the visualisation of a 5D brain EIT dataset. In the following section, an overview of EIT5DVis system is presented. Then some visualisation examples are given to illustrate how EIT5DVis works. Finally, some initial evaluation and discussion of EIT5DVis system is given.

5.5.1 Overview of EIT5DVis

The EIT5DVis system is developed in MATLAB, with support from C++ and VTK (Visualisation Toolkit). MATLAB (The MathWorks Inc 2002) is a high-performance language for technical computing. It is an easy-to-use environment with powerful debug tools and so has been chosen to build up this prototype system. MATLAB provides some visualisation functions; however those functions are not enough for the development of the prototype system. For example, MATLAB does not include a volume rendering feature. VTK is selected to provide visualisation support. VTK is an open-source, portable, object-oriented software system for 3D computer graphics, visualisation and image processing (Schroeder, Avila et al. 2000). VTK includes a core implemented as a compiled C++ class library and supports TCL, Python and JAVA language bindings. However, VTK does not support MATLAB binding directly. Therefore, C++ is used as a bridge between MATLAB and VTK.

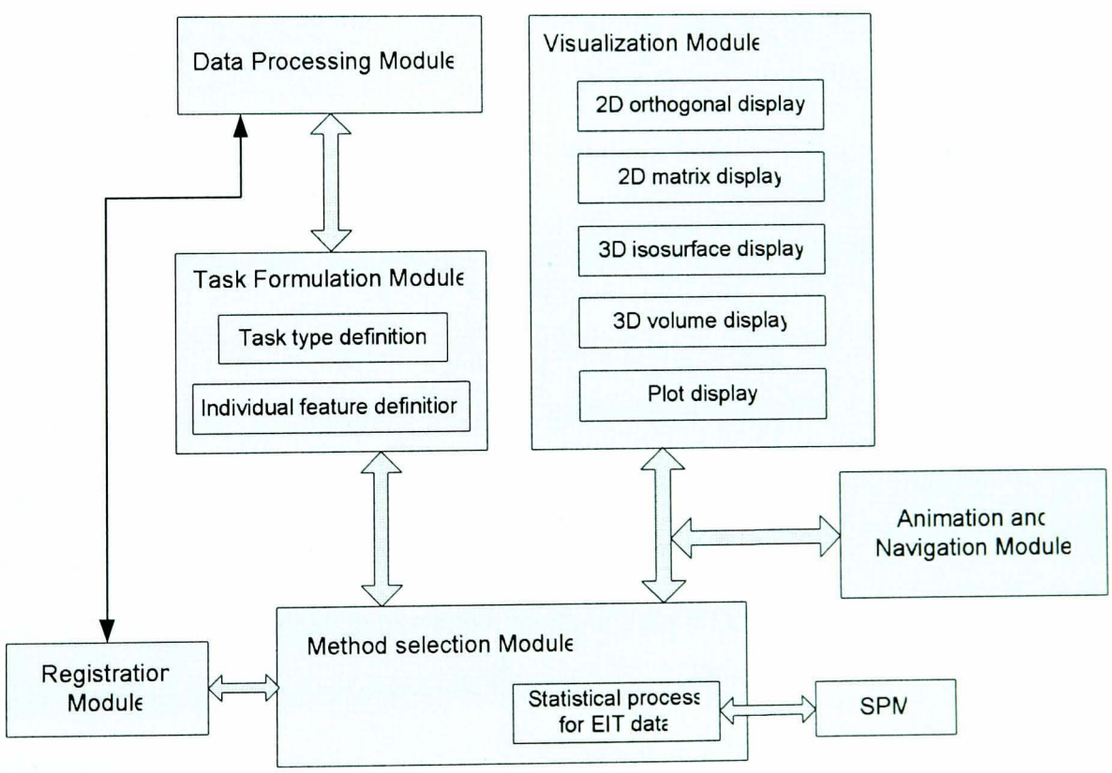

Figure 5.4 Module structure of the EIT5DVis system

EIT5DVis is constituted with relatively independent modules, which mainly include data processing module, task formulation module, method selection module, visualisation module, animation and navigation module, and registration module. Figure 5.4 illustrates communications among modules and main functions contained in those modules. A brief introduction for each module is given below.

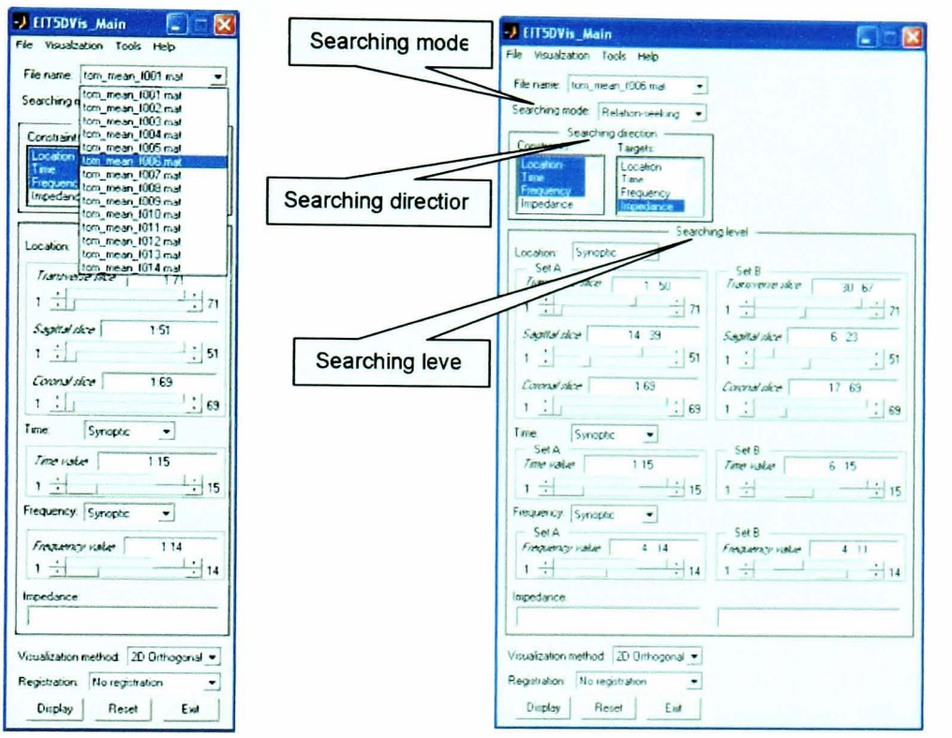

(a) GUI for task specification at lookup searching mode

(b) GUI for task specification at comparison or relatior-seeking searching mode

Figure 5.5 Graphical user interface for task specification

The data processing module in EIT5DVis system handles data input and output. The registration module included the registration algorithm proposed in Chapter 4. The task formulation module provides graphic user interfaces (see figure 5.5). Through these interfaces, users can specify task types by choosing values on the three dimensions of the task typology model, and then define constraints and targets part of tasks. After task specification, EIT5DVis calls the method selection module to choose a processing algorithm to answer the formulated question. The algorithms included in the method selection module are extensible: it is possible to combine new image analysis methods into this module, or communicate with other image processing software from this

module. In the current system, EIT data is processed by SPM in this module. The registration module can also be called from this module.

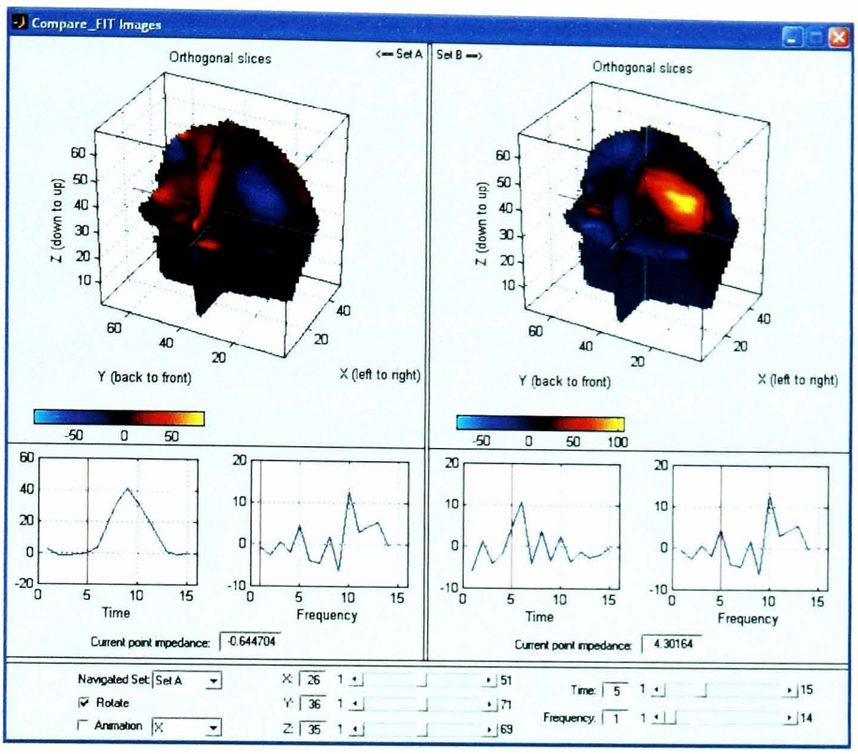

Figure 5.6 Orthogonal display of a direct comparative task

In the visualisation module, four main display methods are provided: 2D orthogonal display, 2D matrix display, 3D isosurface display, and 3D volume display. 2D orthogonal display visualises three orthogonal slices crossed at a selected voxel in one view (as illustrated in figure 5.6). In 2D matrix display, each elementary image within the 'matrix' presents information for a 2D slice, plus the two dimensions provided by 'matrix', theoretically, this method is able to visualise a 4D dataset in one view. Figure 5.7 shows an example of the 2D matrix display. The 3D isosurface display in EIT5DVis combines *isosurfaces* and *isocaps*: isosurfaces are constructed by creating a surface within a volume dataset that has the same value; isocaps are used along with isosurface to show inside slices of a volume. By default, EIT5DVis creates an isosurface corresponding to brain outline. Figure 5.8 presents a 3D isosurface visualisation example. The 3D volume display in EIT5DVis is realized by VTK. VTK provides three main volume rendering techniques: ray casting, 2D texture mapping, and support for

VolumePro volume rendering hardware. The 3D volume rendering presented in figure 5.9 is resulted by making use of the volumetric ray casting function in VTK.

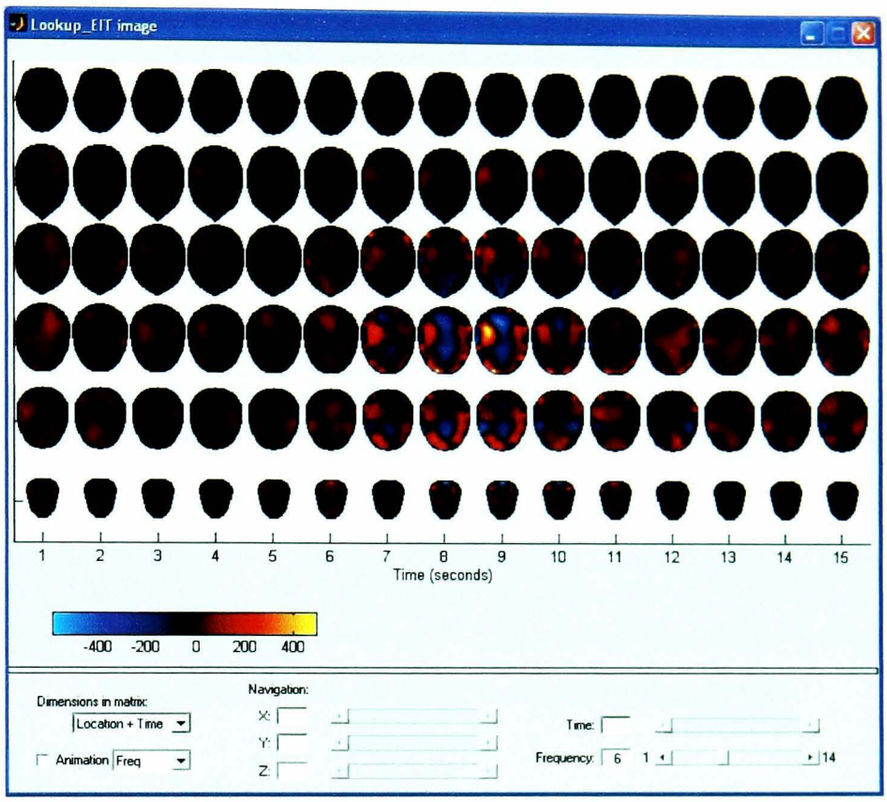

Figure 5.7 2D matrix display of a direct lookup task

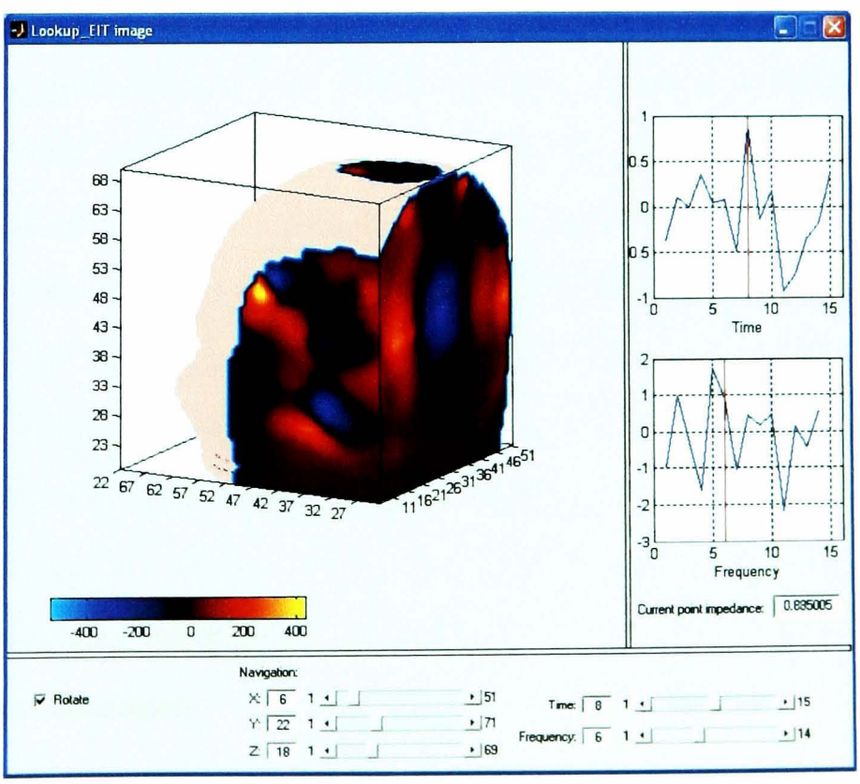

Figure 5.8 3D surface display of a direct lookup task

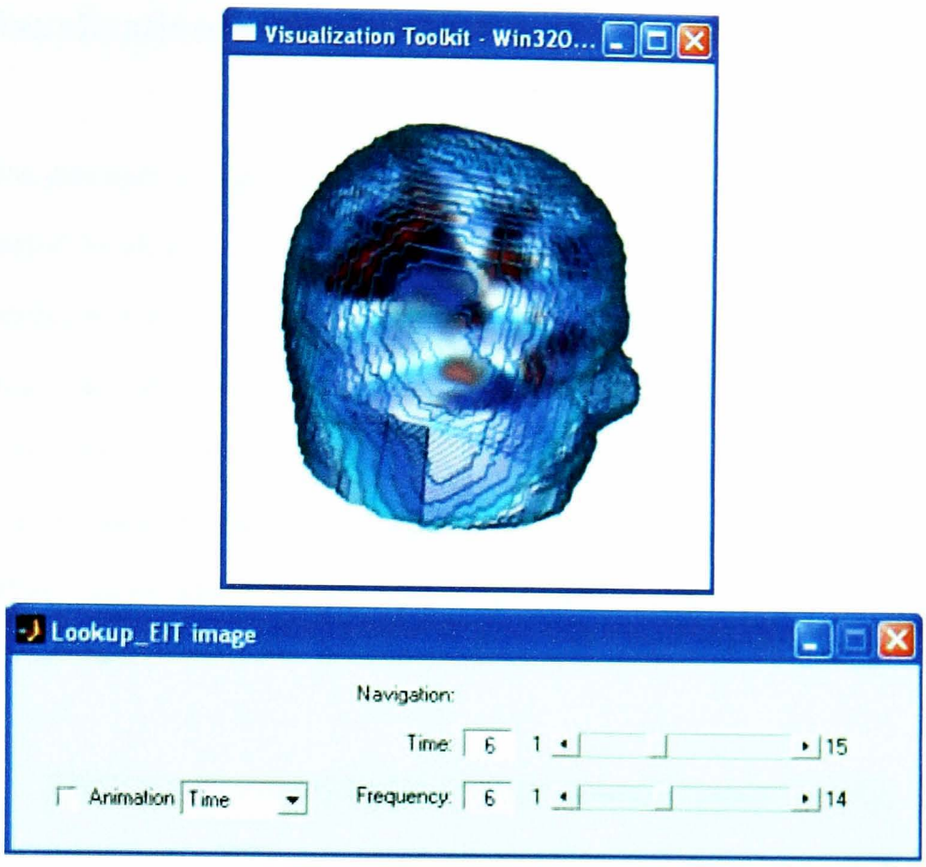

Figure 5.9 3D volume display of a direct lookup task

Task-based subsets, which include target subsets and target-constraint subsets, usually have fewer dimensions than the whole dataset. However, for some tasks, even their target subsets have same dimensions as the whole dataset. A integrated task-based visualisation system should be able to deal with these situations. In EIT5DVis system, the animation and navigation module is developed to visualise subsets of more than four-dimensions and enable browsing of the whole dataset. In other words, the display methods involved in the visualisation module show four dimensions in one view at most, animation can be used to present information along another dimension beside those dimensions which have been displayed in the view. For 2D orthogonal display and 3D surface display, navigation can be conducted along all the five dimensions. For 2D matrix display and 3D volume display, user can navigate the view along time and frequency dimensions. Alternatively, animation can be used as an automatic navigation along a selected dimension.

5.5.2 Visualisation Examples Using EIT5DVis

This section attempts to explain how EIT5DVis works with some concrete visualisation tasks. It would be ideal if a 5D clinical brain EIT dataset is available for this illustration. Unfortunately, only a set of 4D clinical brain EIT datasets obtained in visual stimulation experiments is accessible for this research currently. Instead of creating some simulated 5D brain EIT datasets, these 4D EIT datasets corresponding to different subjects are treated as a 5D dataset collected from one subject at different frequency within a time interval. More details about the 4D clinical brain EIT datasets can be found in section 3.4.2.

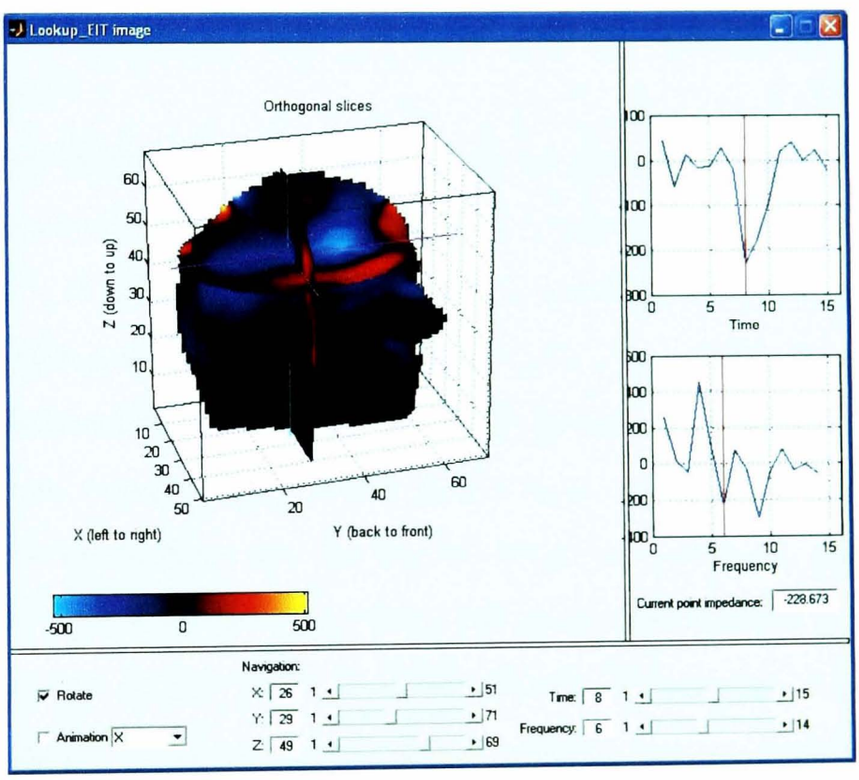

Figure 5.10 2D orthogonal display of the result for question 5_1

There are a range of tasks that can be addressed in EIT5DVis, whose complexity is roughly determined by where they are drawn from on the scale of searching level. For example let us take the first question listed in this chapter as an example:

Question 5_1: "*At a given point position, say* (x_1, y_1, z_1), *how did the impedance change along the time course under different frequencies?*"

This question is a direct lookup task. Figure 5.10 illustrates a 2D orthogonal display of result for this question.

Obviously a comprehensive visualisation system would include implementation of all tasks from all searching levels in the derived task typology model. However the complete implementation of the system is beyond the scope of this thesis. Rather the feasibility of the methodology will be demonstrated by investigating three complex inverse example questions. For the visualisation of a 5D brain EIT dataset collected in visual stimulation experiments, one of the most interesting questions is:

Question 5_17: "*Which part of the brain is activated under the visual stimulation?*"

The expected answer to this question is to display the activated regions. In order to process this question in EIT5DVis, the first phase is to formulate the question. The target of question 5_17 is *Location*, which is a reference according to the data model for a 5D EIT dataset given in formula (5.10) in section 5.3.4.1. Thus question 5_17 is a inverse task. This task considers action inside the brain along the whole experiment time interval and the whole frequency range instead of at a certain time point or under a certain frequency, so the searching level for time and frequency are synoptic. Also, the target locations for this task are 3D regions rather than isolated spatial points, so the reference location is at the synoptic level as well. Put them together, this task is on level H as defined in table 5.1: synoptic location, synoptic time and synoptic frequency. Relations concerned in this question are between references (location) and attribute (impedance), so searching mode of this task is lookup. Table 5.3 summaries the task type of question 5_17.

Table 5.3: Task type of question 5_17

Task dimension	Value
Searching level	Synoptic location, synoptic time and synoptic frequency
Searching mode	Lookup
Searching direction	Inverse

After the specification of task type, the next step in task definition stage is to set the target and constraints. Obviously, the target of question 5_17 is *Location*. There are three constraints in this question: the first one sets the synoptic *Time* as the whole experimental time interval, the second one restricts the synoptic *Frequency* to the whole frequency range in the experiment. The third constraint limits the value of impedance. In the original question, the third constraint is just mentioned as 'activated', and no further information about 'activated' is given. So it is not possible to define the impedance change pattern in an 'activated' region directly. However, those activations are caused by visual stimulations in the experiments and should react to the changes in stimulation. So the on and off pattern of visual stimulation is used as a constraint for impedance change pattern in this task. Specifically, matrix P in formula (5.13) is entered in the editable textbox to set the constraint to impedance change pattern (as shown in figure 5.11).

$$P = \begin{bmatrix} 0&0&0&0&0&0&1&1&1&0&0&0&0&0&0 \\ 0&0&0&0&0&0&1&1&1&0&0&0&0&0&0 \\ 0&0&0&0&0&0&1&1&1&0&0&0&0&0&0 \\ 0&0&0&0&0&0&1&1&1&0&0&0&0&0&0 \\ 0&0&0&0&0&0&1&1&1&0&0&0&0&0&0 \\ 0&0&0&0&0&0&1&1&1&0&0&0&0&0&0 \\ 0&0&0&0&0&0&1&1&1&0&0&0&0&0&0 \\ 0&0&0&0&0&0&1&1&1&0&0&0&0&0&0 \\ 0&0&0&0&0&0&1&1&1&0&0&0&0&0&0 \\ 0&0&0&0&0&0&1&1&1&0&0&0&0&0&0 \\ 0&0&0&0&0&0&1&1&1&0&0&0&0&0&0 \\ 0&0&0&0&0&0&1&1&1&0&0&0&0&0&0 \\ 0&0&0&0&0&0&1&1&1&0&0&0&0&0&0 \\ 0&0&0&0&0&0&1&1&1&0&0&0&0&0&0 \end{bmatrix} \quad (5.13)$$

In the matrix P, "0" denotes that no visual stimulation is presented, "1" indicates that visual stimulation is presented. Each column of this matrix represents a sample time point, and each row corresponds to a different frequency. As mentioned in section 3.4.2, the visual stimulation experiment lasted 6min and 15sec with a scalp impedance dataset acquired every 25sec, and the visual stimulus was presented after the sixth sample time point for 75sec in each experiment. So the visual stimulus accross the experiment time can be represented with six '0', following three '1', and then six '0'. Impedance values under different frequency are measured simultaneously, which means the visual stimulus is the same for each frequency. So same values appear on each row of matrix P.

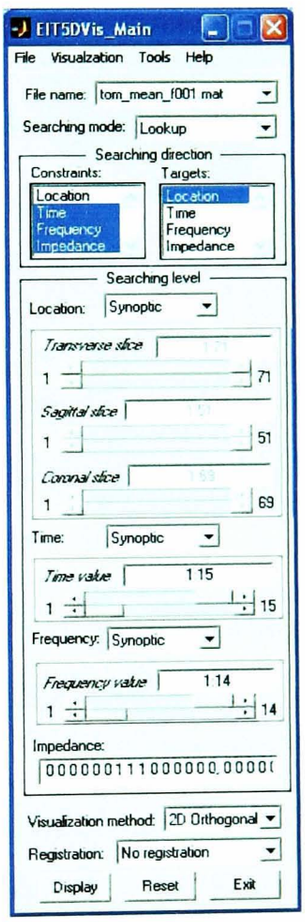

Figure 5.11 Task specification for the question 5_17

After task formulation, EIT5DVis calls the appropriate algorithm included in the task analysis module to process the task. For question 5_17, SPM is called to address the target location. Details about how SPM works with EIT dataset have been presented in Chapter 3. For this question, the target subset is 3D, and the target-constraint subset is

5D. So the target subset is adopted in the final visualisation. Figure 5.12 shows a 2D orthogonal display of the target subset, where locations activated under visual stimulation are presented with colour, and impedance in other parts of the brain are displayed in grey scale.

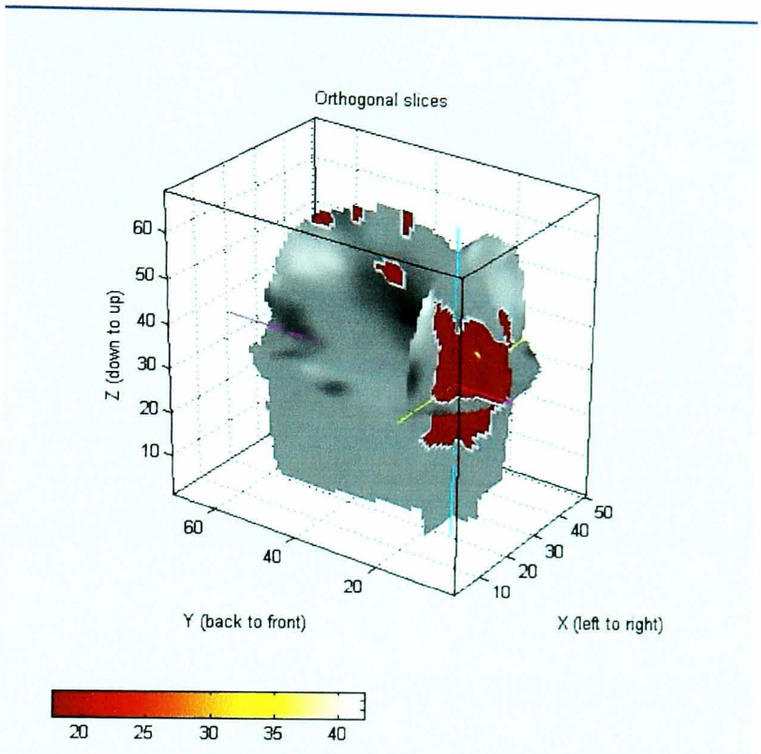

Figure 5.12 2D orthogonal display of the result for question 5_17

After the solution of question 5_17, another question may be presented subsequently:

Question 5_18: "*If the region of the brain activated under visual stimulation is in the visual cortex?*"

This question can be treated as a comparison task. However, as we know, EIT imaging data contain little anatomical information. It is difficult to recognise the visual cortex within EIT data. Therefore, it is better to process question 5_18 in two steps instead of as a simple comparison task: first, question 5_17 is processed as a subtask for question 5_18, then the target subset and the EIT dataset for question 5_17 are registered to a MRI dataset with the scheme proposed in chapter 4, and the final visualisation combine the registered target subset, the registered EIT dataset, and the MRI dataset. Figure 5.13 present a 2D orthogonal display of the target subset in the anatomical contours provided

by MRI dataset, where locations activated under visual stimulation are presented with color, and impedance in other parts of the brain are displayed in grey scale.

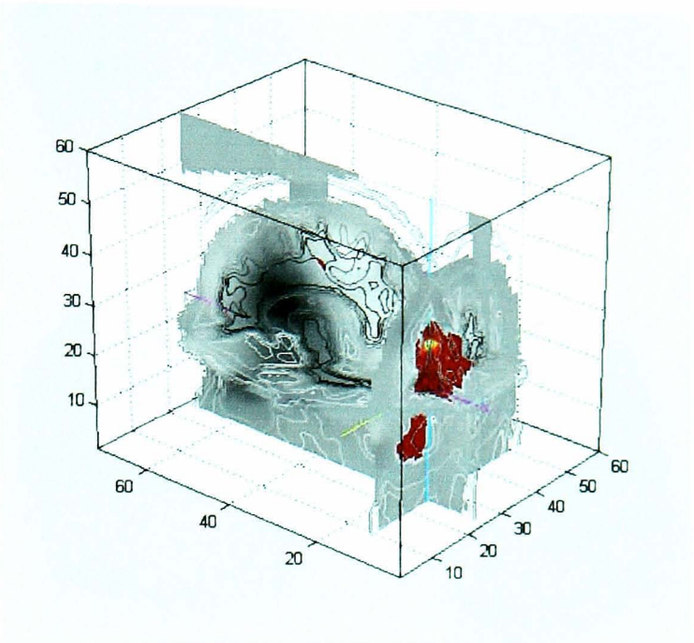

Figure 5.13 2D orthogonal display of the result for question 5_18

As pointed out in section 5.3.1.3, diverse relations can potentially exist in tasks. Apart from the commonest same/different relation, Boolean spatial operators as used in Constructive Solid Geometry (CSG), such as union, intersection and difference, commonly appears in tasks as well. Question 5_19 is a task involving a relation in the form of a CSG operation.

Question 5_19: "*For two specified frequencies, supposing L1 and L2 are the parts of brain activated under visual stimulation under these two frequency separately, then how is the union and intersection result of L1 and L2 ?*"

Question 5_19 is an inverse comparison task. According to section 5.3.2, inverse comparison tasks can be formed with "inverse lookup" subtasks and subtasks to"identify relations existing between two specified references". Actually, the inverse lookup subtasks contained in this question are similar to question 5_14. So same method can be adopted to deal with these "inverse lookup" subtasks for question 5_19. Figure 5.14 visualises the result for those "inverse lookup" subtasks and question 5_19.

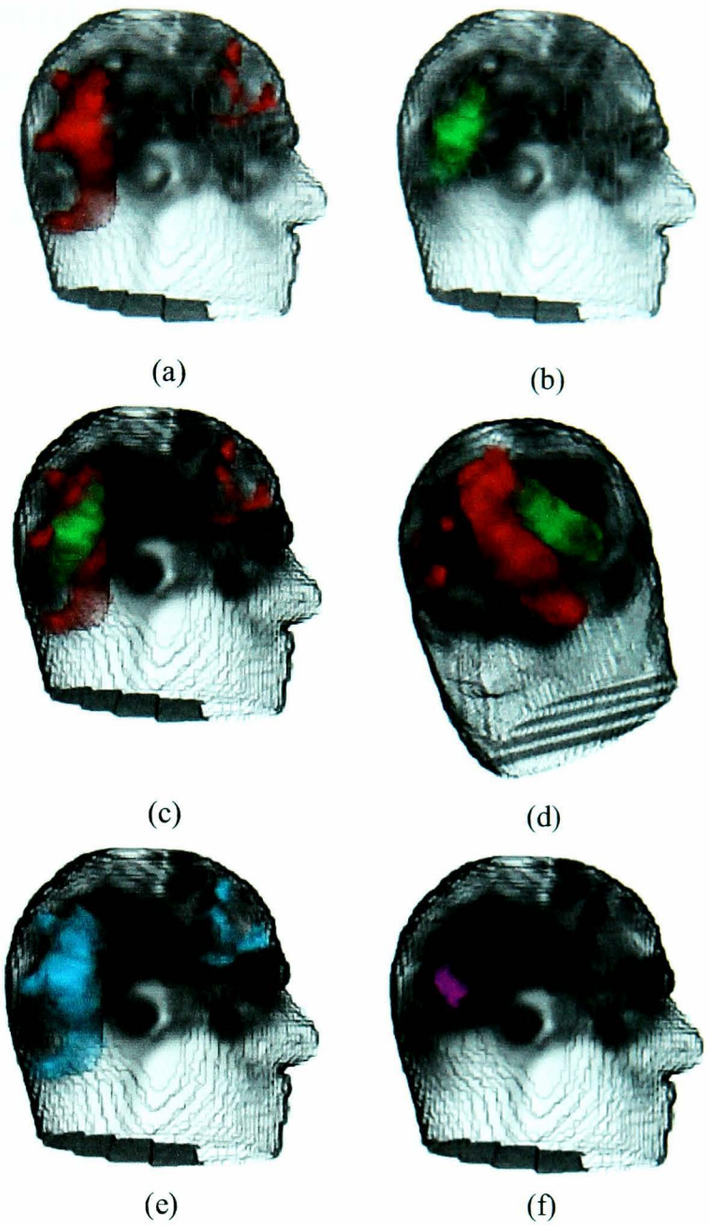

Figure 5.14 3D volume display of the result for question 5_19

Image (a) and (b) show volume rendering of the activated regions detected under two specified frequencies respectively; Images (c) and (d) display the activated regions included in (a) and (b) simultaneously from different viewing positions; Image (e) and (f) present the union and intersection of the activated regions detected under two specified frequencies.

5.5.3 Evaluation and Discussion

The EIT5DVis prototype system provides various display methods to visualisation 5D brain EIT dataset according to the users' requirements. Users can navigate in multi-

dimensional dataset freely. The EIT5DVis prototype system also presents some new ways to visualise EIT data. The major goal of EIT5DVis is to demonstrate the feasibility of the proposed system development methodology for multi-dimensional medical data rather than providing a comprehensive software tool. Naturally some analysis or display methods involved in other visualisation systems may not be included in the current version. However, given the modular structure of EIT5DVis, it is not difficult to extend the system and incorporate more analysis and display approaches.

To further evaluate the EIT5DVis system, an informal interview was conducted with a senior researcher in the EIT imaging area, three research associates from other medical imaging fields, one researcher in data mining, and one from computer science. Because EIT has not been used routinely in clinical use, no clinical competent reviewer is available at this moment. The main aspects to be examined in this interview include completeness of the task typology model, utility of the task definition interface, and general impression of the EIT5DVis system.

One aim of the EIT5DVis system is to describe questions which people may put forward and address the questions properly. During the interview, an introduction to the derived task typology model is given. The following question was asked of the respondents both before and after the introduction: "if you are visualising a 5D EIT dataset, what would be the question that most concerned to you?". It is interesting to notice that, before the introduction, most respondents proposed questions belonging to direct lookup tasks, this happened even for the senior researcher in EIT. However, after the introduction, many respondents changed their responses putting more inverse searching tasks and rating them of higher interest. This phenomenon suggested that, given the task typology model, some important while not intuitive tasks can be identified by the user. When using the EIT5DVis system, questions asked commonly by respondents included "identify any disorder and abnormalities correctly", "seeing enough information at once", "showing an overview which will provide general information about the dataset", etc. Almost all the

respondents concluded that the system is able to address their question satisfied, and the task typology model is able to cover all the questions they can construct.

The task specifying interface of EIT5DVis is constructed according to the derived task typology model. It looks different from interfaces used in common visualisation systems. The utility of this task definition interface is another aspect to be examined through the investigation. As expected when respondents tested the system without any instruction, they can formulate direct searching task and control the range of reference variables easily, but were seldom aware other features provided by the system. After some introductions and demonstrations, respondents are able to define different type of tasks through the interface. On the whole, most respondents graded the task definition interface as user-friendly, although some of them thought that the approach for impedance feature setting is not in a satisfactory format: although the task specification interface in EIT5DVis is untypical of image processing systems, it was not difficult for users to learn how to master it, given reasonable help information and examples.

On the question of the most useful feature provided by the EIT5DVis system, a variety of feedback was given by the respondents, partially because of their different research backgrounds. For example, some of them think the multiple viewing formats and choice of animation dimension is quite attractive; some took the analysis function imported from SPM as his/her favourite; some prefer the anatomical information provided by the registered display; and others put the task-based subset selection to reduce the visualisation complexity as the best feature.

Some useful suggestions on how to improve EIT5DVis system were also obtained through the interview. For example, to include more examples in the system, to provide some help document, to enhance the user interface, to enable the simultaneous animation for both sets in a comparison window, etc.

Combining the developer's self evaluation and analysis of the interview results, it is reasonable to conclude that, as a first trail to visualise 5D medical imaging data, EIT5DVis fulfils its main goal, although there are some points to be improved.

5.6 Conclusion

This chapter studied the last objective of this research: To derive a system development methodology for the visualisation of multi-dimensional medical images, and construct a prototype visualisation system for five-dimensional brain EIT datasets. Because of the specific features included in medical image data, showing subset of a dataset seems to be the best way among general approaches to visualise multi-dimensional medical image data. The most important step in subset-based visualisation is to select subsets properly. A task-based subset definition scheme is proposed in this chapter first. Then a task typology model is derived to support the task exploration for medical image data. Next, a task-based visualisation system development methodology is proposed. Finally, following the proposed methodology, a prototype visualisation system named EIT5DVis is developed for the 5D brain EIT data.

Up to now, all the three objectives of this research have been fulfilled. The next chapter is a summary of this work, which concludes the achievements made in this research and proposes some objectives for future work.

Chapter 6 Conclusions and Future Work

6.1 Conclusions on Current Work

With the development of new medical imaging technology, more accurate and complex information can be detected. Sequentially, datasets with multiple dimensions are needed to present the information. Visualisation of these multi-dimensional datasets, which is vital for medical research and clinical understanding, presents a big challenge for researchers. This is due to the use of multi-dimensional visualisation methods and dimension reduction methods for dataset from other fields are not suitable for medical image datasets. The work presented in this thesis is a new method of visualising multi-dimensional medical images datasets. The application is demonstrated using EIT images of the human brain function. The main contributions made in this research are:

- A new scheme for the processing of four-dimensional temporal-spatial brain EIT data with SPM is proposed. (Chapter 3)

- First demonstration of the feasibility to process brain EIT data with SPM according to the proposed scheme by using simulated brain EIT imaging data. (Chapter 3)

- First applying SPM to locate the ROI in human brain EIT data obtained under visual stimulation, and the experimental results proves that it is reasonable to use the balloon hemodynamic change model to simulate the impedance change during brain function activity. (Chapter 3)

- A new landmark-based registration scheme is developed to register brain EIT images with standard anatomical brain data. (Chapter 4)

- Experimental results are presented to validate the registration scheme by registering a brain EIT dataset with a Montreal BrainWeb MRI brain reference dataset. (Chapter 4)

- A novel task typology model is derived for task exploration in multi-dimensional medical image visualisation. (Chapter 5)

- A new task-based system development methodology is proposed for the visualisation of multi-dimensional medical images. (Chapter 5)

- A prototype visualisation system, named EIT5DVis, is developed and evaluated for the visualisation of five-dimensional brain EIT dataset. (Chapter 5)

6.2 Future Work

As a result of this research, several questions have arisen which justify further work. Some of them are described below.

- Extending the statistical process to five-dimensional EIT datasets

Currently, the SPM based statistical process scheme has been proposed for four-dimensional spatial-temporal brain EIT images. Five-dimensional spectral-temporal-spatial EIT datasets have to be processed frequency by frequency with this scheme. Future work can extend this scheme to deal with 5D EIT dataset obtained under different frequency simultaneously (as a whole).

- Combining theoretical generation with practical investigation for task exploration in EIT image visualisation

Considering the circumstance that EIT has not been used clinically and few experts in EIT area is available, the derived task typology model has been used to reveal potential tasks for 5D EIT dataset visualisation presently. Once EIT is used clinically, more experts in EIT research and application area will be available; it would be desirable to reveal potential visualisation tasks by combining practical task investigation with theoretical task generation. The combined approach can prompt the refinement of task definition interface; highlight important tasks in the system, etc.

- Registering EIT imaging data with functional imaging data and visualising the multi-dimensional multi-variate medical data

To compensate the poor spatial resolution of EIT imaging, EIT data is registered with anatomical imaging data in this research. That anatomical information is used in the visualisation step instead of the task definition stage at present. A possible future work is to register EIT data and functional imaging data with high spatial resolution, for example, fMRI data. In this way, fMRI is not only supposed to provide a anatomical visualisation background, the functional information included in it is more interesting. The EIT-fMRI registration results a multi-dimensional multi-variate dataset. The task typology model can still be employed to reveal potential tasks for the visualisation of an EIT-fMRI

dataset. However, in that case the relations between the two variates, which does not exist for 5D EIT dataset, should be considered.

- Applying the derived task typology model and visualisation system development methodology to other medical imaging modalities

The derived task typology model is adopted for the visualisation of a 5D brain EIT dataset as a demonstration in this research. In fact, the model is proposed as a general model and can be applied to datasets collected with different modalities. It can be employed to reveal visualisation tasks for datasets with less dimension as well as high dimensions. For example, fMRI can be measured under different frequency, although the data under different frequency are not obtained simultaneously at present. If the researcher prefers to analyse fMRI dataset collected under different frequency as a whole, it can be treat as a five-dimensional dataset. Naturally, visualisation tasks for this 5D fMRI data can be revealed in the same way as 5D EIT data by using the task typology model, and the task-based visualisation system development methodology can be utilized subsequently.

References

Adey, W. R., R. T. Kado, et al. (1962). "Impedance measurements in brain tissue of animals using microvolt singals." Experimental Neurology **5**: 47-66.

Adler, A. and W. R. B. Lionheart (2006). "Uses and abuses of EIDORS: an extensible software base for EIT." Physiological measurement **27**(5): S25-S42.

Ahadzi, G. M., O. Gilad, et al. (2004). An EIT electrode protocal for obtaining optimal current density in the primary visual cortex. XII international conference on electrical bioimpedance & V electrical impedance tomography, Gdansk, Poland.

Alpern, B. and L. Carter (1991). The hyperbox. Visualisation, 1991. Visualisation '91, Proceedings., IEEE Conference on.

Anagnostou, K., T. J. Atherton, et al. (2000). 4D volume rendering with the Shear Warp factorisation. Symposium on Volume visualisation, ACM Press.

Anderson, T. W. and T. W. Anderson (1984). An Introduction to Multivariate Statistical Analysis. New York, Wiley-Interscience.

Andrienko, N. and G. Andrienko (2006). Exploratory Analysis of Spatial and Temporal Data. Berlin, Heidelberg, Springer-Verlag.

Andrienko, N., G. Andrienko, et al. (2000). Visualisation of spatio-temporal information in the Internet. Database and Expert Systems Applications, 2000. Proceedings. 11th International Workshop on.

Andrienko, N., G. Andrienko, et al. (2003). "Exploratory spatio-temporal visualisation: an analytical review." Journal of Visual Languages and Computing **14**(6): 503-541.

Arnheim, R. (1997). Visual Thinking, University of California Press, Berkeley.

Arnholt, J. (1997). Development of interactive tools for analysis and visualisation of functional MRI data sets, Mayo Foundation, Rochester, MN.

Artzy, E., G. Frieder, et al. (1980). The theory, design, implementation and evaluation of a three-dimensional surface detection algorithm. International Conference on Computer Graphics and Interactive Techniques, ACM Press.

Arvo, J. and K. Novins (1994). Iso-Contour volume rendering. Symposium on Volume Visualisation, ACM SIGGRAPH.

Avila, R., T. He, et al. (1994). VolVis: a diversified volume visualisation system. Visualisation, 1994. IEEE Conference on.

Avill, R., Y. F. Mangnall, et al. (1987). "Applied potential tomography. A new noninvasive technique for measuring gastric emptying." Gastroenterology **92**(4): 1019-1026.

Bagshaw, A. P., A. D. Liston, et al. (2003). "Electrical Impedance Tomography of human brain function using reconstruction algorithms based on the finite element method." NeuroImage **20**(2): 752-764.

Barber, D. C. and B. H. Brown (1984). "Applied potential tomography." Journal of Physics E: Scientific Instruments **17**: 723-733.

Barber, D. C. and A. D. Seagar (1987). "Fast reconstruction of resistance images." Clinical physics and physiological measurement **8**(A): 47-54.

Bates, L. M., D. P. Hanson, et al. (1998). Implementation of an oblique-sectioning visualisation tool for line-of-sight stereotactic neurosurgical navigation using the AVW toolkit. Proc. SPIE Medical Imaging '98, San Diego, California.

Bayford, R. H., K. G. Boone, et al. (1996). "Improvement of the positional accuracy of EIT images of the head using a Lagrange multiplier reconstruction algorithm with diametric excitation." Physiological measurement **17**: A49-A57.

Bayford, R. H., A. Gibson, et al. (2001). "Solving the forward problem in electrical impedance tomography for the human head using IDEAS (integrated design engineering analysis software), a finite element modelling tool." Physiological measurement **22**: 55-64.

Belliveau, J. W., D. N. Kennedy, et al. (1991). "Functional Mapping of the Human Visual Cortex by Magnetic Resonance Imaging." Science **254**(5032): 716-719.

Bentley, C. L. and M. O. Ward (1996). Animating multidimensional scaling to visualise N-dimensional data sets. Information Visualisation '96, Proceedings IEEE Symposium on.

Bertin, J. (1983). Semiology of Graphics, The University of Wisconsin Press.

Besl, P. J. and N. D. McKay (1992). "A method for registration of 3-D shapes." IEEE Trans. Pattern Anal. Mach. Intell. **14**: 239-56

Binnie, C., A. Rowan, et al. (1982). The 10-20 system. A Manual of Electroencephalographic Technology**:** 325-331.

Blok, C. (2000). "Monitoring change: charateristics of dynamic geo-spatial phenomena for visual exploration." Spatial Cognition II, Lecture notes in Artificial Intelligence **1849**: 16-30.

Boone, K., A. M. Lewis, et al. (1994). "Imaging of cortical spreading depression by EIT: implications for localization of epileptic foci." Physiological measurement **15**: A189-A198.

Brett, M. (1999). "SPM theory introduction." from Been used by transfer.

Briggs, N. M., N. J. Avis, et al. (2000). "A real-time volumetric visualisation system for electrical impedance tomography." Physiological measurement **21**(1): 27-33.

Brinkmann, B. H., T. J. O'Brien, et al. (1998). "Scalp-recorded EEG localization in MRI volume data." Brain Topography **10**(4): 245-253.

Brown, B. H. (2003). "Electrical impedance tomography (EIT): a review." Journal of medical engineering and technology **27**(3): 97-108.

Brown, B. H., D. C. Barber, et al. (1994). "Cardiac and respiratory related electrical impedance changes in the human thorax." Biomedical Engineering, IEEE Transactions on **41**(8): 729-734.

Brown, B. H., R. A. Primhak, et al. (2002a). "Neonatal lungs--can absolute lung resistivity be determined non-invasively?" Medical & biological engineering & computing **40**(4): 388-394.

Brown, B. H., R. A. Primhak, et al. (2002b). "Neonatal lungs: maturational changes in lung resistivity spectra." Medical & biological engineering & computing **40**(5): 506-511.

Buxton, R. B., E. C. Wong, et al. (1998). "Dynamics of Blood Flow and Oxygenation Changes During Brain Activation: The Balloon Model." Magnetic Resonance in Medicine **39**: 855-864.

Canny, J. (1983). Finding Edges and Lines in Images. AI Lab, Massachusetts Institute of Technology.

Canny, J. (1986). "A computational approach to edge detection." IEEE Transaction Pattern Analysis Machine Intelligence **8**(6): 679--698.

Card, S. K., J. Mackinlay, et al. (1999). Readings in Information Visualisation : Using Vision to Think, Morgan Kaufmann.

Cherepenin, V. A., A. Y. Karpov, et al. (2002). "Three-dimensional EIT imaging of breast tissues: system design and clinical testing." Medical Imaging, IEEE Transactions on **21**(6): 662-667.

Chi, E. H. (2002). "Improving Web usability through visualisation." Internet Computing, IEEE **6**(2): 64-71.

Chiueh, T.-C., C.-K. Yang, et al. (1997). Integrated volume compression and visualisation. Visualisation '97., Proceedings, IEEE.

Ciesla, C. M., D. D. Arnone, et al. (2000). Biomedical applications of terahertz pulse imaging. Commercial and Biomedical Applications of Ultrafast Lasers II, SPIE.

Clay, M. T. and T. C. Ferree (2002). "Weighted regularization in electrical impedance tomography with applications to acute cerebral stroke." Medical Imaging, IEEE Transactions on **21**(6): 629-637.

Cleveland, W. S. (1993). Visualising Data. New Jersey, Hobart Press.

Cline, H. E., W. E. Lorensen, et al. (1986). High-resolution Three-Dimensional Reconstruction of Tomograms. Proceedings of RSNA.

Collignon, A., F. Maes, et al. (1995). Automated multi-modality image registration based on information theory. Information Processing in Medical Imaging, Dordrecht: Kluwer Academic.

Collins, B. M. (1993). Data visualisation – Has it all been seen before? Animation and Scientific Visualisation – Tools and Applications. R. A. Earnshaw and D. Watson, Academic Press: 3–28.

Collins, D. L. and A. P. Zijdenbos (1998). "Design and construction of a realistic digital brain phantom." IEEE Tran. on Med. Imaging **17**(3): 463-468.

Course_Notes. (1997). "SPM course notes." from been used by transfer.

Cox, R. W. (1996). "AFNI, software for analysis and visualisation of functional magnetic resonance neuroimages." Comput Biomed Res **29**: 162-173.

Csebfalvi, B. (2001). Interactive Volume-Rendering Techniques for Medical Data Visualisation. Institute of Computer Graphics and Algorithms. Vienna, Vienna University of Technology.

Csébfalvi, B. (1999). Fast Volume Rotation using Binary Shear-Warp Factorization. Joint EUROGRAPHICS-IEEE TCVG Symposium on Visualisation 99, Vienna, Austria, Springer-Verlag Wien.

D.Silver and X. Wang (1998). "Visualising Evolving Scalar Phenomena." Journal of Future Generations of Computer System: Invited Paper.

Dadzie, A. S. and A. Burger (2005). "Providing visualisation support for the analysis of anatomy ontology data." Bmc Bioinformatics **6**: 74.

Delibasis, K. K., G. K. Matsopoulos, et al. (1999). "Efficient Implementation of the Marching Cubes Algorithm for Rendering Medical Data." Lecture Notes In Computer Science **1593**: 989 - 997.

Dobashi, Y., V. Cingoski, et al. (1998). "A fast volume rendering method for time-varying 3-D scalar field visualisation using orthonormal wavelets." Magnetics, IEEE Transactions on **34**(5): 3431-3434.

Draper, N. R. and H. Smith (1981). Applied Regression Analysis. New York, John Wiley & Sons.

Duffy, F. H., P. H. Bartels, et al. (1981). "Significance probability mapping: an aid in the topographic analysis of brain electrical activity." Electroencephalography and clinical neurophysiology **51**(5): 455-462.

Eddy, W. F., M. Fitzgerald, et al. (1996). Functional Imaging Analysis Software-Computational Olio. Proceedings in Computational Statistics, Heidelberg, Physica-Verlag.

Espinosa, O. J., C. Hendrickson, et al. (1999). Domain analysis: a technique to design a user-centered visualisation framework. Information Visualisation, 1999. (Info Vis '99) Proceedings. 1999 IEEE Symposium on.

Eyuboglu, B. M., B. H. Brown, et al. (1989). "In vivo imaging of cardiac related impedance changes." Engineering in Medicine and Biology Magazine, IEEE **8**(1): 39-45.

Fabrizi, L., M. Sparkes, et al. (2004). Electrical Impedance Tomography during epileptic seizures: preliminary clinical studies. XII international conference on electrical bioimpedance & V electrical impedance tomography, Gdansk, Poland.

Faes, T. J. C., H. R. v. Genderingen, et al. (2006). "Some reflections on the EIT Conference." Physiological measurement **27**(5): Foreword.

Feiner, S. K. and C. Beshers (1990a). Worlds within worlds: metaphors for exploring n-dimensional virtual worlds. Proceedings of the 3rd annual ACM SIGGRAPH symposium on User interface software and technology, Snowbird, Utah, United States, ACM Press.

Feiner, S. K. and C. Beshers (1990b). Visualising n-dimensional virtual worlds with n-vision. Proceedings of the 1990 symposium on Interactive 3D graphics, Snowbird, Utah, United States, ACM Press.

Ferreira de Oliveira, M. C. and H. Levkowitz (2003). "From visual data exploration to visual data mining: a survey." Visualisation and Computer Graphics, IEEE Transactions on **9**(3): 378-394.

Fisher, R. B., S. Perkins, et al. (1996). HIPR: Hypermedia Image Processing Reference. Chichester, John Wiley and Sons Ltd.

Fishman, E. K., D. R. Ney, et al. (2006). "Volume Rendering versus Maximum Intensity Projection in CT Angiography: What Works Best, When, and Why." Radiographics **26**(3): 905-922.

Frankle, W. G., M. Slifstein, et al. (2005). "Neuroreceptor Imaging in Psychiatry: Theory and Applications." International Review of Neurobiology **67**: 385-440.

Frawley, W., G. Piatetsky-Shapiro, et al. (1992). "Knowledge discovery in databases: An overview." AI Magazine **Fall**: 57--70.

Frerichs, I. (2000). "Electrical impedance tomography (EIT) in applications related to lung and ventilation: a review of experimental and clinical activities." Physiological Measurement **21**(2): R1-R21.

Frerichs, I., M. Bodenstein, et al. (2005). "Effect of lower body negative pressure and gravity on regional lung ventilation determined by EIT." Physiological measurement **26**(2): S27-S37.

Frerichs, I., T. Dudykevych, et al. (2001). "Gravity effects on regional lung ventilation determined by functional EIT during parabolic flights." J Appl Physiol **91**(1): 39-50.

Friston, K. J. (2002). "Statistical Parametric Mapping." from been used by transfer.

Friston, K. J., J. Ashburner, et al. (1995). "Spatial registration and normalisation of images." Human Brain Mapping **2**: 165-189.

Friston, K. J., C. D. Frith, et al. (1991). "Comparing functional (PET) images: the assessment of significant change." Journal of Cerebral Blood Flow Metabolism **11**: 690-699.

Friston, K. J., A. P. Holmes, et al. (1995). "Statistical Parametric Maps in Functional Imaging: A General Linear Approach." Human Brain Mapping **2**: 189-210.

Fuchs, H., Z. M. Kedem, et al. (1977). "Optimal surface reconstruction from planar contours." Source Communications of the ACM **20**(10): 693 - 702.

Geddes, L. A. and L. E. Baker (1967). "The specific resistance of biological material--a compendium of data for the biomedical engineer and physiologist." Medical and Biological Engineering **5**(3): 271-293.

Glaser, D. E., K. J. Friston, et al. (2003). Haemodynamic modelling. Human Brain Function, Academic Press.

Glenn, W. J., R. Johnston, et al. (1975). "Image generation and display techniques for CT scan data. Thin transverse and reconstructed coronal and sagittal planes." Invest. Radiol. **10**(5): 403-416.

Goble, J. C., M. Cheney, et al. (1992). "Electrical Impedance Tomography in Three Dimensions." Applied Computational Electromagnetics Soc. J. **7**: 128-147.

Gold, S., B. Christian, et al. (1998). "Functional MRI Statistical Software Packages: a comparative analysis." Human Brain Mapping **6**(73-84).

Gratta, C. D., V. Pizzella, et al. (2001). "Magnetoencephalography - a noninvasive brain imaging method with 1 ms time resolution." Reports on Progress in Physics **64**(12): 1759-1814.

Gross, M. H., L. Lippert, et al. (1997). "Two Methods for Wavelet-Based Volume Rendering." Computers & Graphics **21**(2): 237-252.

Gross, M. H., L. Lippert, et al. (1995). "A New Method to Approximate the Volume Rendering Equation Using Wavelets and Piecewise Polynomials." Computers & Graphics **19**(1).

Gross, M. H., T. C. Sprenger, et al. (1997). Visualising information on a sphere. Information Visualisation, 1997. Proceedings., IEEE Symposium on.

Haeberli, P. and M. Segal (1993). Texture Mapping as a Fundamental Drawing Primitive. Proc. 4th Eurographics Workshop on Rendering, Paris, France.

Hahn, G., A. Just, et al. (2006). "Imaging pathologic pulmonary air and fluid accumulation by functional and absolute EIT." Physiological Measurement **27**(5): S187-S198.

Henderson, R. P. and J. G. Webster (1978). "An impedance camera for spatially specific measurements of the thorax." IEEE Transactions on Biomedical Engineering **25**(3): 250-254.

Hill, D. L. G., P. G. Batchelor, et al. (2001). "Medical image registration." Physics in medicine & biology **46**: R1-R45.

Holder, D. S. (1992a). "Detection of cerebral ischaemia in the anaesthetised rat by impedance measurement with scalp electrodes: implications for non-invasive imaging of stroke by electrical impedance tomography." Clinical physics and physiological measurement **13**(1): 63-76.

Holder, D. S. (1992b). "Detection of cortical spreading depression in the anaesthetised rat by impedance measurement with scalp electrodes: implications for non-invasive imaging of the brain with electrical impedance tomography." Clinical physics and physiological measurement **13**(1): 77-86.

Holder, D. S. (2005). Electrical Impedance Tomography: methods, history and applications, Institute of Physics Publishing.

Holder, D. S., A. Rao, et al. (1996). "Imaging of physiologically evoked responses by electrical impedance tomography with cortical electrodes in the anaesthetized rabbit." Physiological measurement **17**(4): A179-A186.

Hong, K. and P. Freeny (1999). "Pancreaticoduodenal arcades and dorsal pancreatic artery: comparison of CT angiography with three-dimensional volume rendering, maximum intensity projection, and shaded-surface display." Am. J. Roentgenol. **172**(4): 925-931.

Horbelt, S., M. Unser, et al. (1999). Wavelet Projections for Volume Rendering. Twentieth Annual Conference of the European Association for Computer Graphics (EUROGRAPHICS'99), Milano, Italy.

Horesh, L., R. H. Bayford, et al. (2004). BEYOND THE LINEAR DOMAIN - THE WAY FORWARD IN MFEIT IMAGE RECONSTRUCTION OF THE HUMAN HEAD. XII International Conference on Electrical Bio-Impedance & V Electrical Impedance Tomography, Gdansk, Poland.

Hu, B. B. and M. C. Nuss (1995). "Imaging with Terahertz Waves." Optical Letters **20**(16): 1716-1718.

Huang, J., K. Mueller, et al. (2000). FastSplats: optimized splatting on rectilinear grids. Visualisation 2000. Proceedings.

Huppertz, H. J., M. Otte, et al. (1998). "Estimation of the accuracy of a surface matching technique for registration of EEG and MRI data." Electroencephalography and Clinical Neurophysiology **106**(5): 409-415.

Inselberg, A. and B. Dimsdale (1987). Parallel coordinates for visualising multi-dimensional geometry. CG International '87 on Computer graphics 1987, Karuizawa, Japan, Springer-Verlag.

Inselberg, A. and B. Dimsdale (1990). Parallel coordinates: a tool for visualising multi-dimensional geometry. Visualisation, 1990. Visualisation '90., Proceedings of the First IEEE Conference on.

Inselberg, A., M. Reif, et al. (1987). "Convexity algorithms in parallel coordinates." Journal of the ACM (JACM) **34**(4): 765 - 801.

Isaacson, D., J. L. Mueller, et al. (2006). "Imaging cardiac activity by the D-bar method for electrical impedance tomography." Physiological measurement **27**(5): S43-S50.

Itoh, T. and K. Koyamada (1994). Isosurface generation by using extrema graphs. Visualisation, 1994., Visualisation '94, Proceedings., IEEE Conference on.

Jain, H., D. Isaacson, et al. (1997). "Electrical Impedance Tomography of complex conductivity distributions within noncircular bounbdary." IEEE Trans. Biomed. Eng **44**(12): 1051-1060.

Jiang, D. and J. P. Singh (1997). Improving parallel shear-warp volume rendering on shared address space multiprocessors. Proceedings of the sixth ACM SIGPLAN symposium on Principles and practice of parallel programming, Las Vegas, Nevada, United States, ACM Press.

Joines, W. T., Y. Zhang, et al. (1994). "The measured electrical properties of normal and malignant human tissues from 50 to 900 MHz." Medical Physics **21**(4): 547-550.

Kanitsar, A., D. Fleischmann, et al. (2002). CPR - Curved Planar Reformation. IEEE Visualisation 2002.

Kaufman, A. E. (2000). Volume visualisation in medicine. Handbook of Medical Imaging: Processing and Analysis. I. N. Bankman. San Diego, CA, Academic Press. **Chapter 43:** 713-730.

Kerner, T. E., K. D. Paulsen, et al. (2002). "Electrical impedance spectroscopy of the breast: clinical imaging results in 26 subjects." Medical Imaging, IEEE Transactions on **21**(6): 638-645.

Kohonen, T. (1990). "The self-organizing map." Proceedings of the IEEE **78**(9): 1464-1480.

Kohonen, T., E. Oja, et al. (1996). "Engineering applications of the self-organizing map." Proceedings of the IEEE **84**(10): 1358-1384.

Koussoulakou, A. and M. J. Kraak (1992). "Spatial-temporal maps and cartographic communication." The cartographic journal **29**: 101-108.

Kraak, M.-J. (1999). Visualising spatial distribution. Geographical Information Systems. P. Longley, M. Goodchild, D. Maguire and D. Rhind. New York, JohnWiley and Sons. **1:** 157-73.

Kraemer, E. and J. T. Stasko (1993). "The Visualisation of Parallel Systems - an Overview." Journal of Parallel and Distributed Computing **18**(2): 105-117.

Kreeger, K., I. Bitter, et al. (1998). Adaptive perspective ray casting. Volume Visualisation, 1998. IEEE Symposium on.

Kruskal, J. B. and M. Wish (1978). Multidimensional Scaling. London, Sage Publications, Inc.

Kuszyk, B. S., D. G. Heath, et al. (1996). "Skeletal 3-D CT: advantages of volume rendering over surface rendering." Skeletal Radiology **25**(3): 207 - 214.

Lacroute, P. (1996). "Analysis of a parallel volume rendering system based on the shear-warp factorization." Visualisation and Computer Graphics, IEEE Transactions on **2**(3): 218-231.

Lacroute, P. and M. Levoy (1994). Fast Volume Rendering Using a Shear-Warp Factorization of the Viewing Transformation. Proc. SIGGRAPH '94, Orlando, Florida.

Lamm, C., C. Windischberger, et al. (2001). "Co-registration of EEG and MRI data using matching of spline interpolated and MRI-segmented reconstructions of the scalp surface." Brain Topography **14**(2): 93-100.

Laramee, R. S., D. Weiskopf, et al. (2004). Investigating swirl and tumble flow with a comparison of visualisation techniques. IEEE Visualisation 2004, Austin, Texas, USA.

Laur, D. and P. Hanrahan (1991). Hierarchical splatting: a progressive refinement algorithm for volume rendering. Proceedings of the 18th annual conference on Computer graphics and interactive techniques, ACM Press.

Law, A. and R. Yagel (1996). An Optimal Ray Traversal Scheme for Visualising Colossal Medical Volumes. Proceedings of Visualisation in Biomedical Computing, Hamburg, Germany.

LeBlanc, J., M. O. Ward, et al. (1990). Exploring N-dimensional databases. Visualisation, 1990. Visualisation '90., Proceedings of the First IEEE Conference on.

Levin, D. N., C. A. Pelizzari, et al. (1988). "Retrospective geometric correlation of MR, CT, and PET images." Radiology **169**: 817-23.

Levoy, M. (1992). Volume Rendering using the Fourier Projection-Slice Theorem. Proc. Graphics Interface '92, Vancouver, British Columbia, Canadian Information Processing Society.

Li, J. and P. Agathoklis (1998). "An efficiency enhanced isosurface generation algorithm for volume visualisation." The Visual Computer **13**(9 - 10): 391-400.

Lionheart, W. R. B. (2004). "EIT reconstruction algorithms: pitfalls, challenges and recent developments." Physiological measurement **25**(1): 125-142.

Liston, A. D. (2004). Modles and image reconstruction in Electrical Impedance Tomography of human brain function. London, Middlesex University.

Liston, A. D., R. H. Bayford, et al. (2004). "The effect of layers in imaging brain function using electrical impedance tomography." Physiological measurement **25**(1): 143-158.

Livnat, Y., H.-W. Shen, et al. (1996). "A near optimal isosurface extraction algorithm using the span space." Visualisation and Computer Graphics, IEEE Transactions on **2**(1): 73-84.

Lorensen, W. E. and H. E. Cline (1987). "Marching cubes: A high resolution 3D surface construction algorithm." Computer Graphics **21**(4): 163-169.

Ma, K.-L., D. Smith, et al. (1998). Efficient Encoding and Rendering of Time-Varying Volume Data, ICASE Report No. 98-22 (NAS/CR-1998-208424).

Mackinlay, J. (1986). "Automating the design of graphical presentations of relational information." ACM Transactions on Graphics (TOG) **5**(2): 110 - 141.

Maes, F., A. Collignon, et al. (1997). "Multimodality image registration by maximization of mutual information." IEEE Trans. Med. Imaging **16**: 187-98.

Maintz, J. B. A. and M. A. Viergever (1998). "A Survey of Medical Image Registration." Medical Imaging Analysis **2**(1): 1-36.

Malmivuo, J. and R. Plonsey (1995). Bioelectromagnetism. New Tork, Oxford University Press.

Malzbender, T. (1993). "Fourier volume rendering." ACM Transactions on Graphics (TOG) **12**(3): 233-250.

Mangnall, Y. F., C. Barnish, et al. (1988). "Comparison of applied potential tomography and impedance epigastrography as methods of measuring gastric emptying." Clinical physics and physiological measurement **9**: 249-254.

Mattson, J. and M. Simon (1996). The Pioneers of NMR and Magnetic Resonance in Medicine: The Story of MRI. Jericho & New York, Bar-Ilan University Press.

Matveyev, S. V. (1994). Approximation of isosurface in the Marching Cube: ambiguity problem. Visualisation, 1994., Visualisation '94, Proceedings., IEEE Conference on.

Metherall, P., D. C. Barber, et al. (1996). "Three-dimensional electrical impedance tomography." Nature **380**(6574): 509-512.

Meyers, D. (1994). Reconstruction of Surfaces From Planar Contours. PhD thesis, University of Washington.

Meyers, D., S. Skinner, et al. (1992). "Surfaces from contours." ACM Transactions on Graphics (TOG) **11**(3): 228-258.

Mihalisin, T., E. Gawlinski, et al. (1990). Visualising a scalar field on an N-dimensional lattice. Visualisation, 1990. Visualisation '90., Proceedings of the First IEEE Conference on.

Mihalisin, T., J. Timlin, et al. (1991a). "Visualising multivariate functions, data, and distributions." Computer Graphics and Applications, IEEE **11**(3): 28-35.

Mihalisin, T., J. Timlin, et al. (1991b). Visualisation and analysis of multi-variate data: a technique for all fields. Visualisation, 1991. Visualisation '91, Proceedings., IEEE Conference on.

Montani, C., R. Scateni, et al. (1994a). Discretized Marching Cubes. Visualisation, 1994., Visualisation '94, Proceedings., IEEE Conference on.

Montani, C., R. Scateni, et al. (1994b). "A modified look-up table for implicit disambiguation of Marching Cubes." The Visual Computer **10**(6): 353-355.

Morton, W. J. and E. W. Hammer (1896). The X-ray; Or, Photography of the Invisible and Its Value in Surgery, American Technical Book Co.

Mueller, K., T. Moller, et al. (1999). Splatting without the blur. Visualisation '99. Proceedings.

Mueller, K., T. Moller, et al. (1998). "Splatting errors and antialiasing." Visualisation and Computer Graphics, IEEE Transactions on **4**(2): 178-191.

Mueller, K. and R. Yagel (1996). Fast perspective volume rendering with splatting by utilizing a ray-driven approach. Visualisation '96. Proceedings.

Muraki, S. (1993). "Volume data and wavelet transforms." Computer Graphics and Applications, IEEE **13**(4): 50-56.

Nakakoji, K., A. Takashima, et al. (2001). Cognitive effects of animated visualisation in exploratory visual data analysis. Information Visualisation, 2001. Proceedings. Fifth International Conference on.

Nielsen, F. A. and L. K. Hansen (2000). Experiences with matlab and vrml in functional neuroimaging visualisations. Visualisation development environments 2000 proceedings.

Nielson, G. M. and B. Hamann (1991). The asymptotic decider: resolving the ambiguity in marching cubes. Visualisation, 1991. Visualisation '91, Proceedings., IEEE Conference on.

Ning, P. and L. Hesselink (1992). Vector quantization for volume rendering. Proceedings of the 1992 workshop on Volume visualisation, Boston, Massachusetts, United States, ACM Press.

Ning, P. and L. Hesselink (1993). Fast volume rendering of compressed data. Visualisation, 1993. Visualisation '93, Proceedings., IEEE Conference on.

Nour, S., Y. Mangnall, et al. (1993). "Measurement of gastric emptying in infants with pyloric stenosis using applied potential tomography." Arch Dis Child **68**(4): 484-486.

Odenstedt, H., S. Lindgren, et al. (2005). "Slow moderate pressure recruitment maneuver minimizes negative circulatory and lung mechanic side effects: evaluation of recruitment maneuvers using electric impedance tomography." Intensive Care Medicine **31**(12): 1706-1714.

Ogata, M., T. Ohkami, et al. (1998). A real-time volume rendering architecture using an adaptive resampling scheme for parallel and perspective projections. Volume Visualisation, 1998. IEEE Symposium on.

Orchard, J. and T. Möller (2001). Accelerated splatting using a 3D adjacency data structure. Graphics interface 2001, Ottawa, Ontario, Canada, Canadian Information Processing Society.

Pelizzari, C. A., G. T. Y. Chen, et al. (1989). "Accurate three-dimensional registration of CT, PET, and/or MR images of the brain." J. Comput. Assist. Tomogr. **13** 20-6.

Peuquet, D. J. (1994). It's about time: a conceptual framework for the representation of temporal dynamics in Geographic Information Systems. Annals fo the associstion of american geographers, Blackwell Publishers.

Plonsey, R. (1969). Bioelectric Phenomena. New York, McGraw-Hill.

Plonsey, R. (1984). "Quantitative formulations of electrophysiological sources of potential fields in volume conductors." IEEE Transactions on Biomedical Engineering **31**(12): 868-872.

Poline, J. B., K. J. Friston, et al. (1995). "Estimating Smoothness in Statistical Parametric Maps: Confidence Intervals on p-Values." Journal of Computer Assisted Tomography **19**(5): 788-796.

Polydorides, N. and W. R. B. Lionheart (2002). "A Matlab toolkit for three-dimensional electrical impedance tomography: a contribution to the Electrical Impedance and Diffuse Optical Reconstruction Software project." Measurement Science and Technology **13**(12): 1871-1883.

Prewitt, J. M. (1970). Object Enhancement and Extraction. Picture Processing and Psychopictorics. B. Lipkin and A. Rosenfeld. New York, Academic Press: 75-149.

Price, B. A., R. M. Baecker, et al. (1993). "A Principled Taxonomy of Software Visualisation." Journal of Visual Languages and Computing **4**(3): 211-266.

Pulletz, S., H. R. v. Genderingen, et al. (2006). "Comparison of different methods to define regions of interest for evaluation of regional lung ventilation by EIT." Physiological measurement **27**(5): S115-S127.

Qian, L., M. Wachowicz, et al. (1997). Delineating operations for visualisation and analysis of space-time data in GIS. GIS/LIS'97 conference.

Rabbani, K., M. Hassan, et al. (1996). "3D object localization using EIT measurements at two level." Physiological measurement **17**(3): 189-199.

Ramachandran, P. (2003). Scientific data visualisation with MayaVi. SciPy'03, CalTech.

Ranck, J. B. (1963). "Specific impedance of rabbit cerebral cortex." Exp. Neurol. **7**: 144–152.

Rao, A., A. Gibson, et al. (1997). "EIT images of electrically-induced epileptic activity in anaesthetized rabbits." Medicine biological Engineers Computing **35**: A327-A329.

Ravelli, A. M. and P. J. Milla (1994). "Detection of gastroesophageal reflux by electrical impedance tomography." Journal of Pediatric Gastroenterology and Nutrition **18**(2): 205-213.

Rhodes, M., W. Glenn, et al. (1980). "Extracting Oblique Planes from Serial CT Sections." Journal of Computer Assisted Tomography **4**(5): 649-657.

Richard, F., K. J. Friston, et al. (1997). Human Brain Function. California USA, Academic Press.

Robb, R. A. (1999). "3-D visualisation in biomedical applications." Annu. Rev. Biomed. Eng. **01**: 377-399.

Robb, R. A. (2000). Biomedical Imaging, Visualisation, and Analysis, Wiley-Liss.

Roberts, J. C. (2004A). Exploratory visualisation with multiple linked views. Exploring Geovisualisation, Amsterdam, Elseviers.

Roberts, L. G. (1965). Machine perception of three-dimensional solids. Optical and electrooptical information processing. J. T. Tippett. Cambridge, MIT Press: 125-143.

Robertson, P. K. (1991). "A methodology for choosing data representations." Computer Graphics and Applications, IEEE **11**(3): 56-67.

Rush, S. and D. A. Driscoll (1969). "EEG electrode sensitivity--an application of reciprocity." IEEE Transactions on Biomedical Engineering **16**(1): 15-22.

Sakas, G., M. Grimm, et al. (1995). Optimized Maximum Intensity Projection (MIP). Proceedings 6th Eurographics Workshop on Rendering, Springer-Verlag.

Santos, S. R. d. and K. W. Brodlie (2002). Visualising and investigating multidimensional functions. Proceedings of the symposium on Data Visualisation 2002, Barcelona, Spain, Eurographics Association.

Sato, Y., N. Shiraga, et al. (1998). "LMIP: Local Maximum Intensity Projection." Journal of Computer Assisted Tomography **22**(6).

Saulnier, G. J., R. S. Blue, et al. (2001). "Electrical impedance tomography." Signal Processing Magazine, IEEE **18**(6): 31-43.

Schroeder, W. J., L. S. Avila, et al. (2000). "Visualising with VTK: a tutorial." IEEE Computer Graphics and Applications **20**(5): 20-27.

Schulze, J. P. and U. Lang (2002). The parallelization of the perspective shear-warp volume rendering algorithm. Proceedings of the Fourth Eurographics Workshop on Parallel Graphics and Visualisation, Blaubeuren, Germany, Eurographics Association.

Seagar, A. D., D. C. Barber, et al. (1987). "Theoretical limits to sensitivity and resolution in impedance imaging." Clinical physics and physiological measurement **8**(Suppl. A): 13-31.

Shahidi, R., B. Lorensen, et al. (1996). Surface Rendering Versus Volume Rendering In Medical Imaging: Techniques And Applications. Visualisation '96. Proceedings.

Shannon, C. E. (1948). "The mathematical theory of communication (parts 1 and 2)." Bell Syst. Tech. J. **27**: 379-423, 623-56.

Shantz, M. (1981). "Surface definition for branching, contour-defined objects." ACM SIGGRAPH Computer Graphics **15**(2): 242 - 270.

Shekhar, R., E. Fayyad, et al. (1996). Octree-based decimation of marching cubes surfaces. Visualisation '96. Proceedings.

Shen, H.-W. and C. R. Johnson (1994). Differential volume rendering: a fast volume visualisation technique for flow animation. Visualisation, 1994., Visualisation '94, Proceedings., IEEE Conference on.

Shneiderman, B. (1996). The eyes have it: a task by data type taxonomy for information visualisations. Visual Languages, 1996. Proceedings., IEEE Symposium on.

Singh, K. D., I. E. Holliday, et al. (1997). "Evaluation of MRI-MEG/EEG co-registration strategies using Monte Carlo simulation." Electroencephalography and Clinical Neurophysiology **102**(2): 81-85.

Skudlarski, P., C. Lacadie, et al. (1995). fMRI Manual. Unpublished, New Haven: Yale University.

Smallwood, R. H., A. R. Hampshire, et al. (1999). "A comparison of neonatal and adult lung impedances derived from EIT images." Physiological measurement **20**(4): 401-413.

Smith, L. I. (2002). "A tutorial on Principal Components Analysis." Retrieved July, 2006, from file://E:%5CBibliography%5C2006%5CAdd%20by%20citing%5CA%20tutorial%20on%20Principal%20Components%20Analysis.pdf.

Sobel, I. E. (1970). Camera models and machine perception. Electrical Engineering Department, Stanford University.

Solaiyappan, M. (2000). Visualisation pathways in biomedicine. Handbook of medical imaging: processing and analysis. I. N. Bankman. New York, London, Academic Press: 659-684.

Somersalo, E., M. Cheney, et al. (1992). "Existence and uniqueness for electrode models for electric current computed tomography." SIAM Journal on Applied Mathematics **52**(4): 1023-1040.

Soni, N. K., A. Hartov, et al. (2004). "Multi-frequency electrical impedance tomography of the breast: new clinical results." Physiological measurement **25**(1): 301-314.

Soyer, P., D. Heath, et al. (1996). "Three-Dimensional Helical CT of Intrahepatic Venous Structures: Comparison of Three Rendering Techniques." Journal of Computer Assisted Tomography **20**(1): 122-127.

Spence, R. (2001). Information visualisation, ACM press.

Sprenger, T. C., R. Brunella, et al. (2000). A Hierarchical Visual Clustering Method Using Implicit Surfaces. Zurich, Switzerland, Computer Science Dept., ETH Zurich.

Springmeyer, R. R., M. M. Blattner, et al. (1992). A characterization of the scientific data analysis process. Visualisation, 1992. Visualisation '92, Proceedings., IEEE Conference on.

Sramek, M. and A. Kaufman (2000). "Fast ray-tracing of rectilinear volume data using distance transforms." Visualisation and Computer Graphics, IEEE Transactions on **6**(3): 236-252.

Stefan, H., G. Scheler, et al. (2004). "Magnetoencephalography (MEG) predicts focal epileptogenicity in cavernomas." Journal of Neurology Neurosurgery and Psychiatry **75**(9): 1309-1313.

Strupp, J. P. (1996). "Stimulate: A GUI based fMRI analysis software package." Neuroimage **3**: 607.

Swan, J. E., II, K. Mueller, et al. (1997). An anti-aliasing technique for splatting. Visualisation '97., Proceedings.

The MathWorks Inc. (2002). "MATLAB Release 13: Help documents."

Tian, J., S. Bao, et al. (2003). Medical Image Process and Analysis. Beijing, Publishing House of Electromics Industry.

Tidswell, A. T., A. Gibson, et al. (2001a). "Electrical impedance tomography of human brain activity with a two-dimensional ring of scalp electrodes." Physiological measurement **22**(1): 167-175.

Tidswell, T., A. Gibson, et al. (2001b). "Three-Dimensional Electrical Impedance Tomography of Human Brain Activity." NeuroImage **13**(2): 283-294.

Tietjen, C., T. Isenberg, et al. (2005). Combining Silhouettes, Surface,and Volume Rendering for Surgery Education and Planning. IEEE/Eurographics Symposium on Visualisation (EuroVis).

Toma, K., T. Matsuoka, et al. (2002). "Generators of movement-related cortical potentials: fMRI-constrained EEG dipole source analysis." Neuroimage **17**(1): 161-173.

Tory, M., N. Rober, et al. (2001). 4D space-time techniques: a medical imaging case study. Visualisation, 2001. VIS '01. Proceedings.

Totsuka, T. and M. Levoy (1993). "Frequency Domain Volume Rendering." Computer Graphics (Proceedings SIGGRAPH '93),: 271-278.

Tukey, J. W. (1977). Exploratory Data Analysis., Addison-Wesley.

Tuy, H. K. and L. T. Tuy (1984). "Direct 2-D Display of 3-D Objects." IEEE Computer Graphics and Applications **4**(10): 29--33.

Udupa, J. K. (1982). Interactive segmentation and boundary surface formation for 3D digital images. Computer Graphics and Image Processing.

Udupa, J. K. and D. Odhner (1993). "Shell rendering." Computer Graphics and Applications, IEEE **13**(6): 58-67.

van Genderingen, H. R. and J. P. A. Verbunt (2005). EITviewer: towards a clinical visualisation tool for thoracic EIT. 6th conference on biomedical applications of electrical impedance tomography, London.

van Ooijen, P. M. A., R. J. M. van Geuns, et al. (2003). "Noninvasive Coronary Imaging Using Electron Beam CT: Surface Rendering Versus Volume Rendering." Am. J. Roentgenol. **180**(1): 223-226.

van Wijk, J. J. and R. van Liere (1993). HyperSlice. Visualisation, 1993. Visualisation '93, Proceedings., IEEE Conference on.

Vauhkonen, P. J., M. Vauhkonen, et al. (1999). "Three-dimensional electrical impedance tomography based on the complete electrode model." Biomedical Engineering, IEEE Transactions on **46**(9): 1150-1160.

Veltman, D. and C. Hutton. (2001). "SPM 99 User Manual." from been used by transfer.

Victorino, J. A., J. B. Borges, et al. (2004). "Imbalances in Regional Lung Ventilation: A Validation Study on Electrical Impedance Tomography." Am. J. Respir. Crit. Care Med. **169**(7): 791-800.

Viola, P. A. (1995). Alignment by maximization of mutual information, Massachusetts Institute of Technology.

Wan, M., A. Kaufman, et al. (1999). High performance presence-accelerated ray casting. Visualisation '99. Proceedings.

Ward, M. O. (2002). "A taxonomy of glyph placement strategies for multidimensional data visualisation." Information Visualisation **1**(3-4): 194 - 210.

Wehrend, S. and C. Lewis (1990). A problem-oriented classification of visualisation techniques. Visualisation, 1990. Visualisation '90., Proceedings of the First IEEE Conference on.

Weibel, R. and B. P. Buttenfield (1992). "Improvement of GIS graphics for analysis and decision-making." International Journal of Geographical Information Systems **6**(3): 223-245.

Wells, W. M. I., P. Viola, et al. (1996). "Multi-modal volume registration by maximization of mutual information." Med. Image Anal. **1**: 35-51.

Westermann, R. (1994). A multiresolution framework for volume rendering. Symposium on Volume Visualisation.

Westover, L. (1989). Interactive volume rendering. Proceedings of the 1989 Chapel Hill workshop on Volume visualisation, Chapel Hill, Noth Carolina, United States, ACM Press.

Westover, L. (1990). "Footprint Evaluation for Volume Rendering." Computer Graphics, Proceedings of SIGGRAPH 90: 367--376.

Wilhelms, A. J. and A. V. Gelder (1992). "Octrees for faster isosurface generation." ACM Transactions on Graphics (TOG) **11**(3): 201 - 227.

Wilkinson, L. (1999). The grammar of graphics. New York, Springer Verlag.

Wilson, A. J., P. Milnes, et al. (2001). "Mk3.5: a modular, multi-frequency successor to the Mk3a EIS/EIT system." Physiological measurement **22**(1): 49-55.

Wong, P. C. and A. R. D. Bergeron (1997). 30 Years of Multidimensional Multivariate Visualisation. Scientific Visualisation, Overviews, Methodologies, and Techniques, IEEE Computer Society.

Wong, P. C. and R. D. Bergeron (1997). Multivariate visualisation using metric scaling. Visualisation '97., Proceedings.

Woods, R. P., J. C. Mazziotta, et al. (1993). " MRI-PET registration with automated algorithm." J. Comput. Assist. Tomogr. **17** 536-46.

Yagel, R., D. Cohen, et al. (1992). "Discrete ray tracing." Computer Graphics and Applications, IEEE **12**(5): 19-28.

Yagel, R. and A. Kaufman (1992). Template-based volume viewing. Computer Graphics Forum, Proceedings Eurographics.

Yagel, R. and Z. Shi (1993). Accelerating volume animation by space-leaping. Visualisation, 1993. Visualisation '93, Proceedings., IEEE Conference on.

Yang, C.-k. (2000). Integration of Volume Compression and Visualisation: A Survey, Computer Science Department, State University of New York at Stony Brook.

Yerworth, R. J., R. H. Bayford, et al. (2003). "Electrical impedance tomography spectroscopy (EITS) for human head imaging." Physiological measurement **24**(2): 477-489.

Yerworth, R. J., R. H. Bayford, et al. (2002). "Design and performance of the UCLH Mark 1b 64 channel electrical impedance tomography (EIT) system, optimized for imaging brain function." Physiological measurement **23**: 149-158.

Yerworth, R. J., L. Horesh, et al. (2004). ROBUSTNESS OF LINEAR AND NONLINEAR RECONSTRUCTIONS ALGORITHMS FOR BRAIN EITS Non-linear is it worth the effort? XII International Conference on Electrical Bio-Impedance & V Electrical Impedance Tomography, Gdansk, Poland.

Yu, H., E.-C. Chang, et al. (2004). Fast Rendering of Foveated Volume in the Wavelet Domain. Visualisation, 2004. IEEE.

Yu, H., E.-C. Chang, et al. (2005). Fast Rendering of Foveated Volumes in Wavelet-based Representation. 13th Pacific Conference on Computer Graphics and Applications.

Zhang, J. (1996). "A representational analysis of relational information displays." International Journal of Human-Computer Studies **45**(1): 59-74.

Zhang, X.-C. (1997). Generation and detection of pulsed microwave signals by THz optoelectronics. Microwave and Optoelectronics Conference, 1997. 'Linking to the Next Century'. Proceedings., 1997 SBMO/IEEE MTT-S International.

Zhou, M. X. and S. K. Feiner (1998). Visual task characterization for automated visual discourse synthesis. Proceedings of the SIGCHI conference on Human factors in computing systems, Los Angeles, California, United States, ACM Press.

Zitova, B. and J. Flusser (2003). "image registration methods: a survey." Image and Vision computing **21**: 977-1000.

Appendix A Visualisation Tasks for 5D Brain EIT Data

In section 5.3.3, a task typology has been established for 5D EIT data, and general task formulae in subtasks style have been proposed for each task type. This appendix section is to explore potential visualisation tasks according to the typology. In order to save space, only questions at searching level *G* (synoptic location, synoptic time, and elementary frequency) and *H* (synoptic location, synoptic time, and synoptic frequency) are listed in table A.1. These two levels contain the most complex task types for a 5D brain EIT dataset. As mentioned in section 5.3.1, this research will focus on binary relations between same references or attribute. And only same/different relation will be discussed at this stage.

Symbols used in table A.1:

f : elementary frequency, which corresponds to a particular frequency value.

L : synoptic location, which can be a 2D or 3D location area.

T : synoptic time, which is a time interval defined by a start time point and end time point.

F : synoptic frequency, which corresponds to a range between a lower frequency value and a higher frequency value.

P : synoptic impedance, which means a impedance change pattern over a time interval, and/or a frequency range, and/or a location area.

R_f : same/different relation between two elementary frequency.

R_L : same/different relation between two synoptic location.

R_T : same/different relation between two synoptic time interval.

R_F : same/different relation between two synoptic frequency range.

R_P : same/different relation between two synoptic impedance change pattern.

Table A.1: Visualisation tasks for 5D brain EIT data

Searching Level	Searching Mode	Searching Direction	Tasks
level G: Synoptic location, Synoptic time, Elementary frequency	Lookup	Direct	General formula: $?P:(L,T,f)$ Concrete question: In a given location area L, during a given time interval T and under a given frequency f, find out the corresponding impedance change pattern?
		Inverse	General formula: $?(L,T,f):P$ Concrete question: For a given impedance change pattern P, during which time interval, under which frequency , and in which location area was it attained? In a given location area L, under which frequency and during which time interval was a given impedance change pattern P attained? During a given time interval T, in which location area and under which frequency was a given impedance change pattern P attained? Under a given frequency f, in which location area and during which time interval was a given impedance change pattern P attained? In a given location area L and during a given time interval T, under which frequency was a given impedance change pattern P attained? In a given location area L and under a given frequency f, during which time interval was a given impedance change pattern P attained? During a given time point T and under a given frequency f, in which location area was a given impedance change pattern P attained?
	Comparison	Direct	General formula: $?P_1:(L_1,T_1,f_1)$ $?P_2:(L_2,T_2,f_2)$ $?R_p:(P_1,P_2)$ Concrete question:

			In a given location area L, during a given time interval T and under a given frequency f, what is the relation between the corresponding impedance change pattern P and a given pattern $P1$? During a given time interval T and under a given frequency f, for different location areas $L1$ and $L2$, what is the relation between their corresponding impedance change patterns? In a given location area L and under a given frequency f, for different time interval $T1$ and $T2$, what is the relation between their corresponding impedance change patterns? In a given location area L and during a given time interval T, for different frequency $f1$ and $f2$, what is the relation between their corresponding impedance change patterns? In a given location area L, for different time interval and frequency combinations $(T1, f1)$ and $(T2, f2)$, what is the relation between their corresponding impedance change patterns? During a given time interval T, for different location area and frequency combinations $(L1, f1)$ and $(L2, f2)$, what is the relation between their corresponding impedance change patterns. Under a given frequency f, for different location area and time interval combinations $(L1, T1)$ and $(L2, T2)$, what is the relation betwen their corresponding impedance change patterns. For different location area, time interval, and frequency combinations $(L1, T1, f1)$ and $(L2, T2, f2)$, what is the relation between their corresponding impedance change patterns.
		Inverse	General formula: $?(L_1, T_1, f_1) : P_1$ $?(L_2, T_2, f_2) : P_2$ $?R_L : (L_1, L_2)$ $?R_T : (T_1, T_2)$ $?R_f : (f_1, f_2)$ Concrete question: In a given location area L and during a given time interval T, find out the relation between frequency $f1$, under which a given impedance change pattern $P1$ attained, and a given frequency $f2$? In a given location area L and under a given frequency f, find out the relation between time interval $T1$, during which a given impedance change pattern $P1$ attained, and

			a given time interval $T2$. During a given time interval T and under a given frequency f, find out the relation between location area $L1$, where a given impedance change pattern $P1$ attained, and a given location area $L2$? In a given location area L and during a given time interval T, find out the relation between frequency $f1$, under which a given impedance change pattern $P1$ attained, and frequency $f2$, under which a given impedance change pattern $P2$ attained? In a given location area L and under a given frequency f, find out the relation between time interval $T1$, during which a given impedance change pattern $P1$ attained, and time interval $T2$, during which a given impedance change pattern $P2$ attained. During a given time interval T and under a given frequency f, find out the relation between location area $L1$, where a given impedance change patterns $P1$ attained, and location area $L2$, where a given impedance change pattern $P2$ attained, are near to each other. In a given location area L, find out the relation between the combination of time interval and frequency $(T1, f1)$, which is corresponding to a given impedance change pattern $P1$, and a given combination $(T2, f2)$. During a given time interval T, find out the relation between the combination of location area and frequency $(L1, f1)$, which is corresponding to a given impedance change pattern $P1$, and a given combination $(L2, f2)$. Under a given frequency f, find out the relation between the combination of location area and time interval $(L1, T1)$, which is corresponding to a given impedance change pattern $P1$, and a given combination $(L2, T2)$. In a given location area L, find out the relation between the combinations of time interval and frequency $(T1, f1)$, which is corresponding to a given impedance change pattern $P1$, and $(T2, f2)$, which is corresponding to a given impedance change pattern $P2$. During a given time interval T, find out the relation between the combinations of location area and frequency $(L1, f1)$, which is corresponding to a given impedance change pattern $P1$, and $(L2, f2)$, which is corresponding to a given impedance change pattern $P2$. Under a given frequency f, find out the relation between the combinations of location area and time interval $(L1, T1)$, which is corresponding to a given impedance change pattern $P1$, and $(L2, T2)$, which is corresponding to a given impedance change pattern $P2$. Find out the relation between the combination of

			location area, time interval and frequency $(L1,T1,f1)$, which is corresponding to a given impedance change pattern $P1$, and a given combination $(L2,T2,f2)$. Find out the relation between the combinations of location area, time interval and frequency $(L1,T1,f1)$, which is corresponding to a given impedance change pattern $P1$, and $(L2,T2,f2)$, which is corresponding to a given impedance change pattern $P2$.
	Relation -seeking	Direct	General formula: $?(L_1,T_1,f_1):P_1$ $?L_2:(R_L,L_1)$ $?T_2:(R_T,T_1)$ $?f_2:(R_f,f_1)$ $?P_2:(L_2,T_2,f_2)$ Concrete question: In a given location area L and during a given time interval T, find out an impedance change pattern $P2$ (with corresponding frequency $f2$), satisfying that a specified relation R_f exist between frequency $f2$ and frequency $f1$, under which a given impedance change pattern $P1$ is obtained. In a given location area L and under a given frequency f, find out an impedance change pattern $P2$ (with corresponding time interval $T2$), satisfying that a specified relation R_T exist between time interval $T2$ and time interval $T1$, during which a given impedance change pattern $P1$ is obtained. During a given time interval T and under a given frequency f, find out an impedance change pattern $P2$ (with corresponding location area $L2$), satisfying that a specified relation R_L exist between location area $L2$ and location area $L1$, where a given impedance change pattern $P1$ is obtained. In a given location area L, find out an impedance change pattern $P2$ (with corresponding time interval $T2$ and frequency $f2$), satisfying that a specified relation R_T exist between $T1$ and $T2$, and a specified relation R_f exist between $f1$ and $f2$, where $T1$ and $f1$ corresponding to a given impedance change pattern $P1$. During a given time interval T, find out an impedance change pattern $P2$ (with corresponding location area $L2$ and frequency $f2$), satisfying that a specified relation R_L exist between $L1$ and $L2$, and a specified relation R_f exist between $f1$ and $f2$, where $L1$ and $f1$

			corresponding to a given impedance change pattern $P1$. Under a given frequency f, find out an impedance change pattern $P2$ (with corresponding location area $L2$ and time interval $T2$), satisfying that a specified relation R_L exist between $L1$ and $L2$, and a specified relation R_T exist between $T1$ and $T2$, where $L1$ and $T1$ corresponding to a given impedance change pattern $P1$. Find out an impedance change pattern $P2$ (with corresponding location area $L2$, time interval $T2$ and frequency $f2$), satisfying that a specified relation R_L exist between $L1$ and $L2$, a specified relation R_T exist between $T1$ and $T2$, and a specified relation R_f exist between $f1$ and $f2$, where $L1$, $T1$ and $f1$ corresponding to a given impedance change pattern $P1$.
		Inverse	General formula: $?P_1 : (L_1, T_1, f_1)$ $?P_2 : (R_P, P_1)$ $?(L_2, T_2, f_2) : P_2$ Concrete question: In a given location area L and a given time interval T, find out a frequency $f2$ (with corresponding impedance change pattern $P2$), satisfying that a specified relation exist between $P2$ and $P1$, which was obtained under a given frequency $f1$. In a given location area L and under a given frequency f, find out a time interval $T2$ (with corresponding impedance change pattern $P2$), satisfying that a specified relation exist between $P2$ and $P1$, which was obtained during a given time interval $T1$. During a given time interval T and under a given frequency f, find out a location area $L2$ (with corresponding impedance change pattern $P2$), satisfying that a specified relation exist between $P2$ and $P1$, which was obtained in a given location area $L1$. In a given location area L, find out combination of time interval and frequency $(T2, f2)$ (with corresponding impedance change pattern $P2$), satisfying that a specified relation exist between $P2$ and $P1$, which was obtained during a given time interval $T1$ and under a given frequency $f1$. During a given time interval T, find out combination of location area and frequency $(L2, f2)$ (with corresponding impedance change pattern $P2$), satisfying that a specified relation exist between $P2$ and $P1$, which was obtained in a

			given location area $L1$ and under a given frequency $f1$. Under a given frequency f, find out combination of location area and time interval $(L2, T2)$ (with corresponding impedance change pattern $P2$), satisfying that a specified relation exist between $P2$ and $P1$, which was obtained in a given location area $L1$ and during a given time interval $T1$. Find out combination of location area, time interval and frequency $(L2, T2, f2)$ (with corresponding impedance change pattern $P2$), satisfying that a specified relation exist between $P2$ and $P1$, which was obtained in a given location area $L1$, during a given time interval $T1$ and under a given frequency $f1$.
level H: Synoptic location, Synoptic time, Synoptic frequency	Lookup	Direct	General formula: $?P:(L,T,F)$ Concrete question: In a given location area L, during a given time interval T and a given frequency range F, find out the corresponding impedance change pattern?
		Inverse	General formula: $?(L,T,F):P$ Concrete question: For a given impedance change pattern P, during which time interval, which frequency range, and in which location area was it attained? In a given location area L, during which frequency range and which time interval was a given impedance change pattern P attained? During a given time interval T, in which location area and during which frequency range was a given impedance change pattern P attained? During a given frequency range F, in which location area and during which time interval was a given impedance change pattern P attained? In a given location area L and during a given time interval T, during which frequency range was a given impedance change pattern P attained? In a given location area L and during a given frequency range F, during which time interval was a given impedance change pattern P attained? During a given time point T and during a given frequency range F, in which location area was a given impedance change pattern P attained?
	Comparison	Direct	General formula:

			$?P_1:(L_1,T_1,F_1)$ $?P_2:(L_2,T_2,F_2)$ $?R_p:(P_1,P_2)$ Concrete question: In a given location area L, during a given time interval T and a given frequency range F, what is the relation between the corresponding impedance change pattern P and a given pattern $P1$? During a given time interval T and a given frequency range F, for different location areas $L1$ and $L2$, what is the relation between their corresponding impedance change patterns? In a given location area L and during a given frequency range F, for different time interval $T1$ and $T2$, what is the relation between their corresponding impedance change patterns? In a given location area L and during a given time interval T, for different frequency range $F1$ and $F2$, what is the relation between their corresponding impedance change patterns? In a given location area L, for different time interval and frequency range combinations $(T1, F1)$ and $(T2, F2)$, what is the relation between their corresponding impedance change patterns? During a given time interval T, for different location area and frequency range combinations $(L1, F1)$ and $(L2, F2)$, what is the relation between their corresponding impedance change patterns. During a given frequency range F, for different location area and time interval combinations $(L1, T1)$ and $(L2, T2)$, what is the relation between their corresponding impedance change patterns. For different location area, time interval, and frequency range combinations $(L1, T1, F1)$ and $(L2, T2, F2)$, what is the relation between their corresponding impedance change patterns.
		Inverse	General formula: $?(L_1,T_1,F_1):P_1$ $?(L_2,T_2,F_2):P_2$ $?R_L:(L_1,L_2)$ $?R_T:(T_1,T_2)$ $?R_f:(F_1,F_2)$ Concrete question: In a given location area L and during a given time

			interval T, find out the relation between frequency range $F1$, under which a given impedance change pattern $P1$ attained, and a given frequency $F2$? In a given location area L and during a given frequency range F, find out the relation between time interval $T1$, during which a given impedance change pattern $P1$ attained, and a given time interval $T2$. During a given time interval T and during a given frequency range F, find out the relation between location area $L1$, where a given impedance change pattern $P1$ attained, and a given location area $L2$? In a given location area L and during a given time interval T, find out the relation between frequency range $F1$, under which a given impedance change pattern $P1$ attained, and frequency range $F2$, under which a given impedance change pattern $P2$ attained? In a given location area L and during a given frequency range F, find out the relation between time interval $T1$, during which a given impedance change pattern $P1$ attained, and time interval $T2$, during which a given impedance change pattern $P2$ attained. During a given time interval T and during a given frequency range F, find out the relation between location area $L1$, where a given impedance change patterns $P1$ attained, and location area $L2$, where a given impedance change pattern $P2$ attained, are near to each other. In a given location area L, find out the relation between the combination of time interval and frequency range $(T1, F1)$, which is corresponding to a given impedance change pattern $P1$, and a given combination $(T2, F2)$. During a given time interval T, find out the relation between the combination of location area and frequency range $(L1, F1)$, which is corresponding to a given impedance change pattern $P1$, and a given combination $(L2, F2)$. During a given frequency range F, find out the relation between the combination of location area and time interval $(L1, T1)$, which is corresponding to a given impedance change pattern $P1$, and a given combination $(L2, T2)$. In a given location area L, find out the relation between the combinations of time interval and frequency range $(T1, F1)$, which is corresponding to a given impedance change pattern $P1$, and $(T2, F2)$, which is corresponding to a given impedance change pattern $P2$. During a given time interval T, find out the relation between the combinations of location area and frequency range $(L1, F1)$, which is corresponding to a given impedance change pattern $P1$, and $(L2, F2)$, which is corresponding to a given impedance change pattern $P2$. During a given frequency range F, find out the relation between the combinations of location area and time interval

			$(L1,T1)$, which is corresponding to a given impedance change pattern $P1$, and $(L2,T2)$, which is corresponding to a given impedance change pattern $P2$. Find out the relation between the combination of location area, time interval and frequency range $(L1,T1,F1)$, which is corresponding to a given impedance change pattern $P1$, and a given combination $(L2,T2,F2)$. Find out the relation between the combinations of location area, time interval and frequency range $(L1,T1,F1)$, which is corresponding to a given impedance change pattern $P1$, and $(L2,T2,F2)$, which is corresponding to a given impedance change pattern $P2$.
	Relation -seeking	Direct	General formula: $?(L_1,T_1,F_1):P_1$ $?L_2:(R_L,L_1)$ $?T_2:(R_T,T_1)$ $?F_2:(R_F,F_1)$ $?P_2:(L_2,T_2,F_2)$ Concrete question: In a given location area L and during a given time interval T, find out an impedance change pattern $P2$ (with corresponding frequency range $F2$), satisfying that a specified relation R_F exist between frequency range $F2$ and frequency range $F1$, under which a given impedance change pattern $P1$ is obtained. In a given location area L and during a given frequency range F, find out an impedance change pattern $P2$ (with corresponding time interval $T2$), satisfying that a specified relation R_T exist between time interval $T2$ and time interval $T1$, during which a given impedance change pattern $P1$ is obtained. During a given time interval T and during a given frequency range F, find out an impedance change pattern $P2$ (with corresponding location area $L2$), satisfying that a specified relation R_L exist between location area $L2$ and location area $L1$, where a given impedance change pattern $P1$ is obtained. In a given location area L, find out an impedance change pattern $P2$ (with corresponding time interval $T2$ and frequency range $F2$), satisfying that a specified relation R_T exist between $T1$ and $T2$, and a specified relation R_F exist between $F1$ and $F2$, where $T1$ and $F1$ corresponding to a given impedance change pattern $P1$. During a given time interval T, find out an impedance

			change pattern $P2$ (with corresponding location area $L2$ and frequency range $F2$), satisfying that a specified relation R_L exist between $L1$ and $L2$, and a specified relation R_F exist between $F1$ and $F2$, where $L1$ and $F1$ corresponding to a given impedance change pattern $P1$. During a given frequency range F , find out an impedance change pattern $P2$ (with corresponding location area $L2$ and time interval $T2$), satisfying that a specified relation R_L exist between $L1$ and $L2$, and a specified relation R_T exist between $T1$ and $T2$, where $L1$ and $T1$ corresponding to a given impedance change pattern $P1$. Find out an impedance change pattern $P2$ (with corresponding location area $L2$, time interval $T2$ and frequency range $F2$), satisfying that a specified relation R_L exist between $L1$ and $L2$, a specified relation R_T exist between $T1$ and $T2$, and a specified relation R_F exist between $F1$ and $F2$, where $L1$, $T1$ and $F1$ corresponding to a given impedance change pattern $P1$.
		Inverse	General formula: $?P_1 : (L_1, T_1, F_1)$ $?P_2 : (R_P, P_1)$ $?(L_2, T_2, F_2) : P_2$ Concrete question: In a given location area L and a given time interval T , find out a frequency range $F2$ (with corresponding impedance change pattern $P2$), satisfying that a specified relation exist between $P2$ and $P1$, which was obtained under a given frequency range $F1$. In a given location area L and during a given frequency range F , find out a time interval $T2$ (with corresponding impedance change pattern $P2$), satisfying that a specified relation exist between $P2$ and $P1$, which was obtained during a given time interval $T1$. During a given time interval T and during a given frequency range F , find out a location area $L2$ (with corresponding impedance change pattern $P2$), satisfying that a specified relation exist between $P2$ and $P1$, which was obtained in a given location area $L1$. In a given location area L , find out combination of time interval and frequency range $(T2, F2)$ (with corresponding impedance change pattern $P2$), satisfying that a specified relation exist between $P2$ and $P1$, which was obtained during a given time interval $T1$ and during a given frequency range $F1$. During a given time interval T , find out combination of

			location area and frequency range $(L2, F2)$ (with corresponding impedance change pattern $P2$), satisfying that a specified relation exist between $P2$ and $P1$, which was obtained in a given location area $L1$ and during a given frequency range $F1$. During a given frequency range F, find out combination of location area and time interval $(L2, T2)$ (with corresponding impedance change pattern $P2$), satisfying that a specified relation exist between $P2$ and $P1$, which was obtained in a given location area $L1$ and during a given time interval $T1$. Find out combination of location area, time interval and frequency range $(L2, T2, F2)$ (with corresponding impedance change pattern $P2$), satisfying that a specified relation exist between $P2$ and $P1$, which was obtained in a given location area $L1$, during a given time interval $T1$ and under a given frequency range $F1$.

Appendix B Publications as a Result of This Work

Yerworth R.J., Zhang Y., Tidswell T., Bayford R.H., and Holder D.S. (2007) "Use of statistical parametric mapping (SPM) to enhance electrical impedance tomography (EIT) image sets". Physiological Measurement, 28(7): S141-S152.

Zhang Y., Passmore P.J., and Bayford R.H. "Visualisation and post-processing of 5D brain images". The 27th IEEE Engineering in Biology Society Conference, September 2005, Shanghai, China.

Zhang Y., Passmore P.J., and Bayford R.H. "Registration of Brain EIT Images with an anatomical Brain Model". Proc. of the 1st International Conference on Medical Imaging and Telemedicine, August 2005, China. 40-44.

Zhang Y., Passmore P.J., Yerworth R.J., and Bayford R.H. "Statistical analysis for brain EIT images". Proc. of MediVis05, Jun 2005, London, UK. IEEE Comp. Soc. Press, 60-67.

Zhang Y., Passmore P.J., Yerworth R.J., and Bayford R.H. "A Comparative Analysis of Visualisation Packages for Brain EIT Visualisation". Proc. of BioMED 2005. Feb 2005, Innsbruck, Austria.

Zhang Y., Yerworth R.J., "Visualisation of diagnostic images for brain Electrical Impedance Tomography using VTK". Proc. Of PREP 2004. March 2004, Hertfordshire, UK.